REGULATION OF HPV INFECTION AND CERVICAL CANCER DEVELOPMENT FOLLOWING A HELMINTH INFECTION

Claire Butters

Thesis presented for the Degree of

DOCTOR OF PHILOSOPHY

Clinical Science and Immunology

in the Department of Pathology

Faculty of Health Sciences

UNIVERSITY OF CAPE TOWN

Supervisor: Associate Professor William Horsnell

Co-supervisors: Dr Katherine-Ann Smith and Dr Georgia Schäfer

January 2024

Table of Contents

Acknowledgements

This thesis would not have been possible without the technical and emotional support of many.

Dr William Horsnell: Thank you for your expertise and guidance during this thesis. You were a great source of support and encouragement and I really appreciate you teaching me how to perform to the best of my abilities and how to get the most out of an experiment, even if it goes horribly wrong.

Dr Katie Smith: Thank you for dreaming up this incredible project and choosing me to carry it out. Your support and enthusiasm grew my interest in the field immensely. You were always so positive and friendly, which helped me through the disasters more than you know.

Dr Georgia Schäfer: Thank you for teaching me everything I know about cell culture and various *in vitro* methods. You were a huge source of training, and you were incredibly generous with all the reagents and cells you supplied me with.

Dr Alisha Chetty: Thank you for all your time and help in this project. Thank you for taking hours out of your day to assist me with animal experiments and for training me in various wet lab techniques. I would not be the scientist I am today without you.

Rodney Lucas: Thank you for training me in mouse work and for your patience and understanding.

My mother and father: Thank you for being there to pick up the pieces when I thought everything was falling apart and for reassuring me that I was good enough.

My husband, Hugo: Thank you for not only the verbal support, but also for your small acts of kindness such as bringing me tea and mince pies while I was analysing data or writing.

All other colleagues who helped me throughout this thesis: Thank you to Dr Matthew Darby, Sinead Carse, Dr Tatenda Murangi, Claire Bellis and Dr Brunette Katsandegwaza.

My funders, for both personal financial assistance and for funding the project:

Plagiarism declaration

I know that plagiarism is wrong. Plagiarism is to use another's work and pretend that it is one's own.

I have used the Vancouver convention for citation and referencing. Each contribution to, and quotation in, this thesis from the work(s) of other people has been attributed and has been cited and referenced. Any section taken from an internet source has been referenced to that source.

This thesis is my own work and is in my own words (except where I have attributed it to others).

I have not allowed, and will not allow, anyone to copy my work with the intention of passing it off as his or her own work.

I acknowledge that copying someone else's assignment or essay, or part of it, is wrong, and declare that this is my own work.

Signature _____

Abbreviations

a.u. – arbitrary units

AAM/M2 – alternatively activated macrophages

ADCC – antibody-dependent cellular cytotoxicity

AES – *Ascaris lumbricoides* ES

AIP-1 – anti-inflammatory protein 1

ANOVA – analysis of variance

APC – antigen presenting cell

BCA – bicinchoninic acid

BM – basement membrane

BME – basement membrane extract

CCL – chemokine ligand

CIN – cervical intraepithelial neoplasia

CMC – carboxymethyl cellulose

CRC – colorectal cancer

CTL – cytotoxic T cell lymphocyte

DALY – disability-adjusted life years

DC – dendritic cell

DMEM – Dulbecco's modified eagle medium

DNA – deoxyribonucleic acid

ECM – extracellular matrix

ECP – eosinophil cationic protein

EDN – eosinophil-derived neurotoxin

EDTA – ethylenediaminetetraacetic acid

EMT – epithelial to mesenchymal transition

EPO – erythropoietin

ES – excretory-secretory products

EV – extracellular vesicles

Fc – fragment crystallisable

FGT – female genital tract

fHPV – FLuc plasmid-containing HPV

Fluc – firefly luciferase

FOXP3 – forkhead transcription factor family protein 3

FOXN1 – forkhead box protein N1

GAPDH – glyceraldehyde 3-phosphate dehydrogenase

gHPV – Gluc plasmid-containing HPV

GIT – gastrointestinal tract

Gluc – Gaussia luciferase

GM – geometric mean

GM-CSF – granulocyte-macrophage colony stimulating factor

HEPES – 4-(2-hydroxyethyl)-1-piperazineethanesulfonic acid

HES – *Heligmosomoides polygyrus* ES

HIV – human immunodeficiency virus

Hp – *Heligmosomoides polygyrus bakeri*

HpARI - *Heligmosomoides polygyrus bakeri* Alarmin Release Inhibitor

HPV – human papillomavirus

HRP – horseradish peroxidase

HSB – high salt buffer

HSPG – heparan sulphate proteoglycan

HSV – herpes simplex virus

IBD – inflammatory bowel disease

IFN – interferon

Ig – immunoglobulin

IL – interleukin

ILC2 – innate lymphoid cell 2

iLN – iliac lymph node

IVIS – *in vitro* imaging system

MBP – major basic protein

MCP-1 – monocyte chemoattractant protein 1

MFI – mean fluorescence intensity

miRNA – microRNA

MNV – murine norovirus

MuHV-4 – murine gammaherpesvirus 4

N9 – nonoxynol-9

Nb – *Nippostrongylus brasiliensis*

NES – *Nippostrongylus brasiliensis* ES

NET – neutrophil extracellular trap

P/S – penicillin and streptomycin

PAGE – polyacrylamide gel electrophoresis

PBS – phosphate buffered saline

POI – protein of interest

PRR – pattern recognition receptor

PsV – pseudovirion

PVM – pneumonia virus of mice

RANTES – regulated upon activation, normal T cell expressed and presumably secreted

RIPA – radioimmunoprecipitation assay

RNA – ribonucleic acid

RSV – respiratory syncytial virus

SARS-CoV-2 – severe acute respiratory syndrome coronavirus 2

SAVC – South African Veterinary Council

SCFA – short chain fatty acid

SCID – severe combined immunodeficiency disease

SDS – sodium dodecyl sulphate

SEM – standard error of the mean

SPF – specific pathogen free

SSC – side scatter

STAT6 – signal transducer and activator of transcription 6

STH – soil-transmitted helminth

STVI – sexually transmitted viral infection

t-SNE – t-distributed stochastic neighbour embedding

TAM – tumour associated macrophages

TBS – Tris-buffered saline

TBST – Tris-buffered saline with Tween

TE – Tris-EDTA

Th – helper T cell

TLR – toll-like receptor

TNF – tumour necrosis factor

Treg – regulatory T cell

TSLP – thymic stromal lymphopoietin

USA – United States of America

vDNA – viral DNA

VLP – virus-like particle

WHO – World Health Organisation

Wnt – wingless-related integration site

Abstract

Soil-transmitted helminth (STH) infections elicit systemic immune responses and have the ability to alter susceptibility to other infections in sites uncolonized by the STH. Recent work published by our group demonstrated that hookworm infection increased pathology in the female genital tract (FGT) following infection with the commonly sexually transmitted herpes simplex virus (HSV)-2. Although epidemiological studies have linked helminth infection with an increased prevalence of the most common sexually transmitted infection, human papillomavirus (HPV), studies in our lab have demonstrated that exposure to helminth products can decrease HPV pseudovirion uptake *in vitro*. Persistent infections with high-risk types of HPV can result in cervical cancer, the leading cause of cancer related deaths in women in South Africa. Little is known about the association between these two diseases.

In this thesis, I investigated how HPV pseudovirion (PsV) infection can be altered by an STH infection both *in vitro* and *in vivo. In vitro* experiments demonstrated exposure to somatic helminth antigens from *Nippostrongylus brasiliensis* and *Heligmosomoides polygyrus bakeri* decreased HPV PsV infection in two cervical cancer cell lines and one primary keratinocyte cell line (the target cell of HPV). Similarly, exposure to the excretory-secretory (ES) antigens from *H. polygyrus* decreased HPV PsV infection in two cell lines, and increased HPV PsV infection in the other cervical cancer cell line. When the somatic antigens were heat inactivated, the protection against HPV PsV infection was abrogated, suggesting the molecule involved in this protection is a heat unstable protein. In contrast, when *H. polygyrus* ES antigen was heat inactivated, the previously observed increase in infection was reversed and instead decreased HPV PsV infection. Additionally, western blot analysis revealed that exposure to *N. brasiliensis* somatic antigen resulted in increased expression of vimentin, a molecule known to inhibit HPV infection. These results were then validated *in vivo,* through the development of a physiological murine model for HPV infection, utilising a luminescent HPV PsV and *in vivo* imaging system (IVIS). Following optimisation, I found that HPV PsV infection was significantly reduced following intravaginal exposure to *N. brasiliensis* L3 antigen and at day 9 post-infection with *N. brasiliensis.* This was associated with a significant increase in eosinophil accumulation in the female genital tract (FGT) and iliac lymph node (iLN), the draining lymph node of the FGT. Coinfected mice demonstrated a population of

eosinophils expressing lower levels of Ly6C and higher levels of CD11b, a recruitment marker. When eosinophil recruitment was blocked, the helminth-dependent reduction in HPV infection is lost, suggesting these immune cells may contribute to this observed protection. Additionally, western blot analysis revealed that *N. brasiliensis* infection increased the expression of an HPV receptor, glypican. These data suggest that coinfection with *N. brasiliensis* has a protective effect against the initial infection of HPV.

Finally, to investigate how STH infection may influence the development and growth of HPV-related cervical cancer, I developed a cervical cancer xenograft model using nude mice. Here, my data suggest that engrafted nude mice infected with *N. brasiliensis* displayed reduced growth of cervical cancer tumours compared to naïve mice, with no change to tumour immune cell infiltrates but rather an increase in tumour cell p53 expression and altered epithelial to mesenchymal transition (EMT) marker expression.

Together, these findings show that helminth infection can protect against distal viral infection and suppress the growth and cancer cell behaviour of HPV associated cervical cancer.

Chapter 1: Thesis introduction.

This thesis addresses how soil-transmitted helminth infection affects vaginal immunity towards HPV infection and cervical cancer progression. These infections and diseases are highly prevalent in sub-Saharan Africa, and coinfection has been shown to be common. It is therefore necessary to understand how these two infections may affect the progression of the other as this could lead to the development of novel therapeutics, or alternatively provide further evidence to support the surveillance and treatment of these diseases.

In this introduction, I will introduce helminths and their immunomodulatory abilities, the prevalence and biology of HPV and cervical cancer, as well as how helminths have been shown to alter immunity to other infections and cancers to outline the current knowledge and how this shaped the rationale behind this study.

1.1 Soil-transmitted helminths

1.1.2 Prevalence and burden

Helminths are parasitic worms that infect multiple host species. They have well-developed organ systems and can be either hermaphroditic or bisexual. Helminths infect humans through various mechanisms; the most common infection route is ingestion of eggs or larvae. Some helminths require an intermediate host vector such as arthropods and fish. Helminths can further be divided into platyhelminths (flukes and tapeworms) and nematodes (roundworms)[1]. Soil-transmitted helminths (STHs) are the most common subtype of nematode that are transmitted through contaminated soil. These helminths are endemic in many rural regions with a tropical, humid climate, such as sub-Saharan Africa, south-east Asia and South America (Figure 1.1). The three main types of STHs are hookworms, whipworms and roundworms. STHs infect approximately 1.5 billion people worldwide[2], with the most common human infection being from the hookworm *Ascaris lumbricoides* (up to 1.12 billion)[3]. STH infections are classified as a neglected tropical disease based on the morbidity and disability they cause and the difficulty faced in public health control[3]. While most mild infections are asymptomatic, severe infections may cause diarrhoea, malnutrition, anaemia, decrease in cognitive function and intestinal blockages[2,3]. Death due to STH infection is

uncommon, however it was estimated that in 2010 there were 2824 deaths attributed to *A. lumbricoides* infection[4]. In 2000, STH infections were responsible for over 4 million disability-adjusted life years (DALYs) – years of life lost due to disability and/or premature mortality. This number decreased to 2.7 million DALYs in 2010 and 1.9 million DALYs in 2019, which coincides with an increase in preventative chemotherapy and deworming initiatives[5].

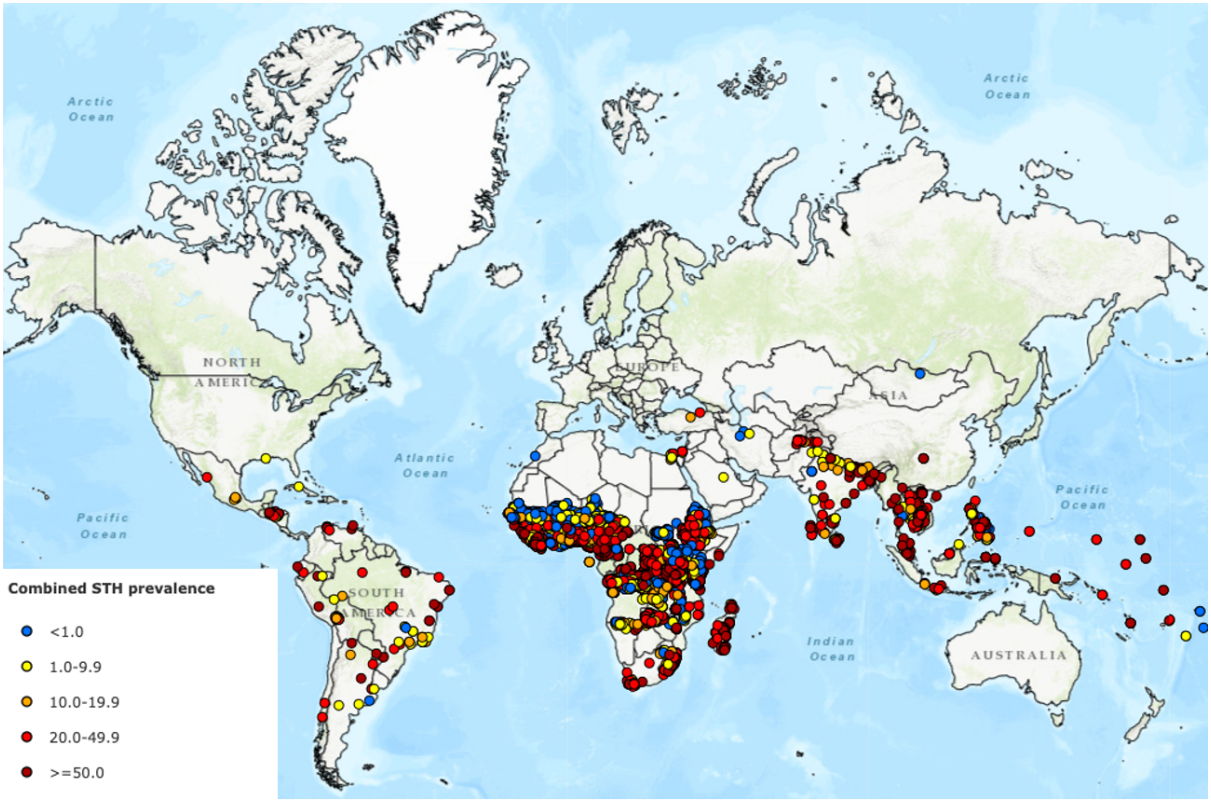

Figure 1.1: Prevalence of soil-transmitted helminth infections. *(Created using Global Atlas of Helminth Infections map creator[6].)*

Due to their persistence in the soil, it is difficult to prevent re-exposure and re-infection with STH's and therefore difficult to eradicate. While humans do develop some level of immunity after infection, this immunity is only partially effective and leaves humans susceptible to repeated low-level infections[7]. The World Health Organization (WHO) recommends periodic preventative chemotherapy and deworming to all at-risk people in endemic areas to reduce worm burden and associated morbidity. Preventative chemotherapy is the use of anthelminthic drugs, alone or in combination, to kill any worms before the infection can causes morbidity. Currently, this is the only treatment available and there are no vaccines against any STHs. In 2021, half a billion children in endemic areas received anthelminthic treatment, representing 62% of all at-risk children[2]. The deworming medications albendazole

and mebendazole are recommended as they are inexpensive and do not need to be administered by healthcare professionals. Albendazole and mebendazole work by inhibiting microtubule formation in the gut of helminths, resulting in energy depletion and death of the helminth. In addition to this, it is important to provide communities with information to educate people about proper sanitation and hygiene practices to prevent soil contamination.

1.1.2 Helminth life cycles

Helminths have diverse life cycles and tissue tropism, reflected by the differing clinical presentation and pathologies. Among the STHs, there are two main biological life cycles: through ingestion of eggs (faecal-oral) or through larval penetration of the skin (percutaneous)[3]. Briefly, faecal-oral transmission occurs through fertilised eggs being ingested. In the case of *A. lumbricoides*, the fertilised eggs develop in the contaminated soil to first-stage larvae (L1), which then moult into L2 and subsequently to L3, the infective larvae. Once these embryonated eggs are ingested, the larvae hatch, penetrate the intestinal mucosa and travel to the lungs through the circulatory system. The larvae then pass through the alveolar wall, and travel through the tracheobronchial tree until they reach the larynx, where they are then swallowed. When they reach the upper small intestine, the larvae moult into L4, and then into adult worms. The male and female adult worms will produce eggs that are then excreted by the infected host in their faeces (Figure 1.2A)[8]. Percutaneous infection by *Ancylostoma duodenale* and *Necator americanus* proceeds when L3 larvae penetrate the skin, usually by walking barefoot on contaminated soil. The larvae travel through the capillaries to the lungs. Much like *A. lumbricoides*, the larvae penetrate the alveolar wall, travel up to the larynx and are swallowed. The larvae moult into L4 and L5 in the gastrointestinal tract (GIT), and finally into adult worms. The worms lay eggs, which are then excreted in faeces. After 5-10 days, the eggs hatch (if in warm and moist soil or faeces) into L1. After moulting twice to L3, the larvae are then infective (Figure 1.2B)[8].

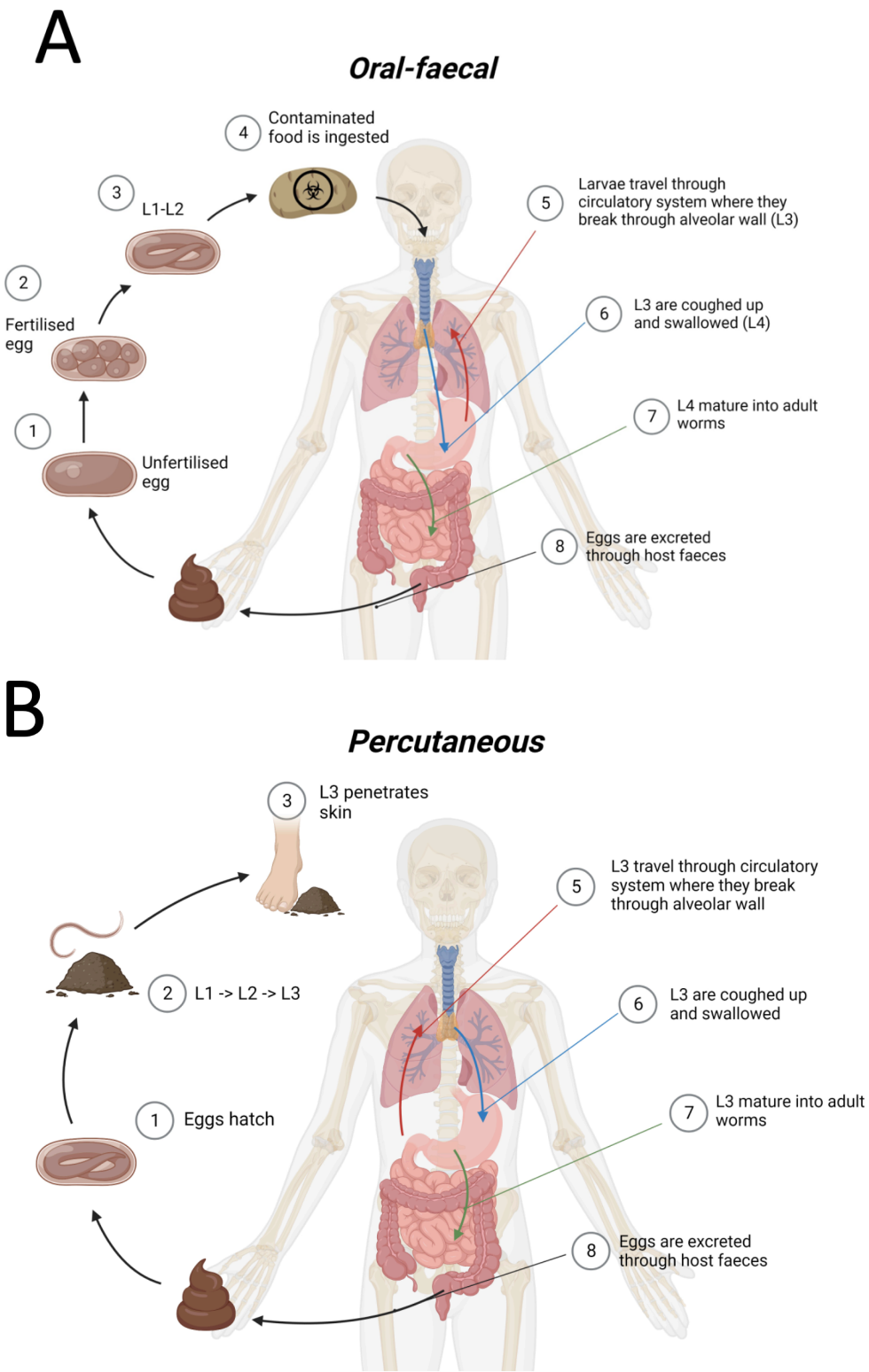

Figure 1.2: Soil transmitted helminth life cycles. *(A) oral-faecal life cycle, (B) percutaneous life cycle*

1.1.3 Mouse models

There are numerous ethical and experimental reasons why experiments are not performed on humans. Therefore, to investigate the effects of helminth infections *in vivo,* it is preferable to perform experiments in animal models[9]. Mouse models are good choices for the following reasons: 1. They are small, and therefore do not take up a lot of space; 2. They reproduce rapidly (gestation approximately 20 days) and have a short lifespan[10]; 3. The mice in all experimental groups are genetically identical (if inbred strains are used), limiting the confounding factors that genetics may pose on outcomes such as susceptibility and immunity to disease[11,12]; 4. Genes can be easily manipulated if required[13]; and 5. Mice have similar, however not identical, immune systems to humans, which makes them biologically comparable and a good model system[14].

Humans have large genetic variability whereas mice are typically inbred to have genetic homozygosity to remove the confounder of genetic variation[10], allowing for smaller sample sizes and reproducible results. Mice have been genetically engineered for various reasons, including alterations to the immune system. For example, the BALB/cJ strain of mice was created by repeated inbreeding of mice with genetically similar backgrounds. This resulted in a genetically homogenous strain with unique immunological characteristics. When challenged with helminths, these mice elicit a type 2 immune response whereas another strain of mouse, C57BL/6J mice, have the genetic characteristic of eliciting a type 1 immune response towards helminths[15], allowing researchers to design and carry out experiments with appropriate immunological conditions for the disease/infection being explored. The difference in immunological traits would obviously effect results of immune-focussed studies and therefore results may not be indicative of how the human immune response would respond. Therefore, the understanding and choice of mouse strain is of utmost importance.

Because BALB/c mice elicit a type 2 immune response against helminths, they are an appropriate choice of mouse strain when investigating acute infection using a murine helminth such as *Nippostrongylus brasiliensis* (as this is how the human immune system responds to an acute infection), whereas C57BL/6 can be used to investigate chronic helminth infections when using a murine helminth such as *Heligmosomoides polygyrus bakerei* (as this

is how the human immune system responds to a chronic infection). The ability to choose a mouse strain that elicits the desired immune response towards STH infection allows researchers to design experiments that would appropriately model a human STH infection, providing reliable data that can be extrapolated to humans. Mouse models are also widely used to study STH infections because the murine equivalent STH species closely resemble those of human STH species. Two of the most common STHs used in mouse models are *N. brasiliensis*, a murine hookworm, and *H. polygyrus,* a murine roundworm. *N. brasiliensis* has a similar life cycle to *A. lumbricoides* and *N. americanus*; the L3 infect their host percutaneously[16] (Figure 1.2). This allows for comparable investigation into human hookworm infection as differences in STH life cycle may cause incomparable pathology (e.g. lung damage caused by migrating larvae) and therefore elicit different immune responses. In an experimental setting, mice are infected through a subcutaneous injection of L3 *N. brasiliensis* to mimic percutaneous infections, while *H. polygyrus* is administered through oral gavage to mimic the faecal-oral transmission[17]. These murine STHs have proteomic similarity to their human STH equivalents, making them useful in the development of vaccines as well as novel drugs from immunomodulatory molecules found in STH ES[18].

1.1.4 Immune response during helminth infection

In an acute infection, there is a dominant type 2 response driven by the production of interleukin (IL)-4, IL-5 and IL-13 (Figure 1.3). In the instance of a percutaneous mode of infection, it has been shown that subcutaneous infection of mice with the filarial helminth *Litosomosoides sigmodontis* resulted in rapid neutrophil accumulation at the site of infection[19]. Here, neutrophils released neutrophil extracellular traps (NETs) to immobilise the larvae and prevent further migration[19]. Following subcutaneous infection with *N. brasiliensis*, mice lacking complement had reduced eosinophil recruitment to the skin and higher lung larval burdens, suggesting an important role for complement in parasite recognition and eosinophil recruitment[20]. Similarly, early recruitment of eosinophils to the skin and subsequent early control of *N. brasiliensis* infection was shown to be dependent on the production of eotaxin in an IL-4- and signal transducer and activator of transcription 6 (STAT6)-dependent manner[21,22]. Analysis of BALB/c mouse lungs following *Ascaris suum* or *A. lumbricoides* infection (timing of peak larval migration through the lung) revealed that there was increased production of IL-6, shortly followed by increased production of tumour necrosis

factor (TNF)-α[23]. An accumulation of neutrophils was also observed, where they initially limited the survival of larvae, but at the expense of furthering lung damage[24] through degranulation of various antimicrobial proteins and proteases[25]. However, neutropenic mice were unable to promote the alternative activation of macrophages (M2), which are important in tissue damage repair and larval trapping, indicating that neutrophils play both a destructive and protective role against larvae in the lung[26]. Following this, there is an IL-5-dependent infiltration of eosinophils, as shown in mice infected with *N. brasiliensis*[27], and was shown in an *in vitro* model to assist with tissue remodelling[28]. Larvae then migrate to the intestine, where epithelial sensor cells, such as tuft cells, produce the alarmins IL-25[29,30], IL-33[31] and thymic stromal lymphopoietin (TSLP)[32], shown in models using various helminth species. Overexpression of IL-25 and IL-33 by tuft cells lead to a goblet cell hyperplasia, an overproduction of mucus[29], and induced worm expulsion in susceptible mice[31], demonstrating their importance in initiating the "weep and sweep" response to physically expel the worms. Additionally, tuft cell deficient mice were unable to mount a complete type 2 antihelminth response against *N. brasiliensis*[30], demonstrating that these cells are vital in the production of these alarmins in initiating a type 2 immune response against helminths. A large increase in eosinophils, neutrophils and mast cells were observed in the gut of mice once *Nematospiroides dubius* larvae had begun invading or burrowing into the gastric mucosa[33], after which these neutrophils were shown to produce eosinophil-recruiting chemokines[34], resulting in intestinal eosinophilia[33]. Additionally, the alarmins activate type 2 innate lymphoid cell (ILC2s)[35], which produce IL-4, IL-5 and IL-13[31,35–37], initiating the polarisation of Th2 cells. Treatment of human neutrophils with IL-4 and IL-13 revealed reduced NET formation and tissue damage, indicating an additional role of these two cytokines on maintaining tissue homeostasis[38,39]. IL-13 overexpression in mice induced goblet cell hyperplasia and increased mucus production, demonstrating that IL-13 production creates a positive feedback loop and enhances the type 2 response[40]. Production of IL-13 by ILC2s was also shown to be critical in promoting the migration of dendritic cells (DCs) to lymph nodes following papain challenge (a potent type 2 promoter)[41]. DCs are antigen-presenting cells; they present helminth antigens (usually secreted helminth products) to naïve T cells in the draining lymph nodes. *In vitro* data have demonstrated that exogenous TSLP potently activated DCs[42]. These human DCs were then cocultured with naïve CD4+ T cells and were able to induce Th2 development and IL-4, IL-5 and IL-13[42–44]. ILC2s have also been shown to

produce CCL17, a helper T cell (Th) chemoattractant, demonstrating the importance of ILC2s in Th2 localisation to the site of infection[45]. Antibody depletion of IL-4 in *N.* brasiliensis-infected mice resulted in no production of IgE by B cells, suggesting IL-4 is necessary for antibody production by B cells[27]. Preclinical models infecting mice with *N. brasiliensis* or *H. polygyrus* both showed that IL-5 production from both ILC2s and Th2 cells, production of eosinophil chemoattractants by neutrophils, as well as the presence of TSLP, was required for eosinophil infiltration and expansion to the site of infection[21,27,36,46].

Eosinophilia is a hallmark feature of a helminth infection. This eosinophilia is evident in increased systemic eosinophils as well as an increase in tissue infiltrating eosinophils at the site of infection. They play an important role in mediating protection from infection with some helminth species[47,48], but not others[49,50]. These cells have been shown to accumulate around diverse nematode species *in vitro*, indicating that, apart from IL-5, there is a conserved molecule produced by helminths that induces eosinophil migration[51]. Eosinophils are directly involved in parasite killing in certain infection models, especially those with tissue migratory larvae[52]. Stimulation of eosinophils with TSLP *in vitro* lead to eosinophil degranulation[53], a process also mediated by antibody binding and/or complement[53,54]. These granules are mostly comprised of cytotoxic and cationic proteins, such as major basic protein (MBP), eosinophil peroxidase (EPO), eosinophilic cationic protein (ECP) and eosinophil-derived neurotoxin (EDN), as well as up to 35 cytokines and chemokines (reviewed in ref[55]). These proteins are highly basic (high pH) and have been shown that *in vitro* treatment of helminth larvae with these granules resulted in tegument damage and worm mortality[56,57]. Eosinophil degranulation occurs through numerous pathways, the first being antibody-dependent cellular cytotoxicity (ADCC). Helminth-specific antibodies opsonise the parasite. Eosinophils from hyper-eosinophilic patients bound to the Fc portion of the antibodies immobilised on beads, which signalled the eosinophils to degranulate[58,59]. Eosinophil degranulation has also been demonstrated to occur through activated complement factors; mice lacking these factors (such as C3a and C5a) understandably had reduced complement deposition on larvae, however eosinophils lacking complement receptors in complement-competent mice were still able to degranulate, indicating eosinophils may use more than one pathway to degranulate[20]. Stimulation of eosinophils with various cytokines, such as IL-5, IL-13, IL-33, granulocyte-macrophage colony stimulating factor (GM-CSF), TNF-α, RANTES and interferon

(IFN)-γ, have also been shown to induce eosinophil degranulation[60–62]. The predominant cytokine released from eosinophils during degranulation is IL-4, which adds to the promotion of naïve T cell polarisation towards Th2 cells[63]. Apart from direct killing, eosinophils may also act as antigen presenting cells (APCs)[63]. It has been shown in an allergic airway mouse model that exposure to antigen in the allergic lung resulted in eosinophil tracking to the site of sensitisation and draining lymph nodes[64]. These antigen-loaded eosinophils expressed MHC class II (MHCII), and during *in vitro* coculture with Th2 cells, lead to the production of IL-4, IL-5 and -13 by antigen-specific CD4+ T cells[64]. Interestingly, it has been shown that the excretory-secretory products (ES) from *N. americanus* contain a protease that specifically cleaves eotaxin, which would in turn prevent eosinophil recruitment, ultimately prolonging the helminths' survival[65].

As mentioned above, eosinophils are an important source of IL-4. IL-4 produced from both eosinophils and Th2 cells promotes the recruitment and activation of AAMs[66–68]. AAMs have been shown to enhance Th2 polarisation through helminth antigen presentation, amplifying the type 2 response[69]. AAMs also express Arg-1, which is involved in muscle hypercontractility and subsequently worm expulsion (weep and sweep response)[68]. AAMs are important in tissue repair inflicted by migrating and burrowing larvae. Macrophages have been shown to secrete Ym1 and FIZZ1 in the presence of IL-4 *in vivo*[70,71], which are both involved in the deposition of extracellular matrix (ECM) and therefore wound healing[72]. The phagocytic ability of AAMs also allows them to remove cellular debris created through tissue damage[73], further contributing to the repair of helminth-induced damage.

As demonstrated above, T cells are an important source of cytokines that drive various helminth-expelling processes. It has been shown in nude mice infected with *N. brasiliensis* or *H. polygyrus* that the absence of T cells results in a delayed worm expulsion with increased intestinal pathology[74–76]. However, goblet cell hyperplasia and mucus production were unaffected, indicating that IL-13 secreted from T cells to increase goblet cell hyperplasia is redundant[74], and its source from other immune cells is sufficient. Long term (chronic) infections are associated with the expansion of regulatory T cells (Tregs)[77]. These cells are important in maintaining a balance between preventing immune-mediated damage to the host and a sufficient immune response to clear an infection[78]. The expansion of Treg

populations can be from the expansion of naturally occurring Treg populations or the differentiation of CD4+ T cells through IL-10 and transforming growth factor (TGF)-β signalling[79,80]. The latter can be accomplished through the production of TGF-β by dendritic cells[81] or AAMs[82], or through the production of IL-10 by dendritic cells[83]. Forkhead transcription factor family protein 3 (*FOXP3*) expression is induced through these signals, and it has been shown *in vitro* that both thymic and peripheral naïve T cells may differentiate into Tregs[79]. Some helminths, such as *H. polygyrus,* secrete a TGF-β mimic that adds to the induction of Tregs and dampened immune response[84,85], which may assist in prolonging their survival within the host. The discovery of Tregs through chronic T cell activation showed that Tregs produce IL-10 and TGF-β[86]. This was shown to induce antibody class switching from IgE to IgG4 by B cells when co-cultured with IL-10 producing Tregs[87]. Mice with no Tregs had increased tissue damage and yet enhanced *H. polygyrus, T. muris and S. mansoni* clearance, indicating that the immunosuppressive effect of Tregs is a fine balance between expelling helminths and limiting immunopathology[88–90].

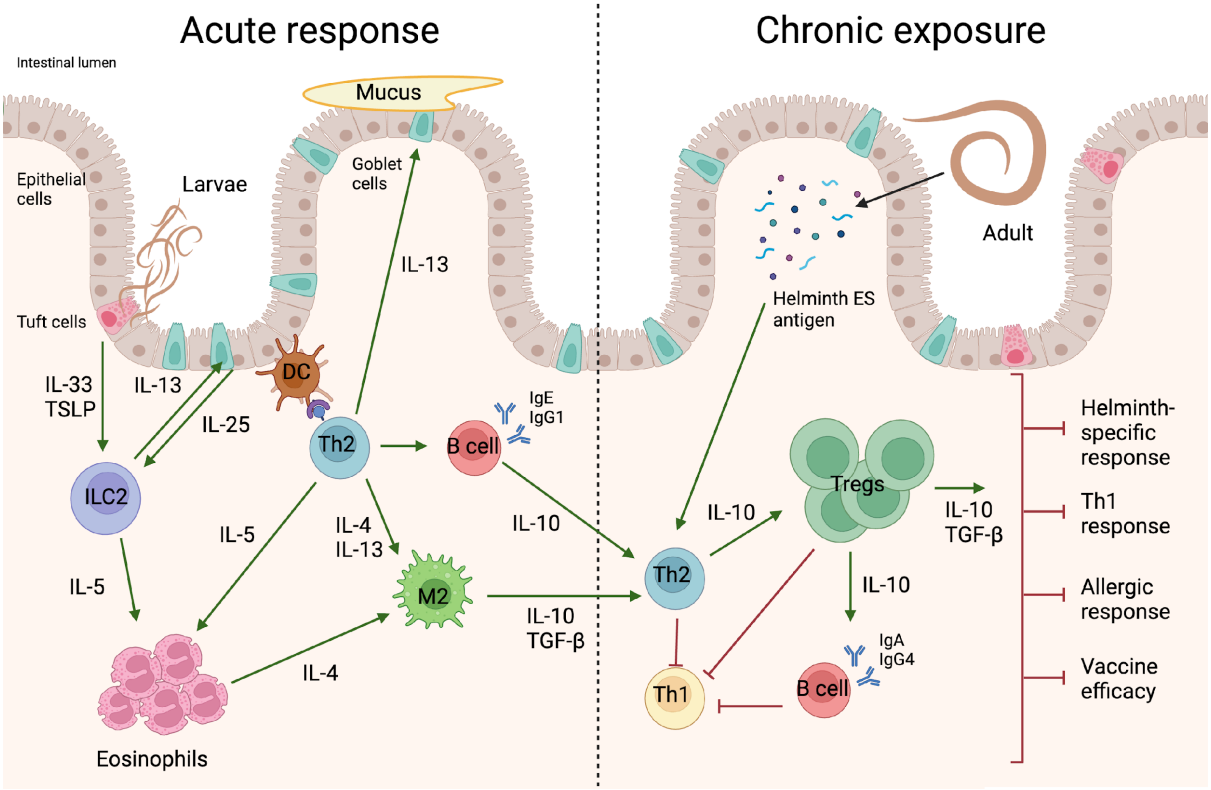

Figure 1.3: Immune response towards helminths. *In the intestinal lumen, STH larvae-induced epithelial damage induces the production of alarmins by intestinal epithelial cells. These alarmins activate ILC2s, which then recruit eosinophils and induce mucus production by goblet cells. Antigen presentation of dendritic cells to T cells*

polarises the T cells towards a Th2 cell. These Th2 cells and eosinophil then alternatively activate macrophages. The Th2 cells also induce IgE and IgG1 antibody production by B cells. In chronic exposure, M2 macrophages will induce the differentiation or expansion of Treg populations, which dampen the immune response and result in antibody class switching by B cells. (Created using Biorender.com.)

1.1.5 Host immunomodulation by helminths

1.1.5.1 Molecules

Helminths secrete potent immunomodulatory molecules within their ES in order to dampen the immune response elicited against them[91]. A favourable consequence of this is that the dampening of the immune response limits immunopathology[78]. There are various molecules within various helminth ES that are responsible for this immunomodulation. For example, cystatins secreted by various helminths have shown to down-regulate IL-4 production, inhibit eosinophil recruitment, induce IL-10 expression by macrophages and interfere with antigen presentation[92–95]. *H. polygyrus* ES (HES) contains a protein named HpARI (*H. polygyrus* Alarmin Release Inhibitor) that inhibits IL-33 release, which in turn prevents production of type 2 cytokines by ILC2s as well as preventing eosinophilia[96,97]. HES also contains a TGF-β mimic that has been shown to induce *FOXP3* expression in T cells, thereby encouraging Treg differentiation and promoting immunosuppression allowing the worm to survive in the host[84].

1.1.5.2. Extracellular vesicles

MicroRNAs (miRNA) can be secreted by various helminths enclosed in extracellular vesicles (EVs). These EVs are approximately 40-2000nm in size, and are derived from the endosome of the cell which then binds to the plasma membrane for release (exosomes) or from plasma membrane budding (microvesicles)[98]. It is not fully understood which cells in the helminth secrete these EVs, however it has been shown that EVs can be released from the gut of a helminth, shown in the murine helminth *H. polygyrus*[99].

The contents of EVs have been shown to contain lipids, proteins and nucleic acids[98]. Some EVs contain unique contents, while they have also been shown to contain the same molecules found in the soluble compartment of the ES[99,100]. One of the primary roles of EV secretion by helminths is to modulate the host immune response. EVs isolated from a number of different helminth species contain miRNAs that interfere with genes involved in immunity[101–104]. For

example, miRNA that was found in EVs isolated from HES have been shown to suppress type 2 innate responses through the suppression of the *IL33r* gene[99] and inhibit the alternative activation of macrophages[101]. The immune modulation of helminth ES is an attractive candidate for the treatment of allergic and autoimmune diseases; recombinant anti-inflammatory protein (AIP-1), which is found in the ES of hookworms, has been shown to reduce colitis-induced inflammation and increase production of immune regulatory cytokines such as IL-10[101].

1.1.5.3. Indirect regulation of systemic inflammation

Another mechanism of host immunomodulation by helminths is through the alteration of the host gut microbiome, a potent modulator of the immune system. Murine infection with *H. polygyrus* has been shown to increase the abundance of bacteria in the ileum compared to uninfected mice[105]. This is largely due to an increase in abundance of *Lactobacillaceae*[105], a family of commensal bacteria in the gut that has been shown to decrease intestinal inflammation through immunosuppression. The increase in the abundance of these bacteria resulted in the increase in short chain fatty acid (SCFA) production of *H. polygyrus*-infected mice, which subsequently induced the expansion of Tregs. This further lead to a reduction in airway inflammation and increased worm burden, demonstrating an indirect mechanism of STHs in modulating host immune responses[106,107]. The adoptive transfer of AAMS from *H. polygyrus*-infected mice was shown to initiate the production of SCFAs by the host microbiota[108]. Additionally, an *H. polygyrus*-infection induced an increase in production of the SCFA isovaleric acid in the small intestine; supplemental administration of isovaleric acid to *H. polygyrus*-infected mice was shown to increase worm fecundity through increased faecal egg counts[109]. Together, these studies demonstrate how helminths may dampen the immune response elicited against them as well as enhance their survival and reproduction.

1.1.5.4. Impact of helminth-immune regulation on vaccine responses

A preclinical study showed that *H. polygyrus*-infected mice that had been immunised against malaria had reduced antibody production when challenged with malarial antigens[110]. Epidemiological evidence has similarly demonstrated reduced antibody production and skewed cytokine production in response to BCG vaccination in helminth-infected individuals,

which was accompanied by increased TGF-β production[111]. Reduced vaccine efficacy has also been demonstrated in viral vaccine challenges; influenza-immunised helminth-infected mice similarly had lower production of influenza-specific antibodies and high viral load following an influenza challenge[112].

While helminth infection has been shown to reduce vaccine efficacy, it does not appear that helminth infection alters immune responses towards the HPV-16/18 vaccine[113]. This demonstrates that the Th2-skewing induced by helminth infections may differentially affect vaccine efficacies based on the immune response induced by the vaccine. For example, the BCG vaccine induces a Th1 memory response[114]. If the immune system is already skewed towards Th2, this may impair the memory response induced by the vaccine. Conversely, the HPV vaccine elicits both a Th1 and Th2 memory response[115,116]. This may explain why reduced efficacy is not seen here.

1.2 HPV and cervical cancer

1.2.1 HPV

Human papillomavirus (HPV) is a group of viruses from the *Papillomaviridae* family that are spread through skin-to-skin contact, primarily (but not exclusively) through sexual contact. There are approximately 120 different types of HPV, with around 14 of these being oncogenic (cancer causing) serotypes. Most men and women will be infected with HPV at some point in their lives, with around 90% of infections being asymptomatic; however, the infection is usually resolved within 2 years[117], but persistent infections may result in oncogenesis. Worldwide, the prevalence of HPV infection among women was estimated to be 10-11.7%, whereas sub-Saharan Africa has the highest prevalence of HPV at 22.9-24%[118] (Figure 1.4).

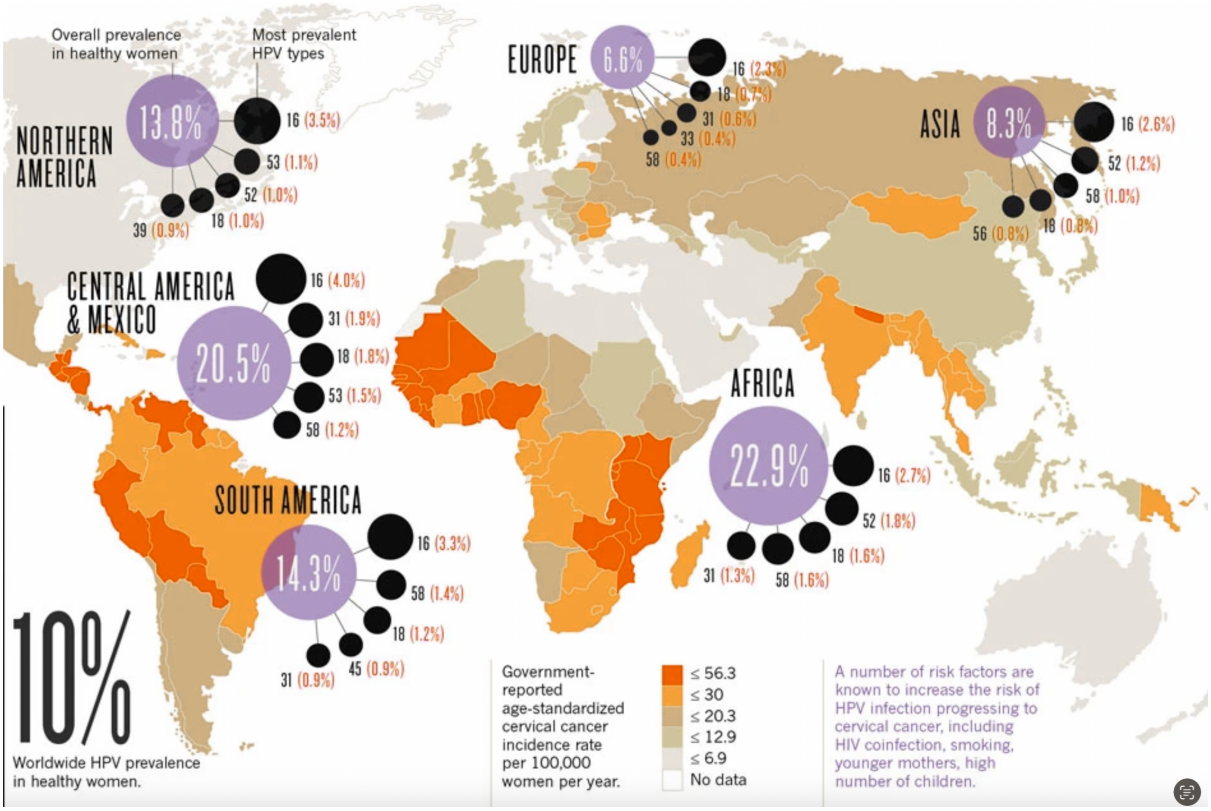

Figure 1.4: Worldwide prevalence of HPV in healthy women. *Geographic prevalence of HPV and HPV subtypes of each continent shown as a percentage of healthy women. Data from WHO/ICO information centre on HPV and cervical cancer. Adapted from Crow, 2012*[119]***.***

HPV is a non-enveloped, icosahedral double-stranded DNA virus and is approximately 52-55nm in size. The viral capsid is made up of two proteins: the major capsid protein L1, and the minor capsid protein L2[120]. HPV infects the basal layer of the epithelium, specifically the basal keratinocytes. Epithelial damage is paramount to a successful infection; *in vivo* experiments show that infection of virus-like particles (VLPs) did not occur in the mouse FGT without chemical or physical epithelial damage[121]. Immunofluorescence microscopy has indicated that this is because the virus binds to the basement membrane (BM)[121], and subsequently binds via the L1 protein to heparan sulphate proteoglycans (HSPG) found on the surface of keratinocytes[122,123]. Binding of the virus to HSPGs causes conformational change of the protein to expose a cleavage site, which is not detectable until 4hrs after the addition of HPV VLPs[124]. The addition of furin inhibitors to cells exposed to HPV VLPs resulted in no infection, suggesting that the conformational change exposes a furin cleavage site[124]. Following this cleavage, there is a loss of affinity of the viral capsid for HSPG and the virus is subsequently transferred to another unknown receptor; some candidates include α6 integrin[125,126] and

Annexin A2[127,128]. The virus is then internalised by the cell through endocytosis[122]. Immunofluorescence microscopy of cells infected with HPV VLPs showed that HPV is trafficked to the nucleus of the host cell through early endosomes to late lysosomes, shown by the presence of early endosome and late lysosome markers as trafficking progresses[129,130]. Within the lysosome, the viral capsid, specifically the L1 protein, begins to disassemble due to a reduction in pH, as neutralisation of the endosome resulted in only half of the HPV VLPs passing this stage of infection[131]. A viral DNA (vDNA)/L2 capsid protein complex remains, and it has been shown that L2 facilitates the exit of the vDNA from the lysosome and trafficking of the vDNA to the nucleus through direct interaction with host cell microtubules[132]. Complete progression through the cell cycle has been shown to be essential in HPV infection, as cell cycle arrest affects HPV infection and the vDNA/L2 complex has been shown to only enter the nucleus when the nuclear envelope is broken down during late prophase[133,134]. Once chaperoned into the nucleus by L2, the vDNA remains as circular episomal element[134] and is replicated up to 200 times per cell. These episomes will be present in both daughter cells following cell division.

The HPV genome is circular and about 8 kbp in length (Figure 1.5). This genome encodes eight proteins; six are considered “early proteins”, which are involved in HPV genome transcription and replication, and two are “late proteins”, which encode the L1 and L2 capsid proteins. The first genes to be transcribed are E1 and E2; they encode a DNA helicase (E1) and proteins involved in the downregulation of E6 and E7 expression and increase in proteins for genome replication (E2)[135]. As the basal epithelial cell divides, the daughter cells differentiate and move into the upper epithelial layer. The viral genome is amplified through the assistance of E4. Once the cells become part of the granular epithelial layer, the transcription of the L1 and L2 capsid proteins is initiated. These proteins are produced in the cytoplasm and are transported to the host cell nucleus. L1 and L2 passively assemble around a copy of the vDNA to produce an HPV virion. The release of these virions takes advantage of the natural death of epithelial cells when cells are sloughed off from the top layer of the epithelium, therefore preventing an inflammatory response as would be the case if the virus lysed the cell itself[136]. In the case of oncogenic HPV types such as HPV-16 and HPV-18, the proteins E6 and E7 interfere with p53 and pRb (tumour suppressor proteins) respectively, which results in

terminally differentiated cell division being reactivated and inhibits apoptosis[137,138]. This over-proliferation of epithelial cells results in highly infectious genital warts.

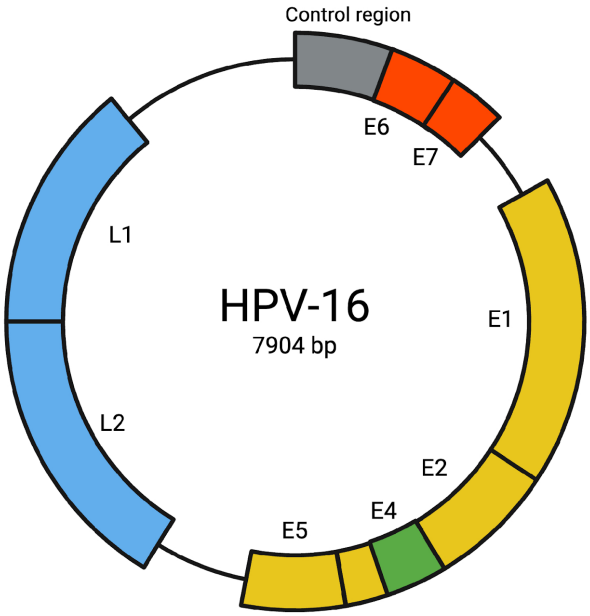

Figure 1.5: Genome structure of HPV-16. *HPV has a circular DNA genome of 7904 bp. The genes encoded in this genome include early proteins (E1, E2, E5; yellow), an amplification protein (E4; green), late proteins (L1 and L2; blue) and oncogenic proteins (E6 and E7; red). (Created using BioRender.com.)*

During persistent infection, the HPV DNA is known to also integrate into the host cell genome later during infection, however this mechanism is poorly understood[139]. This is not strictly part of the HPV life cycle; integration of vDNA prevents vDNA replication and virion assembly as the integration site is commonly found in the E2 gene. In addition to this, E2 is also a negative regulator of E6 and E7 production; therefore a disruption in the gene and consequently a lack of expression would allow E6 and E7 to be constitutively expressed[135,140]. This would result in increased interference of p53 and pRb and a further dysregulated cell cycle, leading to over proliferation. Integration of HPV vDNA is detected in 80-100% of cervical tumours[141].

1.2.2 Cervical cancer

HPV infects the skin or mucous membranes, such as the mouth, throat (oropharyngeal), cervix, anus, and penis[117]. Infection commonly causes highly infectious genital warts, or even pre-cancerous lesions. If these precancerous lesions do not heal, this may lead to cervical, anogenital or head and neck cancer. It usually takes 15-20 years for lesions to develop into cancer, or 5-10 years in immunocompromised individuals[142]. When HPV DNA is integrated

into the host cell genome, there is an upregulation of E6 and E7 mRNA[117], resulting in the interference of host cell cycle protein function, as mentioned above[137,138]. Around 99% of all cervical cancer cases can be attributed to an HPV infection[142].

Briefly, cancer is a disease that occurs when cells divide abnormally and uncontrollably and eventually destroy healthy body tissue. Despite strict cell cycle checkpoints, a mutation in or inhibition of one or more of the proteins involved in normal cell division may allow the cell to bypass a checkpoint. One such checkpoint is the G_1 checkpoint where DNA damage is assessed. If this checkpoint is bypassed, apoptosis is not initiated to kill the mutated cell, but rather it continues dividing uncontrollably. DNA damage is caused by a variety of exogenous and endogenous factors[143]. One of these endogenous factors is parasites, which will be discussed later.

HPV-induced cervical cancer forms from unresolved lesions and can be categorised into different grades based on the amount of epithelium the tumour covers: cervical intraepithelial neoplasia (CIN) grade I (lower third of epithelium), grade II and grade III (full thickness of epithelium)[144]. Once the tumour breaks through the basement membrane, it has the ability to invade surrounding tissue. This is made possible through a process called epithelial to mesenchymal transition (EMT)[145]. This occurs when a cell changes from an epithelial phenotype to a motile, mesenchymal phenotype[146]. A number of changes occur within the cells to cause this transition, such as reduction of cell adhesion molecules and remodelling of the cytoskeleton among others[147–149]. This increases the invasive potential of a cancer cell, allowing it to invade surrounding tissue, the circulatory or lymphatic system and ultimately a secondary tissue[150]. Once cells reach these distal tissues, EMT is reversed to allow the cells to proliferate and form secondary tumours[150].

Within South Africa, cervical cancer is the second most common cancer among women. One in every 42 women has a lifetime risk of being diagnosed with cervical cancer[151]. It is estimated that there are approximately 10,702 new cervical cancer cases with 5,870 associated deaths each year[152]. This makes cervical cancer the leading cause of female cancer-related deaths in South Africa. Cervical cancer is very preventable through regular screening and vaccinations. The HPV vaccine was recently introduced to helminth endemic regions in

South Africa. However, this is restricted to schoolgirls and is only effective against two oncogenic HPV serotypes, namely HPV-16 and HPV-18[153]. Due to multiple factors, such as price, healthcare infrastructure and awareness, the vaccine is administered more often in higher income countries[154]. In the last 20 years in the United States of America (USA), the rate of cervical cancer has decreased (9.6 to 6.8 cases per 100 000 women from 2000 to 2020) through the use of the Papanicolaou (Pap) smear test (early detection) and HPV vaccinations (prevention)[155]. In the USA, the incidence rate of cervical cancer is 6.2 per 100 000 women compared to 35.3 per 100 000 women in South Africa (Figure 1.6)[156]. Because of the high costs of pap smears and HPV vaccines, coupled with poor education around cervical cancer, approximately 90% of deaths due to cervical cancer worldwide occur in low- and middle-income countries[142].

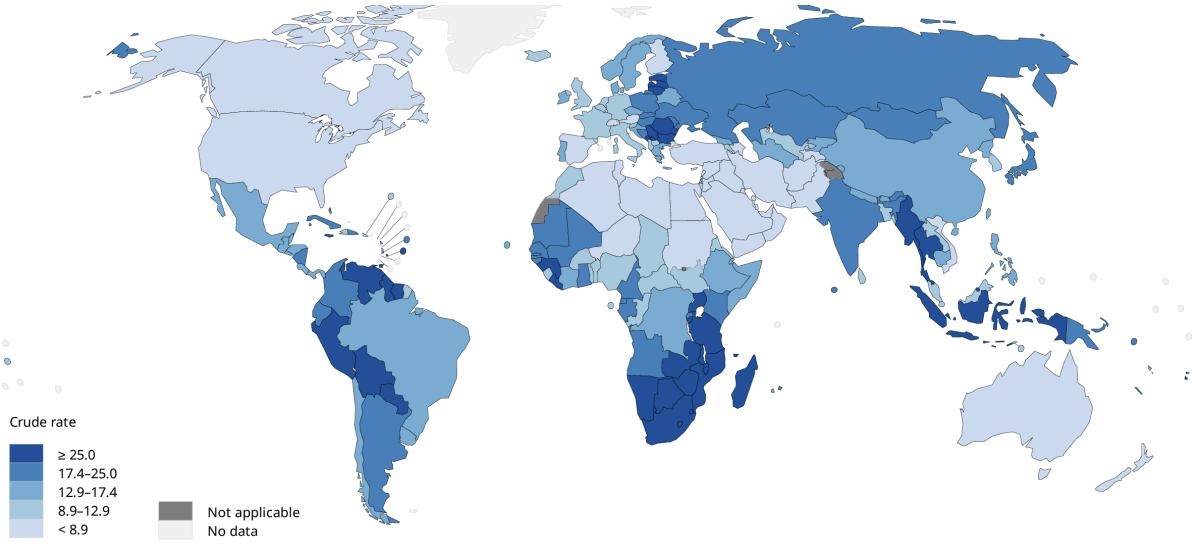

Figure 1.6: Worldwide crude incidence rate of cervical cancer per 100 000. *Geographic distribution of incidence rate of cervical cancer per 100 000 women, described per country. (Created using data from GLOBOCAN[157].)*

One of the most frequently used cell lines used in laboratories around the world is the HeLa cell line. HeLa cells are derived from a cervical cancer tumour of a patient named Henrietta Lacks. Their most common usage is in preclinical drug evaluation and virus cultivation[158–160]. However, there were great injustices and human rights violations in their acquisition and commercial use.

Henrietta Lacks died at the age of 31 in 1951 from aggressive cervical cancer. In a routine biopsy performed a few months before her death, doctors at Johns Hopkins Hospital in Baltimore, USA, cancer cells were taken for the purpose of diagnosis and treatment. However, without Henrietta Lacks' knowledge or consent, these doctors gave part of the biopsy to a researcher. These cells were found to be able to survive and reproduce in the laboratory, essentially becoming the basis of modern medicine[158].

The propagation and sharing of her cells demonstrate the racial inequities of the time. Henrietta Lacks was a black woman, and the hospital that was treating her was one of the few that provided medical care to black people. Billions of dollars have been made from selling her tumour cells, and none of this money has ever been passed back to her family. In the months between the collection of her cells and her death, she or her family were never approached for consent, and her name and medical records were made public. Shockingly, her genome was made publicly available (which has since been removed). There have been calls to end the use of HeLa cells entirely in recent years, based on the unethical means of their acquisition and the injustices behind them[161].

1.2.3 Host immunity to HPV

As mentioned, HPV infects the basal keratinocytes of the epithelium. These keratinocytes are labelled as "nonprofessional immune cells" as they express pattern recognition receptors (PRR), which includes toll-like receptors (TLR). These PRRs can identify pathogens or danger signals. For example, during viral replication, there is an accumulation of viral nucleic acid which can be recognised by TLRs. The binding between the TLR and nucleic acid activates a signalling cascade to initiate host defence mechanisms such as the release of proinflammatory cytokines and type 1 interferon. However, HPV possesses several qualities that allows it to evade the host immune system. Keratinocytes are short lived, and HPV takes advantage of the natural cell death of differentiated keratinocytes to avoid eliciting an inflammatory response upon virion release, as would occur if HPV was cytotoxic, allowing it to largely evade the immune system[136]. Additionally, certain oncogenic strains of HPV are able to downregulate the expression of TLRs[162,163]. Infection of cervical keratinocytes with retroviruses encoding HPV-16 E6 and E7 had altered expression of 80 genes, which included downregulation of interferon-responsive genes that alert immune cells to the infection,

demonstrating that HPV can interact with the interferon pathway to avoid detection by the host immune system[164,165].

If the infection is recognised, APCs will recognise the viral nucleic acid presented by the keratinocyte. Macrophages will become activated in the presence of certain cytokines and chemokines, which causes them to release additional inflammatory cytokines or even kill the infected cell[166]. However, HPV-16 E6 has been shown to interfere with the expression of monocyte chemoattractant protein 1 (MCP-1), a chemokine released by keratinocytes to recruit macrophages and other monocytes, which reduces the recruitment of these cells[167]. Once an APC has sampled the viral antigen, it translocates to the lymph nodes and are presented to T cells. CD4+ T cells will elicit a Th1 response towards HPV virions, which is followed by CD4+ and CD8+ T cell infiltration and pro-inflammatory cytokine production[168]. Once presented with the viral antigen, a CD8+ T cell may differentiate into a cytotoxic T cell lymphocyte (CTL). In the presence of pro-inflammatory cytokines, these cells will become activated effector T cells that are able to kill the infected cell[166]. During HPV vDNA amplification, there is a low frequency of T cells that recognise E2 and E6 proteins shown in a canine model of HPV infection[169]. This response rapidly regressed after the genital lesion had regressed. Additionally, antibody production against the L1 capsid protein increase as genital lesions regress[169]. It takes approximately 5-6 months for the immune system to clear the HPV infection (e.g. HPV-6 and -8), and 8-14 months for high-risk HPV, demonstrated by a negative PCR for HPV vDNA[170,171].

1.3 Helminth bystander effects

1.3.1 Helminths and viral coinfections

Due to the immunomodulatory effects of STHs (discussed in section 1.1.5 above), it is reasonable to hypothesise that infection with a helminth may alter the immune response towards another pathogen at the same site. Viral clearance requires a Th1 polarised immune response, whereas a helminth infection induces a Th2 polarised immune response, along with general immune response dampening[172]. A murine model using the strictly intestinal helminth *H. polygyrus* infection found that helminth infection significantly reduced gastrointestinal norovirus clearance where these mice did not mount a robust virus-specific CD4+ T cell

response[173]. The expansion of various cell types induced by a helminth infection may therefore increase the target cell of a virus, allowing it to replicate freely. For example, murine norovirus has a tropism for tuft cells[174], which are known to be increased in STH infection. STH-infected mice were shown to have higher viral loads compared to norovirus-only infected mice, likely due to this increase in intestinal tuft cells, but it was also shown to be due to a change in gut microbiota composition[173].

As discussed in section 1.1.2, some STH species traverse the lung as part of their life cycle. While the exact mechanism has not been determined, it has been shown in two murine models that infection with STHs traversing the lung (*N. brasiliensis* and *Ascaris suum*) resulted in significantly higher (and quicker) mortality rates and greater lung damage following influenza infection, when compared to influenza-only infected mice[175,176].

In the case of respiratory viruses, some pathology to the lung is attributed to viral replication and cellular release; however, an impact on lung function can be due to the excessive infiltration of immune cells[177]. Viral infection will cause swelling of the airway and excess production of mucus and exudate, which can fill the alveoli and reduce their ability to perform gaseous exchange, and therefore inadequate oxygen uptake[178]. Additionally, a murine model suggested that a prior *N. brasiliensis* infection may protect against the respiratory virus SARS-CoV-2 by reducing viral load through pre-priming the lung for enhanced antigen presentation[179].

Helminths that do not traverse through the lung may alter susceptibility to respiratory viruses through systemic immunomodulation, rather than local immunomodulation as described above. Limiting the infiltration of immune cells and/or altering the immune environment by reducing inflammation may therefore limit lung disease. These data regarding helminths other than STHs can be found in Table 1.1. With regards to STHs, *H. polygyrus* infection was shown to associate with naïve B and T cell accumulation in the mesenteric lymph node, which would remove these cells from circulation. Mice that were infected with *H. polygyrus* had lower proportions of lymphocytes in non-draining lymph nodes and higher proportions of lymphocytes in the mesenteric lymph node (the draining lymph node of the gut) compared to *H. polygyrus*-uninfected mice, suggesting that STH infection redistributes circulating

lymphocytes[180]. With fewer circulating lymphocytes to sample antigen from APCs, there is a lower chance of an anti-viral immune response being elicited and may be in part responsible for the reduced protection. However, it was shown that the reduction in $CD8^+$ T cell response in fact did not result in an increased viral load[173,180]. Infection with the intestinal helminth *H. polygyrus* showed that coinfection with respiratory syncytial virus (RSV) resulted in reduced viral load in the lung through the upregulation of type 1 interferon signalling[181]. However, *H. polygyrus* infection resulted in impaired anti-viral immunity towards murine norovirus (MNV) through the production of Ym1 (chitinase-like protein 3) by AAMs, which subsequently inhibit antiviral T cell responses[173]. Together, these data largely suggest that STHs that coinfect at the same site as the virus may be detrimental, while those that colonise distal sites to the virus may be beneficial. However, a definitive link has not yet been established.

Table 1.1: Effect of helminth infection on viral control at various anatomical sites.

Helminth species (infection site)	Virus (infection site)	Experimental model	Findings	Reference
Fasciola hepatica (liver)	SARS-CoV-2 (lung)	*In vitro*	Antigen exposure reduced SARS-CoV-2 infection in Vero cells.	Serrat et al., 2023[182]
S. mansoni (intestine)	MuHV-4 (lungs)	*In vivo*	*S. mansoni* infection expanded CD8+ T cells and their effector responses through IL-4 signalling.	Rolot et al., 2018[183]
S. mansoni (intestine)	PR8 and PVM (lungs)	*In vivo*	*S. mansoni*-induced mucus indirectly protected from virus, and induced CD8+ T cell expansion.	Scheer et al., 2014[184]
T. spiralis (intestine/muscle)	Influenza (lung)	*In vivo*	Reduced influenza-induced lung pathology through the inhibition of immune cell infiltration.	Furze et al., 2006[185]
L. sigmodontis	Friend Virus Retrovirus	*In vitro*	Filarial infection impaired control of FV infection	Dietze et al., 2016[186]

(pleural cavity/blood)	(blood)		through reduced FV-specific IgG.	

The relationship between sexually transmitted viral infections (STVI) and human helminth schistosomiasis has been well explored. These helminths may lay their eggs in the bladder of their host, which may cause sandy patches (tissue damage) in the genital tract. This infection has been shown in various helminth-endemic regions to be a risk factor for human immunodeficiency virus (HIV)[187,188]. This has been correlated with an increase of HIV target cells, namely CD4+ T cells, in the genital mucosa of women with schistosomiasis[189]. Interestingly, one study found that the treatment of schistosomiasis reduced the entry of HIV into $CD4^+$ T cells due to an increase in the production of IFN-α2a, a cytokine known to inhibit HIV entry[190]. This further supports the concept that helminths that traverse the site of viral infection may be detrimental to the host. However, Kjetland et al. showed that in a cohort of over 500 Zimbabwean women, there was no increase in HPV infection if infected with *S. haematobium*[188].

Studies regarding the relationship between STVIs and STH infection remain sparse. A study by Chetty et al. discovered that *N. brasiliensis* and herpes simplex virus 2 (HSV-2) coinfection resulted in worse pathology compared to HSV-2-only infected mice. This was due to an increase in eosinophils in the FGT of *N. brasiliensis*-infected mice, which increased the amount of vaginal epithelial damage, as eosinophil-depleted *N. brasiliensis*-infected mice had rescued pathology that was comparable to *N. brasiliensis*-uninfected mice[191]. This epithelial damage led to an increase in the production of IL-33, which increased the production of IL-5 by, and expansion of, ILC2s, which led to a further increase in eosinophilia and worsened pathology.
In an *in vitro* study, Jacobs et al. discovered that exposure to *N. brasiliensis* somatic antigen resulted in a decrease in HPV uptake by HeLa cells[192]. Conversely, epidemiological studies have largely contradicted this finding. In 2017, a study was published showing that Peruvian women from a helminth-endemic region who had an STH infection had a 60% higher prevalence of HPV infection compared to those from a helminth non-endemic area. This was associated with a Th2 immune profile in cervical fluid taken from women with STH Infection; this immune profile was not observed in STH-uninfected women. Interestingly, IL-5 was

elevated, which is indicative of eosinophilia. However, the canonical Th2 cytokines IL-4 and IL-13 were not found to be significantly elevated. The most common helminth species found in the helminth-endemic population was *A. lumbricoides, Trichuris trichiura, Strongyloides stercoralis* and *A. duodenale*[193]. Another study carried out in Togo found that the most common helminth infection was from hookworm, and similarly that women with a hookworm infection had a 2.22 odds ratio of HPV infection[194]. It was also shown that these women had a mixed type 1/type 2 immune profile in their vaginal flushes, a different profile of HPV serotypes, and increased viral load. When these women were stratified as HPV +/- and helminth +/-, it was clear that women with a coinfection of HPV and hookworm had an elevated type 2 immune response in their vaginal flushes. Overall, there did not appear to be a type 1 or type 2 immune profile in their plasma, showing that the type 2 immune response was not entirely systemic[195].

1.3.2 Helminths and cancer

The effect of non-soil transmitted helminth infections on various cancers has been extensively studied and are summarized in Table 1.2. However, research on the relationship between STH infection and cancer is sparse. Murine infection with *H. polygyrus* exacerbated tumour formation in an experimentally-induced colitis-associated colorectal cancer (CRC) model[196]. This was not due to a reduction in colonic inflammation, but rather due to the activation of local immune cells that further promoted tumour development. An *in vitro* study showed that exposure of the colorectal cancer cell lines CT26.WT (murine) and HCT116 (human) to *H. polygyrus* antigen resulted in reduced cell proliferation and viability but increased cell migration, suggesting helminth exposure may slow cancer growth but increases its invasive potential[197]. An *in vitro* study found that exposure of the cervical cancer cell line HeLa to *N. brasiliensis* somatic antigen had no effect on cell proliferation, but reduced cell migration. Paired with this, these HeLa cells had reduced expression of the epithelial to mesenchymal transition (EMT) markers vimentin and N-cadherin. The same was seen in the FGT of mice with an *N. brasiliensis* infection[192]. Similarly, infection with *Trichuris muris* had greater tumour formation in APC min/+ (colon cancer mouse model) mice compared to uninfected APC min/+ mice, suggesting that infection with *T. muris* may increase tumour formation[198].

Table 1.2: Effect of non-soil transmitted helminths on cancer progression

Helminth species (location)	Cancer location	Model	Findings	Reference
S. haematobium	Bladder	*In vivo*	*S. haematobium* eggs transformed bladder cells	Chala et al., 2017[199]
S. mansoni and *S. haematobium*	Prostate	*In vitro*	Egg antigen exposure increased proliferation and reduced apoptosis	Tuffour et al., 2018[200]
S. japonicum (intestine)	Colorectal	*In vivo*	Egg antigen promoted colorectal cancer progression	Wu et al., 2020[201]
S. mansoni and *S. haematobium*	Liver	Tumour biopsies	Mutation in p53 was more common in infected patients	Habib et al., 2006[202]
T. crassiceps	Colitis-induced colorectal	*In vivo*	ES reduced inflammation and prevented tumourigenesis	Callejas et al., 2019[203]
T. crassiceps	Colitis-induced colorectal	*In vivo*	Infection reduced inflammation and tumourigenesis	Leon-Cabrera et al., 2014[204]

Infection with hookworm was shown to result in a type 2 immune response in the FGT, characterised by the production of canonical type 2 cytokines as well as eosinophilia[191,195]. Bais et al. demonstrated that a type 2 cytokine profile present during cervical cancer carcinogenesis was associated with CIN grade III or carcinoma. Elevated levels of IL-10 were found in the plasma and serum of women with CIN III, carcinoma and invasive cervical cancer compared to lesion-free women and women with lower grade CIN[205,206]. In agreement, Feng et al. showed that the immunosuppressive microenvironment created through Th2 cytokine production promoted the progression of HPV+ cervical epithelial cells to carcinoma. An increased production of the alarmin and driver of a type 2 immune response, TSLP, was found in cervical epithelial cells as well as *FOXP3* expression, indicative of an increase in Treg populations and therefore immunosuppression, allowing tumours to grow[205]. It could therefore be argued that since helminths prime the FGT towards a Th2 environment and ultimately an immunosuppressive environment, a helminth infection at a distal site may increase the carcinogenesis of cervical lesions through dampening host anti-tumour immune responses.

1.4 Study rationale

The rationale behind the current study is that due to the endemicity of helminth infections and the high prevalence HPV infections in largely overlapping regions (Figure 1.7), it is likely that coinfections will be common, which is supported by epidemiological studies showing that they are coincident[193,194]. It is important to understand how these two infections may influence each other and to determine if one infection renders one more susceptible to the other. Similarly, cervical cancer is a huge burden in sub-Saharan Africa, with the highest rates of cervical cancer worldwide found in this area. If helminth infections promote progression and/or metastasis of cervical cancer, it is imperative that deworming initiatives are prioritised to prevent the progression of this highly prevalent cancer. Alternatively, should helminth infection reduce cervical cancer progression and/or metastasis, this may open doors towards developing anti-cancer therapies.

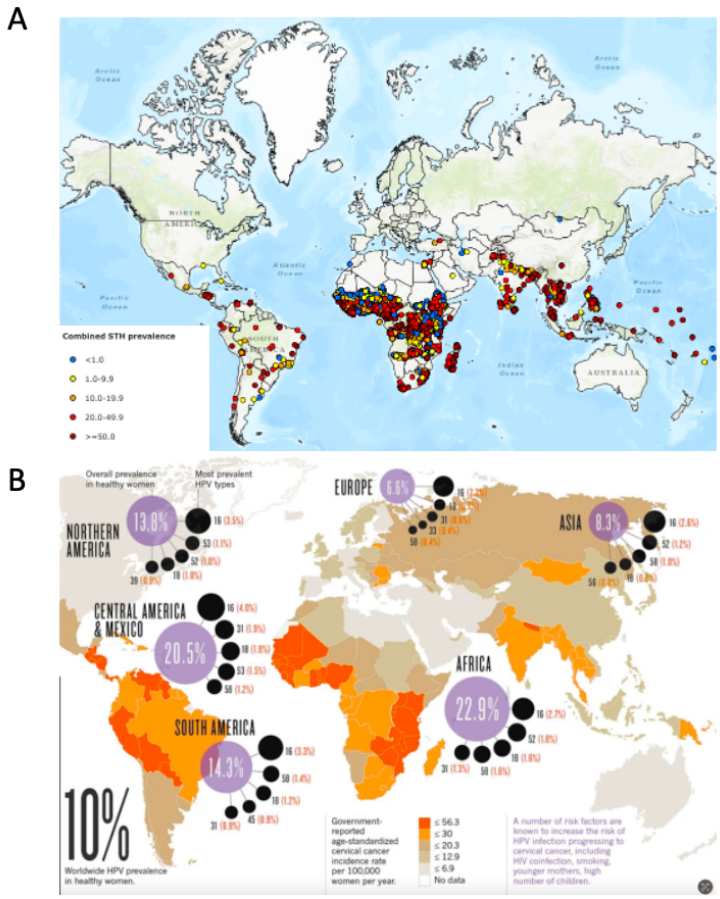

Figure 1.7: Overlap of (A) STH infection and (B) HPV infection prevalence worldwide. (*Created using Global Atlas of Helminth Infection map creator[6] and adapted from Crow 2012[119].)*

1.5 Aims and objectives

1. Does STH antigen exposure alter HPV-16 pseudovirion (PsV) infection?

   This aim will identify how helminth antigens alter HPV-16 PsV infection in the target cells of HPV as well as the potential mechanisms underlying any change. I will achieve this by:

   a. Developing an *in vitro* model to assess how helminth exposure alters HPV-16 PsV infection as a model of a coinfection.
   b. Identifying whether the molecule responsible for any change is heat liable.
   c. Assessing how helminth antigen exposure alters the expression of HPV receptors and restriction molecules.

2. Does an STH infection alter HPV-16 pseudovirion infection *in vivo*?

   This aim will determine whether an STH infection alters immunity in the FGT and how this relates to subsequent susceptibility to an HPV infection. I will achieve this by:

   a. Developing an *in vivo* model to assess the relationship between helminths and HPV.
   b. Identifying the immune cell profiles in the FGT and how the phenotype of individual immune cell options differs between HPV only and HPV and STH coinfected mice, and how these immune cells contribute to protection or susceptibility.
   c. Exploring how helminths alter the HPV infection mechanisms.

3. Can STH derived antigen, ES products and live STH infection affect cervical cancer development and metastasis *in vivo*?

   Here I will test how a helminth infection or challenge with helminth antigen alters anti-cancer immunity and how this affects cervical cancer growth and metastasis. I will achieve this by:

   a. Developing an *in vivo* model using nude mice to determine how the growth of cervical tumours differs between STH infected/challenged and STH-naïve mice.
   b. Investigating any differences in tumour immune cell infiltrates.

c. Assessing the EMT marker expression of tumours cells from helminth infected vs uninfected mice.

My hypothesis is that, based on the work of Jacobs et al., treatment of cells with STH antigen will reduce HPV pseudovirion infection. However, I believe this result may change once the model is validated *in vivo* with the effect of the immune system. I hypothesise that the STH-induced eosinophilia in the mouse FGT will, as shown in the work of Chetty et al., result in increased epithelial damage and therefore increased HPV pseudovirion infection, as greater damage will allow for greater access to the basal keratinocytes.

Lastly, I hypothesise that, because of the Th2 environment created in the FGT of STH-infected mice, cervical cancer tumours will grow more rapidly, as cervical tumours with a Th2 environment had a worse prognosis as discussed above. While this cannot be tested in the athymic mouse model used in this thesis, the role of the effects of STH infection on the innate immune system and its effect on cancer growth and progression may still be assessed in this model.

Chapter 2: Materials and Methods.

2.1. Cells

The human cervical cancer cell lines HeLa (ATCC® CCL-2™, Manassas, VA, USA), and C-33A (ATCC® HTB-31™, Manassas, VA, USA) were maintained in complete Dulbecco's Modified Eagle Medium (DMEM; Appendix 2). The primary keratinocyte cell line NIKS (ATCC® CRL-12191, Manassas, VA, USA) was maintained in F media (Appendix 2). All cell lines were kept at 37°C in an atmosphere of 5% CO_2 and 95% humidity and handled in sterile conditions. Cells were passaged using 0.025% Trypsin/0.01% ethylenediaminetetraacetic acid (EDTA) once they reached confluency. Cells were tested every 3 months for mycoplasma infection. HeLa cells were genetically tested (HeLa Marker STR profile and interspecies contamination test) prior to the start of this project to ensure there was no contamination of other cell types (Idexx BioResearch).

2.2. Animals

Specific pathogen-free level 2 (SPF2) female 6–8-week-old BALB/c that were approximately 20g in body weight were used for all HPV-16 PsV experiments, or C57BL/6 mice for *H. polygyrus* maintenance. Mice were bred in a South African Veterinary Council (SAVC)-authorised facility at the Faculty of Health Science, University of Cape Town. These mice were clear of all Federation of European Laboratory Animal Science Associations (FELASA)-listed pathogens. Mice were issued when they reached 6-8 weeks and were randomly sorted into experimental groups, using a random number generator (Google random number generator, https://g.co/kgs/TX9n3p). The number of mice in each experimental group is indicated in the figure legends. These mice were housed in cages of 4-5 mice with controlled temperature and photoperiods. Food and water were always available throughout the acclimatisation period and experimental period. Cages contained environmental enrichment such as tubes, wooden blocks and red plastic houses. After 5 days of acclimating, all mice were treated with 2mg/20g Depo-Provera® (Pfizer) in phosphate-buffered saline (PBS) to hormonally synchronise mice to ensure all mice were in the same phase of their oestrus cycle to account for changes in epithelial thickness of the FGT. Mice were monitored and weighed daily from date of issue

(Appendix 1). All experiments were carried out by authorized researchers in accordance with ethics protocol 019/010 and 019/032.

SPF2 female Balb/c (JAX) nude mice that were 6-8 weeks old were bred in an SAVC-authorised facility at the Faculty of Health Science, University of Cape Town. Mice were issued when they reached 6-8 weeks and were randomly sorted into experimental groups. These mice were housed in isolation cages of 4-5 mice with controlled temperature and photoperiods. Food and autoclaved water were always available throughout the acclimatisation period and experimental period. Mice were handled in a dedicated biosafety cabinet for immunocompromised mice use, with all precautions taken to work in a sterile environment. All experiments were carried out by authorized researchers in accordance with ethics protocol 019/032.

2.3. Helminth maintenance

2.3.1. *N. brasiliensis*

Nippostrongylus brasiliensis were maintained in Sprague-Dawley rats as previously described[16]. Rats were subcutaneously infected with 5000 L3 larvae. Faeces were collected on days 6-8 post infection and were incubated in 0.25µg/ml fungizone until soft. The mixture was then mixed with equal volumes of granulated charcoal and plated on wet raised filter paper in 140mm petri dishes. The petri dishes were placed in a dark, humid cupboard. Once the eggs hatched, the larvae migrated to the edge of the filter paper. On day 7, four strips of filter paper were cut from the edge of each disk and placed along the edge of a new, raised dampened filter paper until needed. The natural life cycle of *N. brasiliensis* can be seen in Figure 2.1.

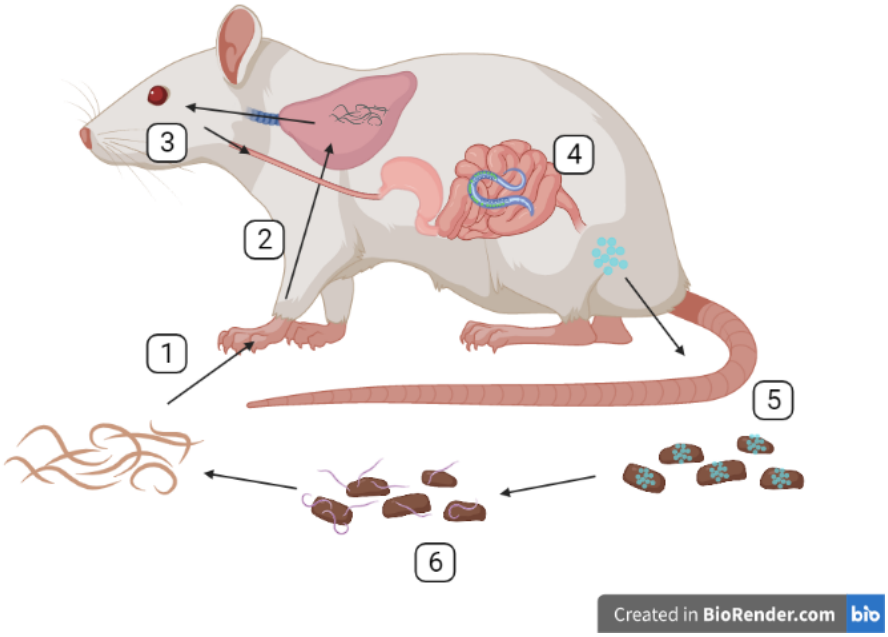

***Figure 2.1: Life cycle of* N. brasiliensis.** *1. L3 larvae penetrate the skin of the host. 2. The larvae travel through the circulatory system until they reach the lungs. 3. The larvae break through the alveolar wall and are coughed up and swallowed. 4. The larvae reach the intestines and mature into adult worms. 5. The adult worms produce eggs that are excreted with the faeces of the host. 6. The eggs hatch and the larvae mature to their infective stage. (Created using BioRender.com.)*

2.3.2. *H. polygyrus*

H. polygyrus were maintained in C57BL/6 mice as previously described[17]. Briefly, mice were infected with 400 L3 larvae suspended in distilled water by oral gavage. Mice were euthanised 14 days later and the gastrointestinal tract (below stomach to the end of colon) was excised. Faeces were removed from the cecum and colon and were mixed with washed, activated charcoal at roughly a 1:1 ratio. This mixture was placed on damp filter paper and incubated in a dark, humid box. From day 7, L3 larvae were collected twice a week for two weeks from the edge of the filter paper by gently dislodging, using sterile water and a Pasteur pipette. L3 larvae were washed three times with distilled water after collection and were stored at 4°C in distilled water until needed. The natural life cycle of *H. polygyrus* can be seen in Figure 2.2.

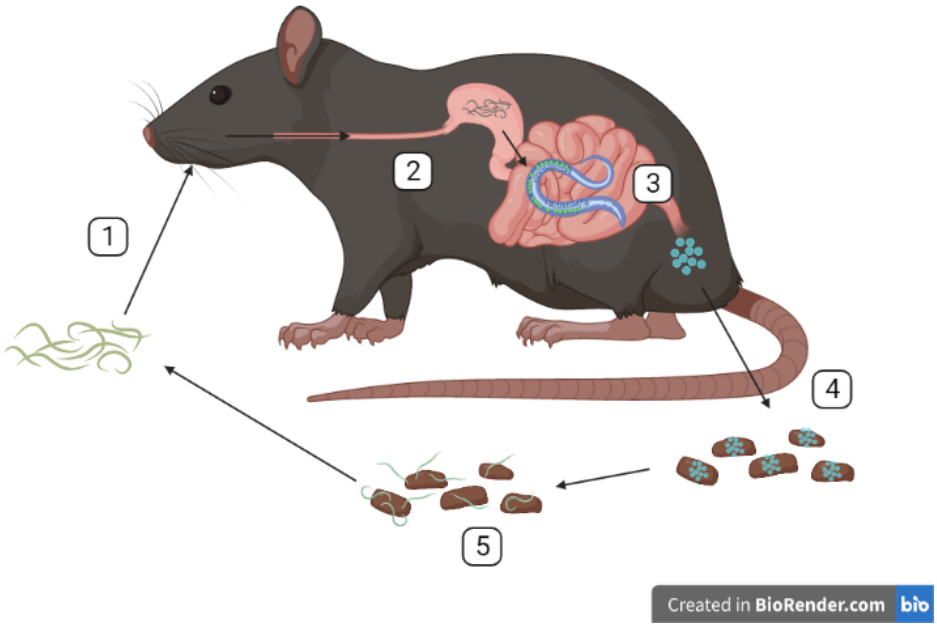

***Figure 2.2: Life cycle of* H. polygyrus.** *1. L3 larvae are orally ingested by eating contaminated food or faeces. 2. The larvae are swallowed and mature into adult worms in the intestines. 3. The adult worms produce eggs. 4. The eggs are excreted in the host faeces. 5. The eggs hatch and mature into their infective stage. (Created using BioRender.com.)*

2.4. Helminth antigen preparation

2.4.1. *N. brasiliensis* L3 somatic antigen

L3 larvae were collected as described above. The L3 larvae were washed in 0.25µg/ml fungizone (Amphotericin) and then resuspended in PBS containing 1% protease inhibitor cocktail (Sigma Aldrich®). The larvae were homogenised using a bead beater. The homogenate was centrifuged at 700 x g, and supernatant was collected and stored at -80°C until needed. Protein concentration was determined using a Pierce Bicinchoninic acid (BCA) Protein Assay Kit (Thermo Fisher Scientific). Antigen was diluted to 500µg/ml and stored in aliquots at -80°C until needed.

2.4.2. *N. brasiliensis* excretory-secretory (NES) antigen

NES was prepared as previously described[16]. Briefly, adult L5 larvae were harvested from the intestine of infected Sprague-Dawley rats on day 7 post infection. The worms were washed extensively in PBS containing 5% gentamycin and 5% penicillin/streptomycin (P/S) and were cultured in T25 flasks in NES culturing solution (Appendix 3) for two days. The supernatant

was collected and concentrated using a 3000MW filter (Merck Millipore™) and Amicon concentrator (Merck Millipore™) and dialysed into 1xPBS under nitrogen gas. Protein concentration was determined using a Pierce BCA Protein Assay Kit. NES was stored in aliquots at a concentration of 250µg/ml at -80°C until needed.

2.4.3. *H. polygyrus* excretory-secretory (HES) antigen

HES was prepared as previously described[17]. Intestinal content from the small intestine of the C57BL/6 mice from above was harvested by placing the small intestine in a petri dish with Hank's media (Sigma Aldrich®), and longitudinally opening the full length of the intestine and scraping out intestinal content using glass slides. The intestinal content was placed in muslin bags and secured to the edge of a funnel attached to a T75 flask, filled with Hank's media and incubated for 1-2 hours at 37°C, agitating halfway to dislodge any faecal content blocking the muslin bags. The worms that had settled at the bottom of the flask were collected, washed six times with Hank's media, and a further six times with Hank's media supplemented with P/S. Worms were steeped in 10% Gentamycin (Thermo Fisher Scientific) for 20min. Worms were then washed six times in Hank's media supplemented with P/S and then incubated in T25 flasks with culturing media (Appendix 3) at 37°C. Twice a week, for three weeks, the medium was collected and concentrated using a 3000MW filter (Merck Millipore™) in an Amicon concentrator, and dialysed into 1xPBS under nitrogen gas. Protein concentration was determined using a Pierce BCA Protein Assay Kit. HES was diluted to 250µg/ml and the aliquoted HES was stored at -80°C until needed.

2.4.4. *H. polygyrus* somatic antigen

The worms from the production of HES were collected after three weeks and homogenised in PBS using a bead beater. The homogenate was centrifuged at 700 x g, and the supernatant was collected. Protein concentration was determined using a Pierce BCA Protein Assay Kit. The antigen was diluted to 1mg/ml and the aliquoted antigen was stored at -80°C until needed.

2.4.5. *A. Lumbricoides* excretory-secretory (AES) antigen

A. lumbricoides adult worms were collected from a patient at Red Cross War Memorial Children's Hospital with parental consent and ethical approval (HREC 174/2017). Worms were extensively washed with water to remove host faecal content. Worms were then placed in a 5-litre bucket with DMEM and 10% P/S overnight at 37°C. Worms were then washed in PBS and transferred to T175 culture flasks containing DMEM with 1% P/S, 1% L-glutamine (Merck), 1% gentamycin and 22% of a 45% glucose solution. The media was removed and replaced every three days. Each day, removed media was centrifuged at 400 x g for 5min to remove eggs. After three days, the ES was concentrated in an Amicon concentrator using a 3000MW filter (Merck Millipore™). The protein concentration was determined using a Pierce BCA Protein Assay Kit. The AES was at a concentration of 90µg/ml and was aliquoted and stored at -80°C until needed.

2.4.6. *A. lumbricoides* exosome isolation

Exosomes were purified from AES as described[100]. Concentrated AES was centrifuged at 15 000 x g for 45min. The supernatant was removed and centrifuged at 120 000 x g for 3h. The supernatant (exosome-depleted) was stored, and the remaining pellet (containing the exosomes) was resuspended in 70µl PBS.

In an ultracentrifugation tube, 1ml decreasing densities of 40, 20, 10, and 5% iodixanol (prepared with 0.25M sucrose and 10mM Tri-HCl, pH 7.2) were layered. The sample containing the exosomes was added to the top layer and ultracentrifuged at 120 000 x g for 18h at 4°C. Numerous fractions were recovered. The absorbance at 340nm was measured in each fraction, and the density was calculated from known standards. Protein concentration was measured using a Pierce BCA Protein Assay Kit. The exosome concentration was determined to be 227µg/ml. Fractions were kept at -80°C until needed.

2.5. HPV-16 PsV production

HPV PsVs containing either the Gaussia luciferase reporter plasmid (pCMV-Gluc2; New England Biolabs) or the Firefly luciferase reporter plasmid (pGL3; New England Biolabs) were produced in HEK-293TT cells [transformed HEK293T (ATCC® CRL-11268™) using modified

human adenovirus] following published protocols[207,208]. Briefly, ten T175 flasks of HEK-293TT cells were cultured in complete DMEM at 37°C and 5% CO_2 and were co-transfected with 150µg HPV-16 capsid protein plasmid (pXULL), which encodes the L1 and L2 capsid proteins of HPV-16, along with 360µg of one of the luciferase plasmids (pCMV-Gluc2 or pGL3) per flask using the calcium phosphate transfection method. The plasmid DNA was diluted with Tris-EDTA (TE) to a final volume of 5250µl and precipitated with 750µl 2.5M $CaCl_2$ and 6000µl HSB (Appendix 4) per flask. After 30min incubation at room temperature, the transfection mixture was added dropwise to the flasks (1.2ml per flask). The PsVs self-assembled within the producer cells, encapsidating the luciferase reporter plasmid. Two days post transfection, the cell supernatants were removed, and cells were trypsinised, washed with PBS and resuspended in PBS in a siliconised tube. Cells were centrifuged at 3000 x g for 3min and resuspended in PBS. Cell lysis buffer (Appendix 4) was added, and the mixture was incubated at 37°C for 24h with occasional mixing. The cell lysate was then chilled on ice for 5min. To this, 0.17 volumes PBS and 5M NaCl was added and incubated on ice for 10min. The sample was then freeze-thawed three times at -80°C and room temperature before proceeding with virus purification.

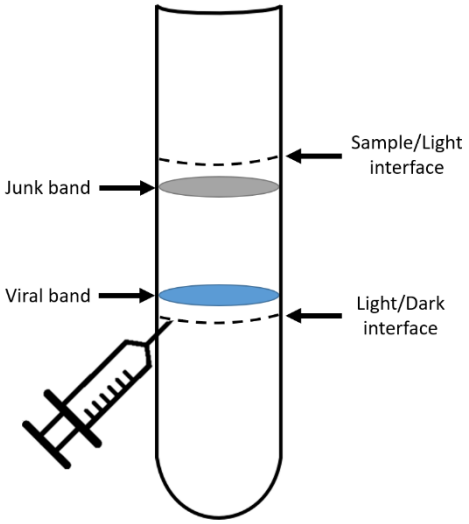

Figure 2.3: HPV-16 PsV purification. *Sample containing HPV-16 PsVs was ultracentrifuged in a CsCl gradient. Purified PsVs were removed with a syringe at the light/dark CsCl interface.*

To purify the PsVs, the cell lysate was centrifuged at 8000 x g for 10min at 4°C. The pellet was washed 1-2 times in 400µl HSB and made to a final volume of 3.5ml using HSB. A discontinuous CsCl gradient was prepared as follows: 4ml light CsCl (Appendix 4; Figure 2.3) was pipetted into a siliconized Ultra-Clear™ centrifuge tube (Beckman Coulter). Heavy CsCl (Appendix 4) was underlaid by plunging the pipette to the bottom of the tube and slowly

expelling 4ml heavy CsCl. Towards the end of the 4ml, the pipette was slowly lifted towards the interface while still expelling the heavy CsCl.

The PsV sample was gently pipetted onto the top of the CsCl. The interface between the heavy and light CsCl and the interface between the light CsCl and sample were marked. This tube was immediately ultracentrifuged for 16-17h at 20 000 x g at 4°C. Thereafter, a 5ml syringe with an 18G needle was inserted into the tube just below the marked interface of the heavy and light CsCl and the sample was sucked up until the junk band (which contains cellular debris) was close to the needle (Figure 2.3). The sample in the syringe was transferred to an Amicon Ultra-4 filter device (Merck Millipore™) with a 100 000kDa MWCO filter (Merck Millipore™) to concentrate the sample by centrifugation at 3000 x g for 10min. Concentrated samples were washed in HSB and centrifuged again to a final volume of approximately 100µl. The purified and concentrated PsVs were stored in a siliconised tube (Sigma Aldrich®) at -80°C.

The concentration of the PsVs was determined using a Pierce BCA Protein Assay Kit. The purity of the PsVs was determined through sodium dodecyl sulphate (SDS)-polyacrylamide gel electrophoresis (PAGE) and subsequent silver staining (Figure 2.4A). To quantify luciferase activity, approximately 3pg of newly prepared PsVs was added to $2x10^5$ seeded HeLa cells for 24h and luminescence recorded following addition of luciferin (Figure 2.4B, and section 2.6).

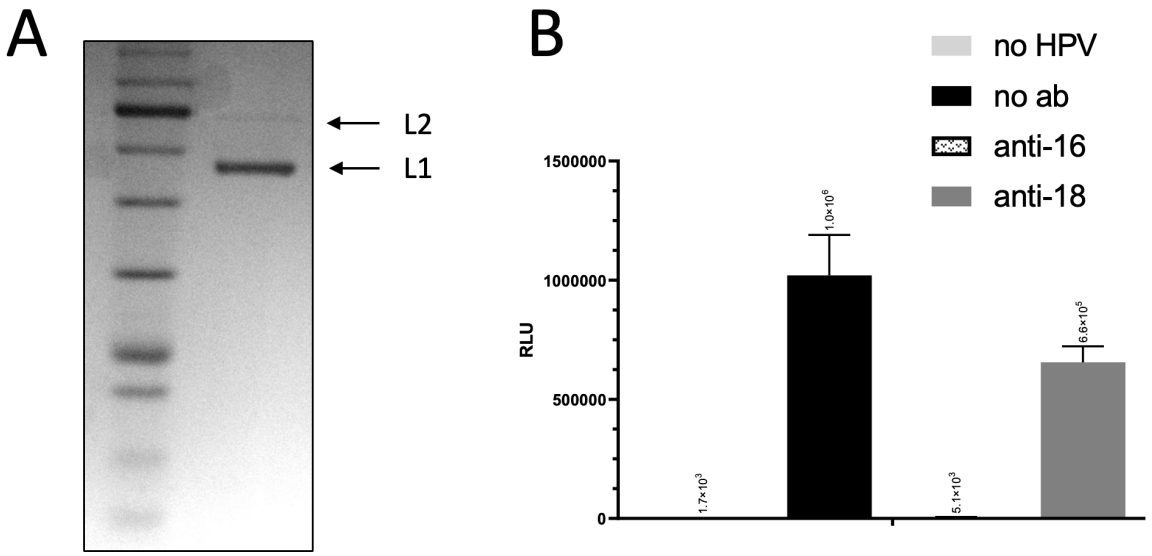

Figure 2.4: Quality control outputs of HPV-16 pseudovirion production*. (A) Representative silver stain gel to confirm purity of sample. Top arrow indicates L2 capsid protein and bottom arrow indicates the more abundant L1 capsid protein. (B) Representative luciferase activity test to confirm luciferase plasmid encapsidation. Neutralising antibodies against HPV-16 and HPV-18 were also used to check for HPV type specificity.*

2.6. gHPV-16 PsV *in vitro* infection assay

HPV-16 pseudovirions (HPV-16 PsVs) encapsidate reporter plasmids under the control of the cytomegalovirus promoter, leading to their constitutive expression of the reporter gene, either Gaussia or Firefly luciferase. The PsVs bind to the same receptors as the native HPV virus and are endocytosed by the cell. Upon successful entry into a cell, the HPV-16 PsV capsid proteins disassemble, and the plasmid is transported into the cell's nucleus. This gene is transcribed and translated using host enzymes and the Gaussia luciferase (Gluc) is secreted from the cell cytoplasm into the surrounding cell culture medium whereas firefly luciferase (Fluc) remains within the cell. The amount of light produced after the addition of D-luciferin is measured with a luminometer. The intensity of light produced will represent the amount of Gluc or Fluc produced, and therefore will represent the level of infection in the cells in each well. A diagram of the HPV-16 PsV model of infection can be seen in Figure 2.5.

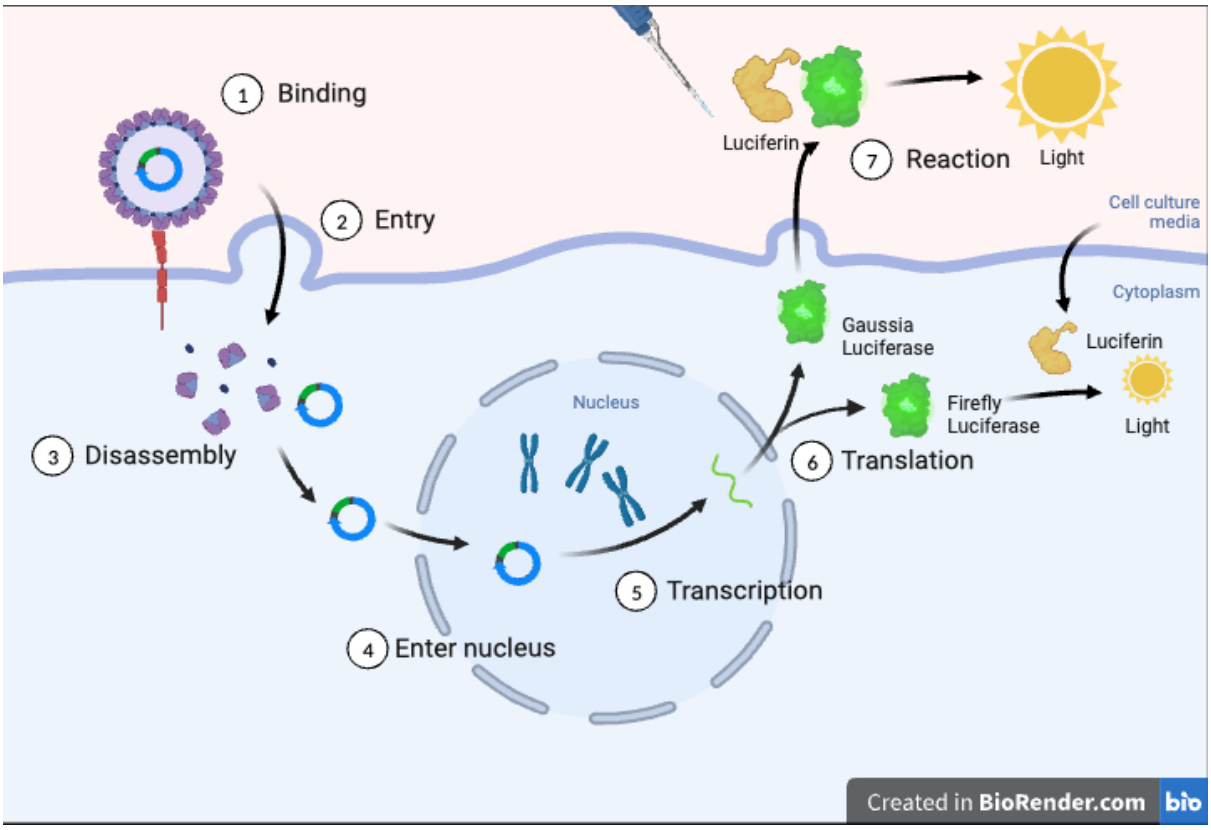

Figure 2.5: HPV-16 PsVs model of infection. *HPV-16 pseudovirions enter the host cell and disassemble. The Gluc or Fluc plasmid is transported to the cell nucleus. The gene is transcribed and translated and the Gluc is transported out of the cell into the cell culture media whereas the Fluc remains within the cell cytoplasm. (Adapted from "Genetic viral life cycle" by BioRender.com[209].)*

To test the effect of various helminth antigens for HPV infection, HPV-16 PsVs containing the Gluc plasmid (gHPV-16 PsV) were used (Figure 2.6). This has been validated in many *in vitro* models[210,211]. Briefly, the media of cultured HeLa cells, C-33A cells or NIKS cells were removed, and cells were lifted using 5ml Trypsin-EDTA. Once detached from the flask, cells were resuspended in the appropriate media (complete DMEM or F media, respectively). Cells were counted on a Neubauer haemocytometer (Marienfeld) and were seeded in a 96-well plate at a density of $5x10^3$ cells per well and incubated at 37°C in an atmosphere of 5% CO_2 and 95% humidity. After attachment to the bottom of the well, helminth antigens were added at 0.1µg/ml, 1µg/ml, 10µg/ml or 50µg/ml (well volume = 100µl). Twelve hours later, 2pg per cell of gHPV-16 PsVs were added to each well. Two days later, 10µl of the supernatant of each well was harvested and placed in an opaque white 96-well plate (Nunc). These plates were used to prevent light spilling over into neighbouring wells, and to amplify the light signal. The plates were read using a Fluoroscan Ascent FL (Thermo fisher Scientific) or GloMax® Explorer

Multimode Microplate Reader (Promega). Light emission was recorded after the addition of 50µl Gluc Assay Solution (1% BioLux substrate in BioLux Assay Buffer; New England Biolabs) with a 2s lag time and 10s integration time. Each treatment condition was plated in quadruplicate and each experiment was repeated three times, with the exception of cells exposed to AES and *A. lumbricoides* exosomes due to low availability.

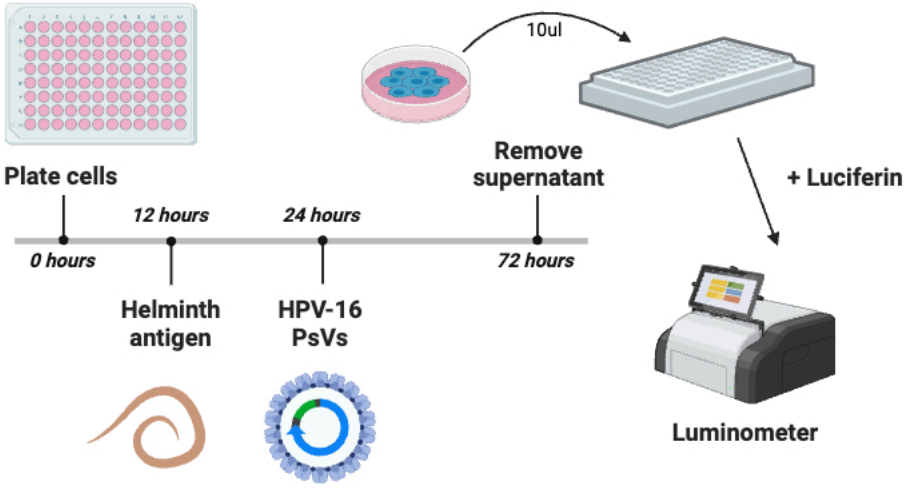

Figure 2.6:* In vitro *model to assess the effect of helminth antigen exposure on gHPV-16 PsV infection. *$5x10^3$ cells per well were plated in a 96 well plate. Twelve hours later, helminth antigen was added at varying concentrations. Twelve hours after exposure, cells were infected with 2pg/cell gHPV-16 PsVs. After two days, the luciferase activity was measured. (Created using BioRender.com.)*

2.7. *In vivo* assays

2.7.1. Parasite infection

N. brasiliensis L3 larvae were collected from maintained culture by placing the filter paper (with L3 larvae around the edges) in a 50ml Falcon tube with Fungizone and incubated for 1h at 37°C to allow for larval detachment from the filter paper. The larvae were washed three times in sterile PBS and made up to a concentration of 500 L3 larvae per 100µl in PBS. Four days after hormonal synchronisation, female BALB/c mice or nude mice were subcutaneously infected with 500 L3 larvae. Mice were monitored and weighed daily (Appendix 1).

2.7.2. fHPV-16 PsV infection and quantification by *in vivo* imaging

Nine days after parasite infection, female BALB/c mice aged 6-8 weeks were anaesthetised and treated intravaginally with 4% nonoxynol-9 (N9; Pharmacopeia) in 3% carboxymethylcellulose (CMC; Sigma Aldrich). N9 is a chemical surfactant and spermicide that is used to disrupt vaginal epithelium to allow HPV PsVs to reach the basal keratinocytes (target cell of HPV). The number of mice in each group was dependent on stock, which was usually between 3 and 5 mice per experimental group. Six hours later, mice were anaesthetised and intravaginally infected with 1µg HPV-16 PsVs containing the Fluc plasmid (fHPV-16 PsV) in 3% CMC. Where indicated, the fHPV-16 PsVs were mixed with 6.25µg *N. brasiliensis* somatic antigen (Figure 2.7). For PsV infection quantification, mice were anaesthetised and intravaginally injected with D-luciferin (Promega). Light emission was measured using an IVIS Spectrum *in vivo* imaging system (Perkin Elmer). Analysis of total flux (photons/second) of a fixed region of interest was performed using Living Image V4.7.3 (Perkin Elmer). Mice were then sacrificed and the FGT and iliac lymph node (iLN) of each mouse was excised for analysis (Figure 2.8).

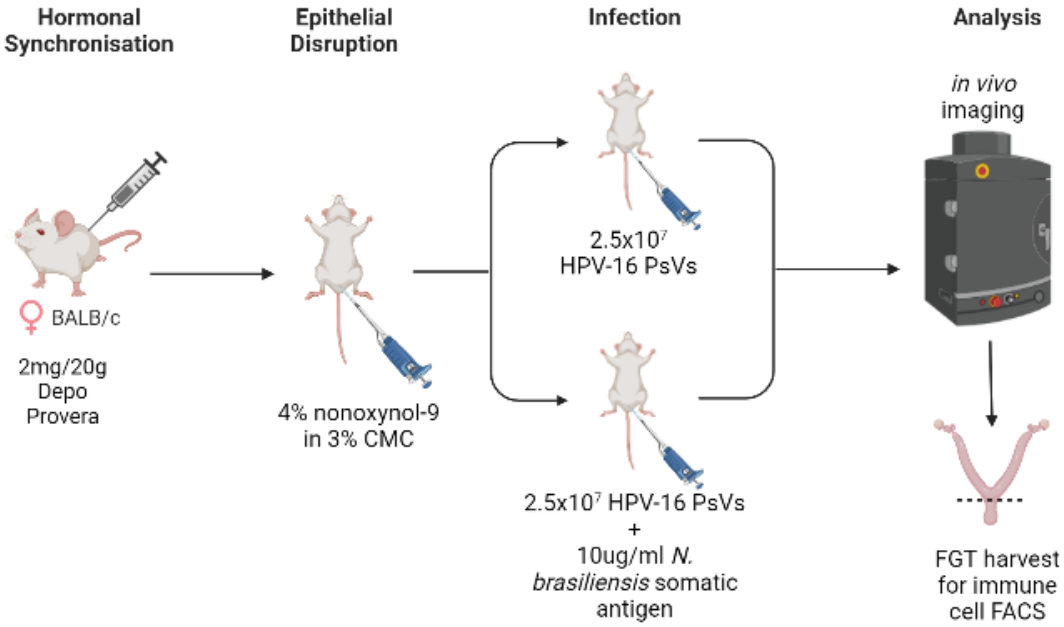

***Figure 2.7: Effect of helminth antigen on fHPV-16 PsV infection* in vivo.** *Female mice were hormonally synchronised. After four days, mice were intravaginally pre-treated with N9 and later infected with fHPV-16 PsVs with or without* N. brasiliensis *somatic antigen. Mice were imaged on the IVIS after 2 days and the FGT was excised. (Created using BioRender.com.)*

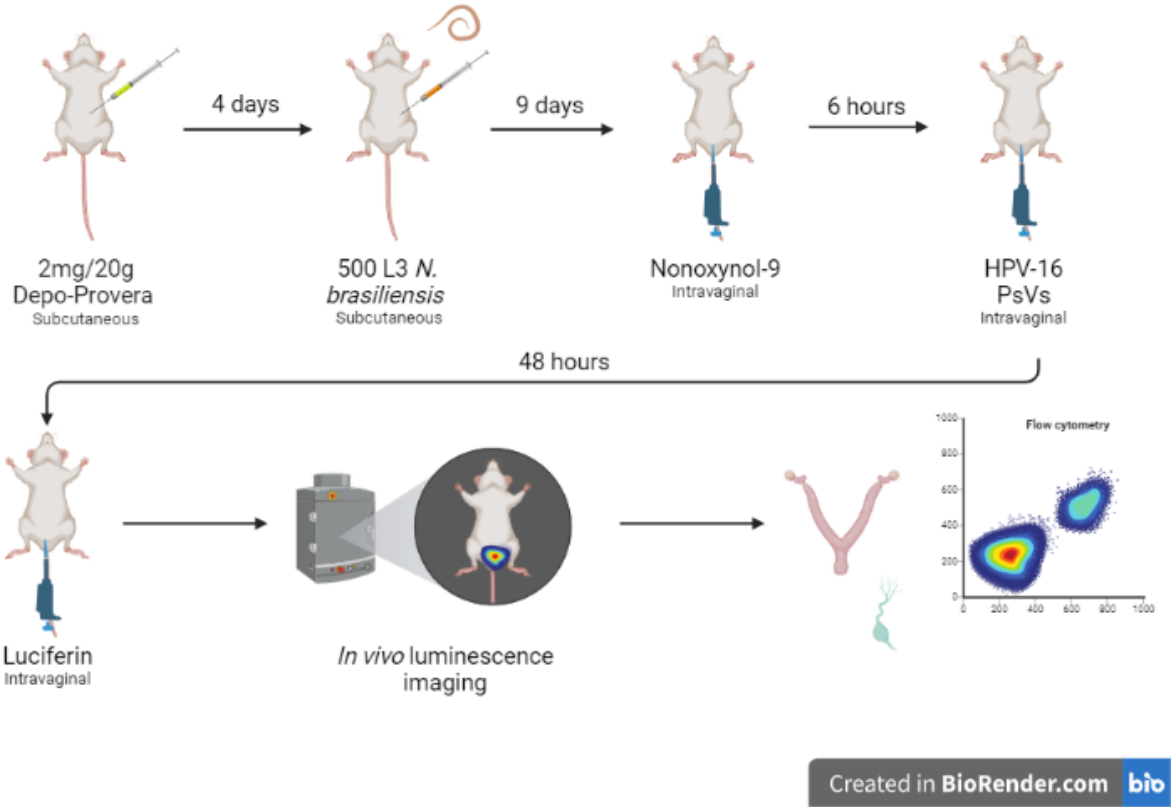

***Figure 2.8: Effect of helminth infection on fHPV-16 PsV infection* in vivo.** *Female mice were hormonally synchronised. After four days, mice were or were not infected with* N. brasiliensis *L3 larvae. After nine days, mice were intravaginally pre-treated with N9 and later infected with fHPV-16 PsVs. Mice were imaged on the IVIS after 2 days and the FGT and iLN were excised for analysis. (Created using BioRender.com.)*

2.7.3. Anti-IL-5 treatment

To prevent the eosinophilia observed following *N. brasiliensis* infection, mice received intraperitoneal injections containing 20µg anti-IL-5 monoclonal antibody or rat IgG1 isotype control antibody (Table 2.1) on days 7 and 9 post-*N. brasiliensis* infection. On day nine post infection, mice were infected with fHPV-16 PsVs and imaged two days later as described above (Figure 2.9).

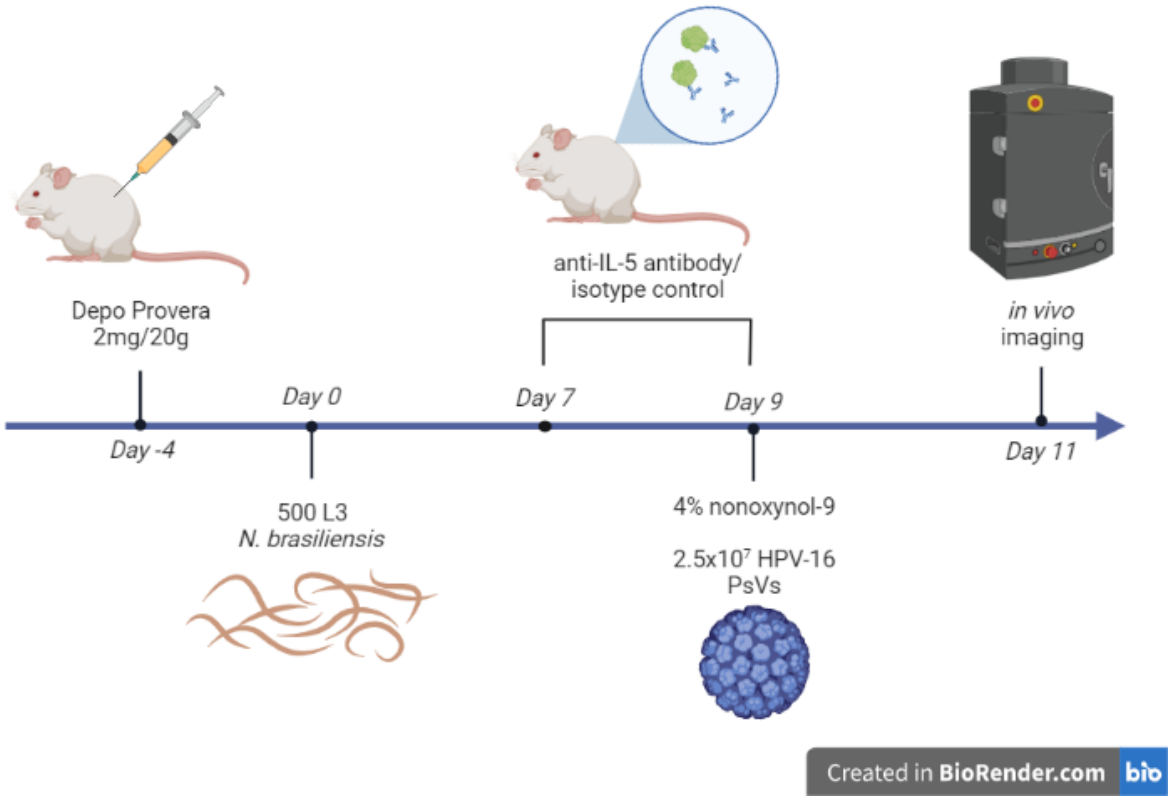

***Figure 2.9: IL-5 depletion model to assess the effects of helminth-induced eosinophilia on fHPV-16 PsV infection* in vivo.** *Female mice were treated with an anti-IL-5 antibody or isotype control on days 7 and 9 post* N. brasiliensis *infection. (Created using BioRender.com.)*

2.7.4. Xenograft model

The nude mouse strain has a mutation within the *Foxn1* gene, resulting in hair loss and a deteriorated or absent thymus[212]. A resultant reduction in the number of T cells and consequent inability to reject engrafted tissue or tumour cells makes this strain a valuable pre-clinical model for tumour research[213].

Nine days after parasite infection, the female nude mice were inoculated subcutaneously on their right flank with $5x10^6$ HeLa cells. This cell suspension was made up of HeLa cells in 1:1 ratio of PBS and Cultrex PathClear basement membrane extract (BME), Type 3 (R&D Systems) and was kept on ice until inoculation using a 25G needle (Surgi Plus Medical). The number of mice in each experimental group was dependent on stock, which was usually between 3 and 5 mice. Tumour lengths were measured daily using digital callipers (Mastercraft). After 48 days, mice were sacrificed and the tumours were excised, weighed, and analysed (Figure 2.10).

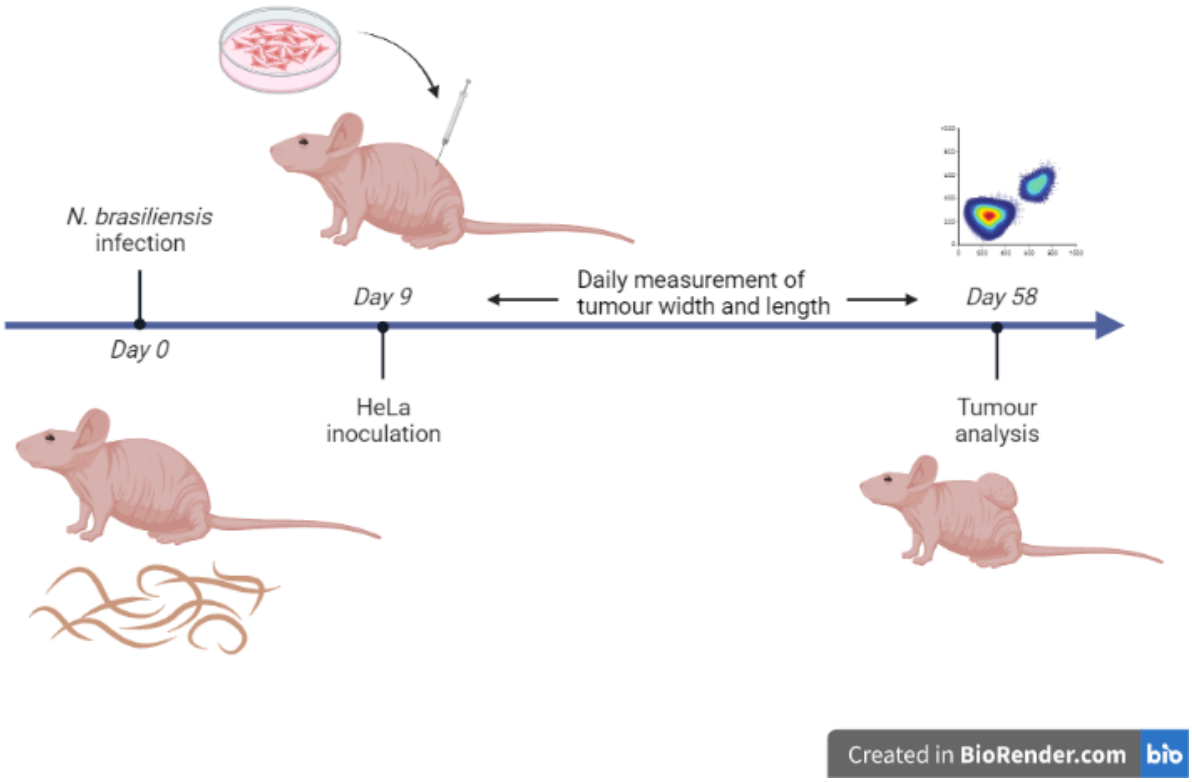

Figure 2.10:* In vivo *xenograft model. *Half of the mice were infected with 500 L3* N. brasiliensis*. After nine days, all mice were inoculated with 5x10^5 HeLa cells. Tumours were measured daily with digital callipers. Tumours were excised after 48 days for analysis.*

2.8. Tissue processing

Processing of FGT and iLN tissue was performed as published[191]. Briefly, mice were euthanised and the FGT and iLN of each mouse was removed. The FGT was placed in DMEM supplemented with 1% HEPES (BioWhittaker™, Lonza) and 20µg/ml Liberase™ TL (Roche) for 1h at 37°C with gentle agitation. The digested FGT was passed through a 70µm cell strainer (Corning) to create a single-cell suspension. This was resuspended in fresh complete DMEM. The iLN and tumour were placed in complete DMEM and passed through a 40µm or 70µm cell strainer, respectively, to create a single-cell suspension. Cells of FGT, iLN or tumour were counted on a haemocytometer using Trypan Blue to exclude dead cells.

2.9. Flow cytometry

Single cell suspensions were stained as published[191]. Briefly, cells were stained in MACs buffer (Appendix 5) with 2% heat-inactivated rat serum and the relevant fluorochrome-conjugated

antibodies in V-bottom 96-well plates (Corning®, NY, USA) at 4°C for 20min covered in foil. The antibody panels used can be found in Table 2.1. Cells were washed twice and resuspended in MACs buffer to a final volume of 200µl.

Sample data were acquired on a BD LSR Fortessa flow cytometer (BD Biosciences). Data analysis was performed using FlowJo V10.8.1 (Treestar, Ashland, OR). Compensation beads stained with the relevant fluorochromes were used for spectral overlap compensation. The gating strategy used to obtain CD45+CD11b+ singlets can be found in Supplementary Figure 4.1. T-distributed stochastic neighbour embedding (t-SNE) was performed on eosinophils by down-sampling each sample to 250 events. These subgroups were concatenated. t-SNE populations were created and compared between HPV-only and HPV-*N. brasiliensis* coinfected mice.

Table 2.1: List of depletion and conjugated antibodies

	Fluorochrome	Clone	Source	Catalogue num
Depletion Antibodies				
Anti-IL-5 Monoclonal Rat IgG1	N/A	TRFK5	eBioscience™, Thermo Fisher Scientific™	16-7052-81
Monoclonal Rat IgG2A Isotype Control	N/A	54447	R&D Systems	MAB006
Myeloid panel				
CD45	Alexa Fluor® 700	30-F11	BioLegend	304024
CD11b	BV421™	M1/70	BioLegend	101236
F4/80	BV605™	BM8	BioLegend	123133
Ly6C	FITC	HK1.4	BioLegend	128006
Ly6G	APC/Cy7	1A8	BioLegend	127624
Siglec-F	PE	S17007L	BioLegend	155506
EMT panel				
N-cadherin	PE	8C11	BioLegend	350805
E-cadherin	BV421™	DECMA-1	BioLegend	147319
Beta catenin	APC	12F7	BioLegend	645804

2.10. Western blots

2.10.1. Sample preparation

***Cell lysates**:*

HeLa cells were plated at a density of $2.5x10^6$ cells per well in a 24-well plate. After adherence, cells were treated with 50µg/ml *N. brasiliensis* somatic or ES antigen, *H. polygyrus* somatic or ES antigen, or AES. Cells were plated in triplicate or quadruplicate, depending on antigen availability. Twelve hours later, the plate was placed on ice and washed with ice cold Tris-buffered saline (TBS). Ice cold radioimmunoprecipitation assay (RIPA) buffer (Merck) was added, and adherent cells were scraped off using a precooled plastic cell scraper. The cell suspension was transferred into 1.5ml Eppendorf tubes and placed in a fridge at 4°C for 30min. Tubes were centrifuged at 16 000 x g for 20min at 4°C. Tubes were placed on ice and the supernatant was removed and pellet discarded. Protein concentration of each sample was measured using a Pierce BCA Protein Assay Kit. Samples were stored at -80°C until needed.

***Tissue homogenates**:*

Following excision, the FGT was snap frozen and stored until needed. The samples were homogenised using a benchtop homogeniser (Kinematica Polytron™ PT 2500E homogeniser) in tissue lysis buffer (Appendix 6) and centrifuged at 10 000rpm for 10min. The protein concentration of each sample was measured using a Pierce BCA Protein Assay Kit. Samples were stored at -80°C until needed.

Sample preparation:

Once samples were prepared or treated, the volume of each sample containing 20µg was diluted to a volume of 20µl with RIPA buffer and added to equal volume Laemmli sample buffer (Appendix 6). The samples were boiled at 95°C for 5min and stored at -4°C for use the next day.

Heparinase III digestion:

Heparinase III digestion was performed as previously described[214]. When indicated, 1mIU/µl Heparinase III (from *Flavobacterium heparinum,* Sigma Aldrich) was added to each sample before the addition of Laemmli sample buffer. Samples were incubated for 2h at 37°C. After incubation, equal volume Laemmli sample buffer was added and treated as above.

2.10.2. SDS-PAGE

Proteins were separated using an 8% resolving gel and 5% stacking gel (Appendix 6). Gels were prepared using a Mini PROTEAN© 3 casting apparatus (BioRad) and were run in a BioRad running tank filled with running buffer (Appendix 6), connected to a BioRad Powerpack 200. Five µl of PageRuler Prestained Protein Ladder (Fermentas, USA) was loaded into the first well of each gel, and equal volumes were loaded into the remaining wells. The gel was run at 120V, 40W and 0.35A. The run was stopped when the blue band from the Laemmli neared the end of the gel.

The separated proteins were transferred to a nitrocellulose membrane (Amersham, GE Healthcare, Life Sciences, Germany) by sandwiching the gel and nitrocellulose membrane between a piece of sponge and Whatman filter paper. This was then placed into the transfer tank filled with transfer buffer (Appendix 6) and an ice brick. The transfer conditions were 100V, 40W and 0.35A for 2h.

Successful transfer was visualised by staining the membrane with Ponceau stain (Appendix 6). This was washed twice with TBST (Appendix 6) to remove the stain. The membrane was then cut at the appropriate places so that one protein of interest (POI) was on one cut portion. Each portion was placed in a small container and the primary antibody (Table 2.2) for the POI diluted in blocking buffer (Appendix 6) was added and incubated overnight at 4°C with constant agitation. Membranes were then washed twice briefly, twice for 5min and twice for 10min with TBST and then incubated with the appropriate secondary antibody (Table 2.2) in blocking buffer for 1h at room temperature. Each portion was washed as before and placed in TBST until visualisation. Proteins were visualised using a BioRad ChemiDoc™ MP Imaging System by covering each portion of membrane with 1:1 chemiluminescent substrate A and B (Advansta or Thermo Fisher Scientific). The chemiluminescent signal from the reaction between horseradish peroxidase (HRP) and substrate was imaged by the chemidoc. Densitometric analysis was performed on ImageJ (1.53t) and readings were normalised to the glyceraldehyde 3-phosphate dehydrogenase (GAPDH) control.

Table 2.2: Western blot antibodies

	Dilution	Source	Catalogue number
Primary antibodies			
P53	1:1000	Santa Cruz	Sc-126
N-cadherin	1:1000	Cell Signalling	14215
Beta catenin	1:1000	Cell Signalling	8480
Vimentin	1:1000	Cell Signalling	3932
HSPG	1:1000	Amsbio	370255-S
GAPDH	1:1000	Cell Signalling	2118
Secondary antibodies			
Anti-mouse IgG	1:5000	Biorad	1706516
Anti-rabbit IgG	1:5000	Biorad	1706515

2.11. Statistics

Statistical analysis was performed using Prism V8.4.3. Where two groups were compared, a student's t-test was used to compare data that was normally distributed; otherwise, a Mann-Whitney t-test was used. Where more than 2 groups were being compared, a one-way analysis of variance (ANOVA) with multiple testing was used for normally distributed data; otherwise, a Kruskal-Wallis test with multiple comparisons was used. Statistical tests are stated in figure legends. Error bars represent mean ± standard error of the mean (SEM). *P* values less than 0.05 were considered significant.

Chapter 3: Impact of helminth antigen on HPV infection *in vitro.*

3.1 Introduction

The overlap in worldwide prevalence of STH infection and HPV infection is large (Figure 1.1 and 1.4). These two infections are endemic to many third world countries; therefore, coinfections are likely. It is therefore important to understand the relationship between an STH and HPV infection. HPV is also known to be the main causative agent of cervical cancer-related deaths[142]. Additionally, helminths have been shown to influence carcinogenesis and cancer progression, which will be further discussed in Chapter 5.

HPV infects the basal keratinocytes of the epithelium. Once the virus reaches the basal cells, it binds to the basement membrane via binding to cell surface HSPGs[122,123]. These molecules are made of a proteoglycan core (syndecan or glypican on epithelial cells) with numerous heparan sulphate side chains. Once the virus has bound, there is a conformational change in the L2 capsid[124] protein, revealing a furin cleavage site. Once cleaved, the virus loses its affinity for the HSPG and subsequently binds to another unknown receptor. Some possible receptors that have been explored include Annexin A2[127,128] and integrin α6 β4[125]. During the search for this unknown receptor, vimentin was identified as being an HPV restriction molecule; vimentin inhibits HPV internalisation by directly binding to the virus[211,215].

While there has been little *in vitro* data assessing the relationship between HPV and STH infections, a previously published study found that HeLa cell exposure to *N. brasiliensis* somatic antigen (homogenised L3 larvae) significantly reduced fluorescently labelled HPV-16 pseudovirion (PsV) internalisation in an *in vitro* model[192]. To further the basic understanding of this relationship, I chose to start with *in vitro* models using the target cells of HPV and exposing these cells to various helminth antigens. Here I hoped to expand on the findings of Jacobs et al.[192] by assessing how an STH infection may affect HPV infection (i.e. expression of a reporter gene), and not just internalisation. I have achieved this by using an established Gaussia luciferase reporter gene pseudovirion assay, which is validated for quantifying HPV

infection *in vitro*, as opposed to the fluorescently labelled HPV-16 PsV used by Jacobs et al., which can only quantify internalisation.

3.2 Results

3.2.1. HeLa cells are more susceptible to gHPV-16 PsV infection, compared to an HPV-negative cervical cancer cell line and a primary immortalised keratinocyte cell line.

HPV-18 is reported to be integrated into the genome of HeLa cells and is thought to have resulted in transformation of this cervical cancer cell line through viral regulation of the host cell cycle[216]. Prior HPV infection is also reported to alter susceptibility to HPV re-infection[217]. Chemical/viral transformation of a cell line might also impact the susceptibility to HPV infection. To determine whether the presence of integrated HPV genome and/or transformation of a cell line altered Gaussia reporter HPV-16 PsV (gHPV-16 PsV) infection, the fold change of gHPV-16 PsV infection (represented by Gaussia luciferase activity, i.e. light emission) was calculated in the HeLa cell line (HPV positive cervical cancer), C-33A cell line (HPV-negative cervical cancer) and NIKS cell line (HPV-negative primary immortalised keratinocytes; HPV target cell), following exposure to gHPV-16 PsV.

HeLa cells were more susceptible to gHPV-16 PsV infection compared to C-33A and NIKS cells, with C-33A cell line having a mean fold change of 0.13 in gHPV-16 PsV infection when compared to HeLa cells ($p=0.0792$), and NIKS cell line having a mean fold change of 0.002 in gHPV-16 PsV infection when compared to HeLa cells ($p=0.0012$; Figure 3.1). It was therefore decided to use HeLa cells in this *in vitro* model (to assess the effect of helminth exposure on HPV infection) due to its high infectivity.

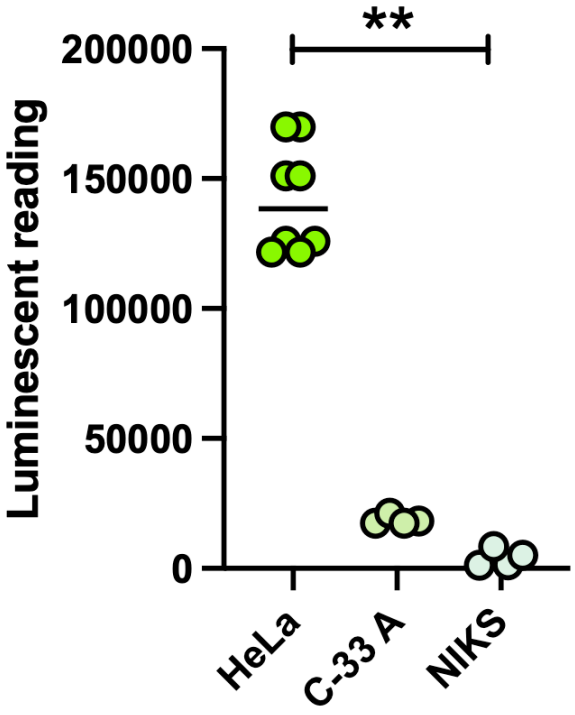

Figure 3.1: HeLa cells are more readily infected than HPV-negative cervical cancer and primary immortalised keratinocyte cell lines*. Light emission readings from gHPV-16 PsV infected HeLa, C-33A and NIKS cells seeded at a density of 5x10^3 per well in a 96-well plate. Error bars represent mean ± SEM. Data are pooled from two independent experiments with 4 technical repeats per cell type. Statistical significance was measured using one-way ANOVA with multiple comparisons. **p<0.01*

3.2.2. Optimisation of cell number and plate size for *in vitro* HPV infection assays.

Published protocols recommend the use of 1x10^5 HeLa cells in a 24-well plate[192] or 12-well plate[211,218]; however, to first establish optimum conditions for experiments whose duration is significantly longer than the above-referenced experiments, a variety of cell densities and plate sizes were assessed together with an amount of 2pg gHPV-16 PsVs per cell[211,218]. A range of cell densities were plated in triplicate in either 96-well (2x10^3, 5x10^3 and 7x10^3 cells) or 24-well plates (1.5x10^4, 2.5x10^4 and 3.5x10^4 cells). A 12-well plate was not explored due to the large volume and scarcity of gHPV-16 PsV and helminth antigens that would be required. Cells were then infected with 2pg gHPV-16 PsVs per cell and two days later, 10µl supernatant was harvested and Gaussia luciferase activity was quantified following addition of 50µl luciferin.

In the 96-well plate there was a trend toward an increase in the luminescent signal from the gHPV-16 PsVs with an increase in cell density, which did not reach significance (Figure 3.2A). However, the cells that were seeded at a density of 7000 cells per well were overly confluent by the end of the experiment 4 days later (data not shown). In the 24-well plate, there was no noticeable increase in luminescence with an increase in cell density (Figure 3.2B). Since the amount of gHPV-16 PsVs required is determined by the number of cells per well, and the

amount of helminth antigen required is determined by the volume of the well, it was decided to use a 96-well plate to minimise the number of cells required (and therefore the amount of gHPV-16 PsVs required) and volume of the well (and therefore volume of helminth antigen required). The cell density of 5000 was chosen due to there being a consistent signal within the limits of detection but preventing the cells becoming overly confluent.

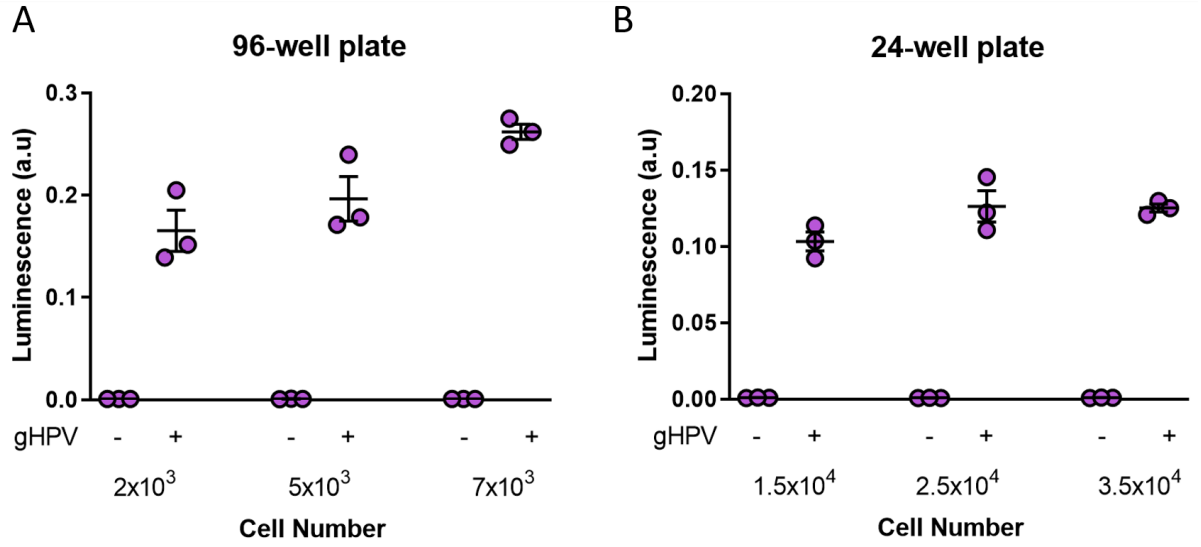

Figure 3.2: Quantification of gHPV-16 PsV infection using different infection formats. *(A) Light emission readings from gHPV-16 PsV infected HeLa cells seeded at $2x10^3$, $5x10^3$ and $7x10^3$ cells per well in a 96-well plate. (B) Light emission readings from gHPV-16 PsV infected HeLa cells seeded at $1.5x10^4$, $2.5x10^4$ and $3.5x10^4$ cells per well in a 24-well plate. Data are from one independent experiment with 3 technical repeats per density. Statistical significance between readings in arbitrary units (a.u.) of gHPV-16 PsV infected cells was calculated using one-way ANOVA with multiple comparisons. Error bars indicate mean ± SEM.*

3.2.3. Optimisation of gHPV-16 PsV concentration and time exposed to helminth antigen.

To optimise the amount of gHPV-16 PsVs required to robustly quantify gHPV-16 PsV infection by Gaussia luciferase production, $5x10^3$ HeLa cells were seeded in a 96-well plate and were infected with three concentrations of gHPV-16 PsVs. As published studies used 2pg/cell of gHPV-16 PsVs to model HPV infection[211,218], the amounts 2pg/cell, 4pg/cell and 6pg/cell were chosen. There was no significant difference in luminescence when cells were infected with 2pg, 4pg or 6pg per cell (Figure 3.3A). It is noted that this lack of significance may be due to the small sample size, however 2pg/cell produced a signal well above the limit of detection. It was therefore decided to use 2pg/cell to minimise the amount of gHPV-16 PsV required for

each experiment due to the time-consuming production process of the pseudovirions, and also in keeping with published methods.

A previous study showed that entry of 4pg of Alexa-488 labelled HPV-16 PsVs into HeLa cells was significantly decreased when HeLa cells were exposed to 10 and 50µg *N. brasiliensis* somatic antigen for 12hrs[192]. To determine if Gaussia luciferase activity (as a proxy for gHPV-16 PsV infection) changed with the length of time that HeLa cells were exposed to helminth antigens, HeLa cells were exposed to 10µg/ml *N. brasiliensis* somatic antigen for 8hrs, 12hrs and 24hrs. There was a noticeable decrease in gHPV-16 PsV infection at 8hrs, 12hrs, and 24hrs of antigen exposure, however it was only deemed significant with 12hrs (p=0.034) of exposure (8hrs, 0=0.124; 24hrs, p=0.059) (Figure 3.3B). Due to the significance observed as well as the abovementioned published literature, 12hrs of exposure was chosen for the assay.

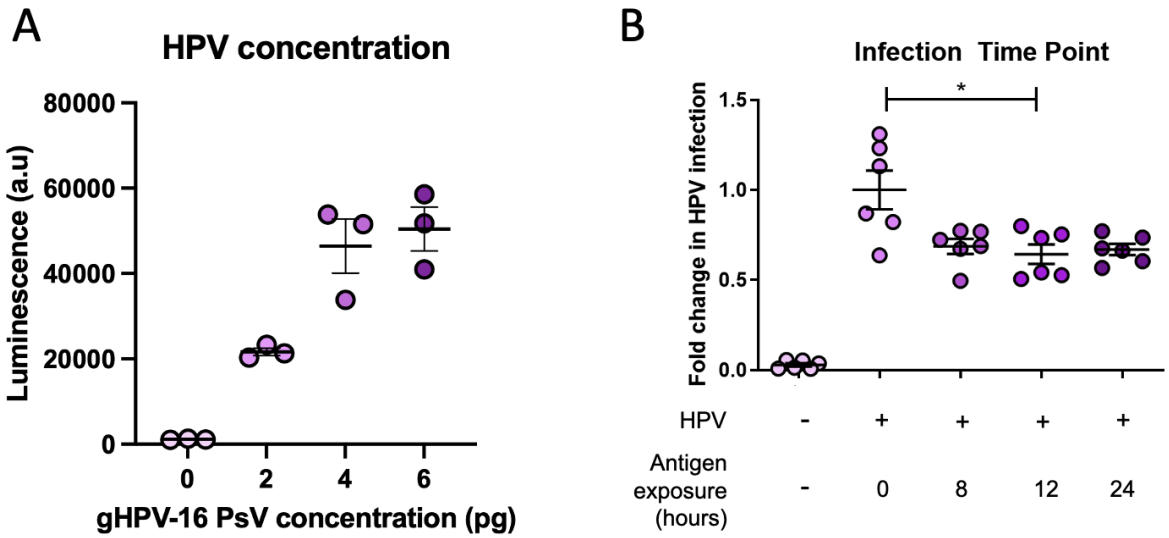

Figure 3.3: **N. brasiliensis** ***antigen significantly reduces 2pg/cell gHPV-16 PsV infection in HeLa cells, independently of the time of antigen exposure.*** *(A) Light emission readings from media of HeLa cells infected with gHPV-16 PsVs at concentrations of 2pg/cell, 4pg/cell and 6pg/cell. (B) Fold change in gHPV-16 PsV infection measured by light emission from media of HeLa cells exposed to 10µg/ml* N. brasiliensis *antigen for 8hrs, 12hrs and 24hrs, where HPV only was set as 1. Data are from one (A) and two (B) independent experiments with 3 technical repeats per concentration or time point. Statistical significance was measured using one-way ANOVA with multiple comparisons. Error bars represent mean ± SEM. *p<0.05.*

3.2.4 Exposure of HeLa cells to rodent nematode somatic antigens significantly reduced gHPV-16 PsV infection in a dose-dependent manner.

Given that exposure of 10µg *N. brasiliensis* somatic antigen significantly reduced gHPV-16 PsV infection of HeLa cells after 12 hours (Figure 3.3B), the impact of exposure of varying somatic antigen doses from two rodent hookworms, *N. brasiliensis* and *H. polygyrus*, on gHPV-16 PsV infection was assessed. There was no significant change in gHPV-16 PsV infection when HeLa cells were exposed to 0.1µg/ml or 10µg/ml *N. brasiliensis* somatic antigen, however HeLa cells exposed to 1µg/ml or 50µg/ml showed a significant reduction in gHPV-16 PsV infection (p=0.05 and p=0.0005 respectively; Figure 3.4A). Similarly, there was no significant change in gHPV-16 PsV infection when HeLa cells were exposed to 0.1µg/ml or 1µg/ml *H. polygyrus* somatic antigen. However, when HeLa cells were exposed to 10 µg/ml or 50µg/ml *H. polygyrus* somatic antigen, a significant decrease in gHPV-16 PsV infection was observed (p=0.0189 and p=0.0005 respectively; Figure 3.4B).

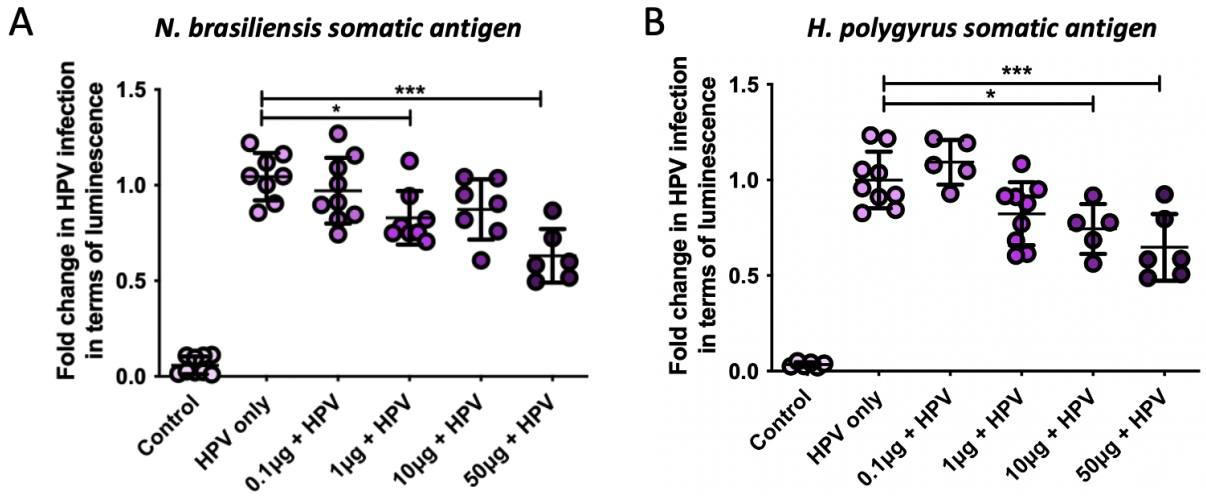

Figure 3.4: Murine nematode somatic antigen exposure reduces gHPV-16 PsV infection in HeLa cells. *(A) Light emission from gHPV-16 PsV infected HeLa cells after exposure to various concentrations of* N. brasiliensis *somatic antigen. (B) Light emission from gHPV-16 PsV infected HeLa cells after exposure to various concentrations of* H. polygyrus *somatic antigen. Error bars represent mean ± SEM. Data are pooled from 3 independent experiments with up to 4 technical repeats per group. Statistical significance was calculated using one-way ANOVA with multiple comparisons. *p<0.05, ***p<0.001.*

3.2.5. HES increases susceptibility to gHPV-16 PsV infection.

Helminths produces a range of excretory-secretory products (ES) that have been shown to suppress immune responses, including the production of IFN-gamma by CD4+ T cells, classically associated with viral control[219]. HeLa cells were exposed to increasing concentrations of *H. polygyrus* ES (HES) to determine whether these secreted molecules may alter gHPV-16 PsV infection in a more realistic model of coinfection. When HeLa cells were exposed to 0.1µg/ml HES, there was no significant effect on gHPV-16 PsV infection (Figure 3.5). Interestingly, when HeLa cells were exposed to 1µg/ml, 10µg/ml and 50µg/ml there was a significant increase in gHPV-16 PsV infection ($p=0.0145$, $p<0.0001$ and $p=0.0056$, respectively). Exposure to 50µg/ml resulted in a 1.89-fold increase in gHPV-16 PsV infection compared to HES-unexposed HeLa cells (Figure 3.5).

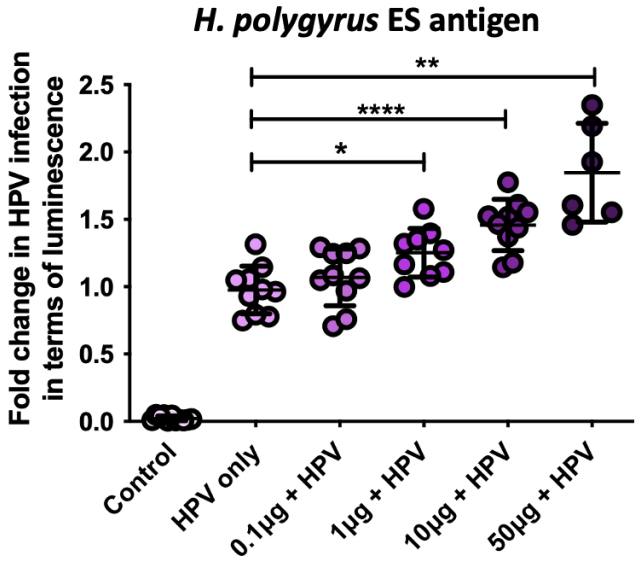

Figure 3.5: Murine helminth excretory-secretory products increase gHPV-16 PsV infection in HeLa cells. *Light emission from gHPV-16 PsV infected HeLa cells after exposure to various concentrations of H. polygyrus excretory-secretory (ES) antigen. Error bars represent mean ± SEM. Data are pooled from 3 independent experiments with up to 4 technical repeats per group. Statistical significance was measured using one way ANOVA with multiple comparisons. *p<0.05, **p<0.01, ****p<0.0001.*

3.2.6. Results of dose-dependent effects of somatic antigens validated in HPV-negative cervical cancer and primary immortalised keratinocyte cell lines.

Although C-33A and NIKS cell lines are less susceptible to gHPV-16-PsV infection than HeLa cells (Figure 3.1), I aimed to validate whether exposure to helminth somatic antigen could also significantly reduce gHPV-16 PsV infection of these less susceptible cell lines, removing the confounder of prior HPV exposure and cell transformation.

Exposure of C-33A cervical cancer cell lines to increasing doses of *N. brasiliensis* somatic antigen revealed a significant decrease in gHPV-16 PsV at concentrations of 10µg/ml and

50µg/ml (p=0.0320 and 0.0228 respectively, Figure 3.6A). Exposure of C-33A to 1µg/ml, 10µg/ml and 50µg/ml *H. polygyrus* somatic antigen resulted in significant decreases in gHPV-16 PsV infection (p=0.0046, p<0.001, p<0.0001 respectively; Figure 3.6B).

Similar to C-33A cells, there was no difference in gHPV-16 PsV infection in NIKS cells when exposed to 0.1µg/ml or 1µg/ml *H. polygyrus* somatic antigen. However, NIKS cell exposure to all four concentrations of *N. brasiliensis* (p=0.0366; p=0.0235; p=0.0257 and p<0.0001 respectively) and 10µg/ml or 50µg/ml *H. polygyrus* (p=0.0339 and p<0.0001 respectively) somatic antigens significantly decreased gHPV-16 PsV infection (Figure 3.6C and D).

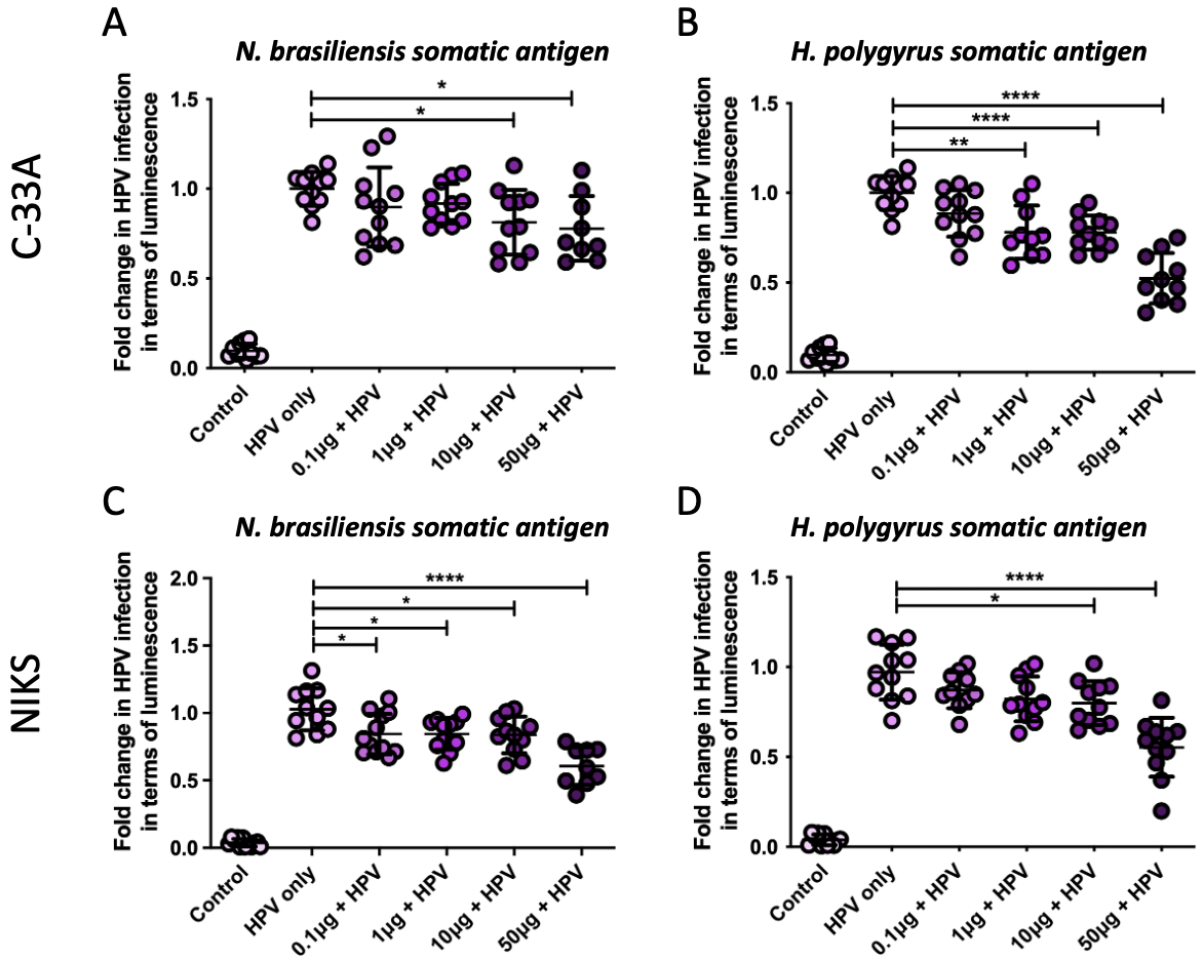

Figure 3.6: Exposure to helminth somatic antigens decrease gHPV-16 PsV infection in C-33A and NIKS cells. *(A) Light emission from gHPV-16 PsV infected C-33A cells after exposure to various concentrations of* N. brasiliensis *somatic antigen. (B) Light emission from gHPV-16 PsV infected C-33A cells after exposure to various concentrations of* H. polygyrus *somatic antigen. (C) Light emission from gHPV-16 PsV infected NIKS cells after exposure to various concentrations of* N. brasiliensis *somatic antigen. (D) Light emission from gHPV-16 PsV infected NIKS cells after exposure to various concentrations of* H. polygyrus *somatic antigen. Data are pooled*

*from 3 independent experiments with up to 4 technical repeats per group. Significance was calculated using a one-way ANOVA with multiple comparisons. *p<0.05, **p<0.01, ***p<0.001, ****p<0.0001.*

3.2.7 Exposure of C-33A and NIKS cells to HES significantly reduces gHPV-16 PsV infection.

Due to the inverse effect observed when HeLa cells were exposed to HES, I repeated this experiment with two other cell lines. In opposition to findings from Figure 3.5, there was a significant decrease in gHPV-16 PsV infection when C-33A and NIKS cells were exposed to increasing doses of HES. When C-33A cells were exposed to all four doses of HES, there were significant decreases in gHPV-16 PsV infection (0.1µg/ml p=0.0050, 1µg/ml p=0.0021, 10µg/ml p=0.0067 and 50µg/ml p=0.0006; Figure 3.7A). Exposure of NIKS cells to 0.1µg/ml and 1µg/ml did not associate with any significant decrease in gHPV-16 PsV infection; however, there was a significant decrease in gHPV-16 PsV infection when exposed to 10µg/ml (p=0.0063) and 50µg/ml (p=0.0010) of HES (Figure 3.7B).

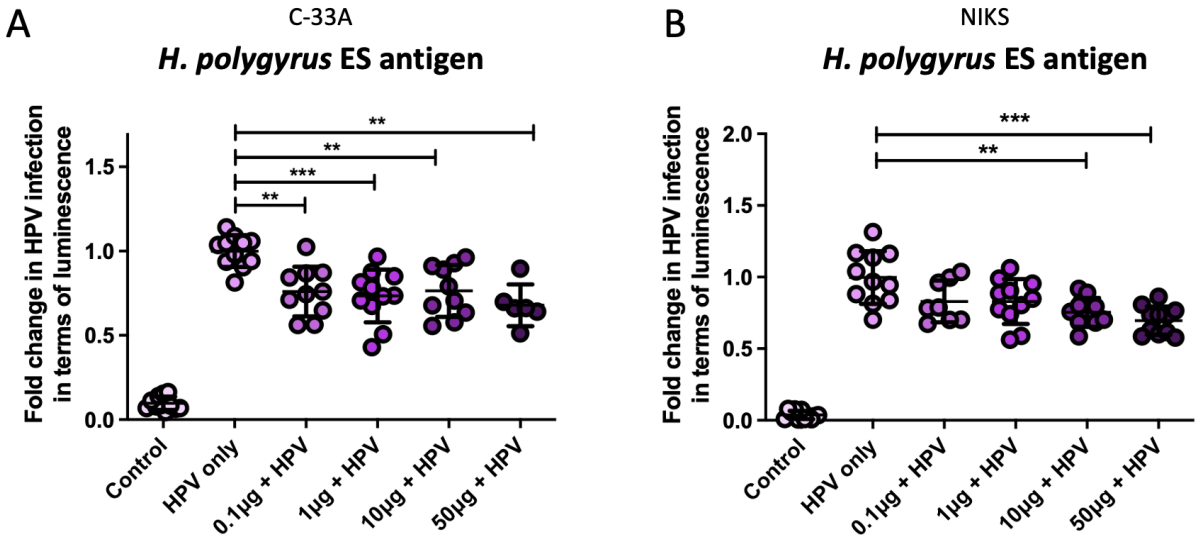

Figure 3.7: Murine helminth excretory-secretory products decrease gHPV-16 PsV infection in C-33A and NIKS cells*. (A) Light emission from gHPV-16 PsV infected C-33A cells after exposure to various concentrations of* H. polygyrus *excretory-secretory (ES) antigen. (B) Light emission from gHPV-16 PsV infected NIKS cells after exposure to various concentrations of* H. polygyrus *ES antigen. Error bars represent mean ± SEM. Data are pooled from 3 independent experiments with up to 4 technical repeats per group. Statistical significance was measured using one-way ANOVA with multiple comparisons. *p<0.05, **p<0.01, ***p<0.001.*

3.2.8. Exposure to ES antigen and exosomes of the human nematode *A. lumbricoides* decreases gHPV-16 PsV infection in HeLa cells.

The human nematode *A. lumbricoides* is one of the most common STH infections across the globe[2]. To more realistically model a human STH infection *in vitro,* HeLa cells were exposed to *A. lumbricoides* ES (AES). Exposure to 50µg/ml AES resulted in a significant decrease in gHPV-16 PsV infection (p=0.0308; Figure 3.8A).

A. lumbricoides is known to release a large number of exosomes containing immunomodulatory molecules in their ES. It was therefore explored whether this component of the ES was responsible for the decrease in gHPV-16 PsV infection. When HeLa cells were exposed to *A. lumbricoides* exosomes, there was also significant difference in gHPV-16 PsV infection when exposed to 50µg/ml AES exosomes (p=0.0189; Figure 3.8B). This may indicate that the exosomes present in the AES may be the contributing factor to this change in infection.

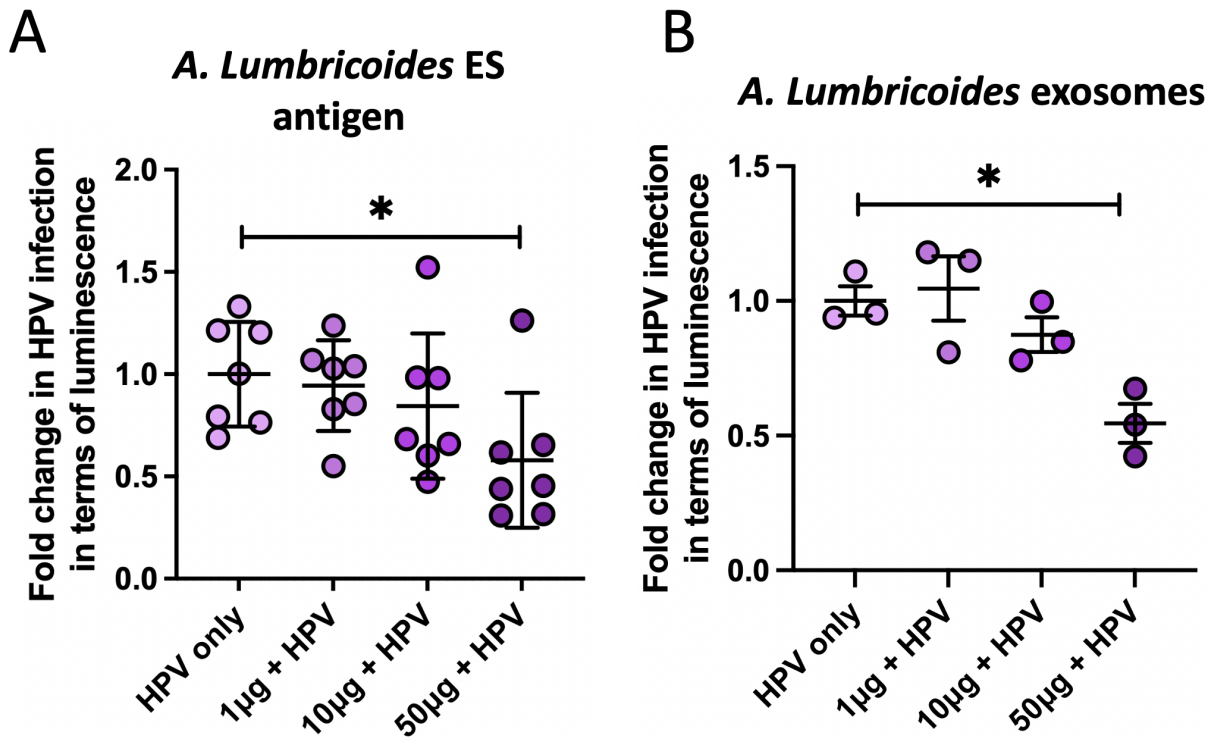

Figure 3.8:* A. Lumbricoides *ES antigen decreases gHPV-16 PsV infection in HeLa cells. *(A) Light emission from gHPV-16 PsV infected HeLa cells after exposure to various concentrations of* A. lumbricoides *excretory-secretory (ES) antigen. (B) Light emission from gHPV-16 PsV infected HeLa cells after exposure to various concentrations of* A. lumbricoides *exosomes. Error bars represent mean ± SEM. Data are pooled from 2 independent experiments*

*(A) or one (B) experiment with 3 or 4 technical repeats per group. Statistical significance was measured using one-way ANOVA with multiple comparisons. *p<0.05.*

3.2.9. Heat inactivation of somatic antigen abrogates protection against gHPV-16 PsV infection and reverses protection from ES antigen exposure.

To determine whether the molecule(s) involved in altered susceptibility to gHPV-16 PsV infection was heat liable, the three murine helminth antigens (*N. brasiliensis* somatic, *H. polygyrus* somatic and HES) were heat inactivated by incubation at 100°C for 30mins. Heat inactivation of both somatic antigens resulted in complete abrogation of protection against gHPV-16 PsV infection, shown through no change in gHPV-16 PsV infection following exposure to increasing concentrations of these antigens (Figure 3.9A and B). However, when HeLa cells were exposed to heat inactivated HES, the increased susceptibility seen before (Figure 3.5) was reversed, and instead a protection against gHPV-16 PsV was observed when exposed to 50µg/ml heat inactivated HES ($p=0.0165$; Figure 3.9C).

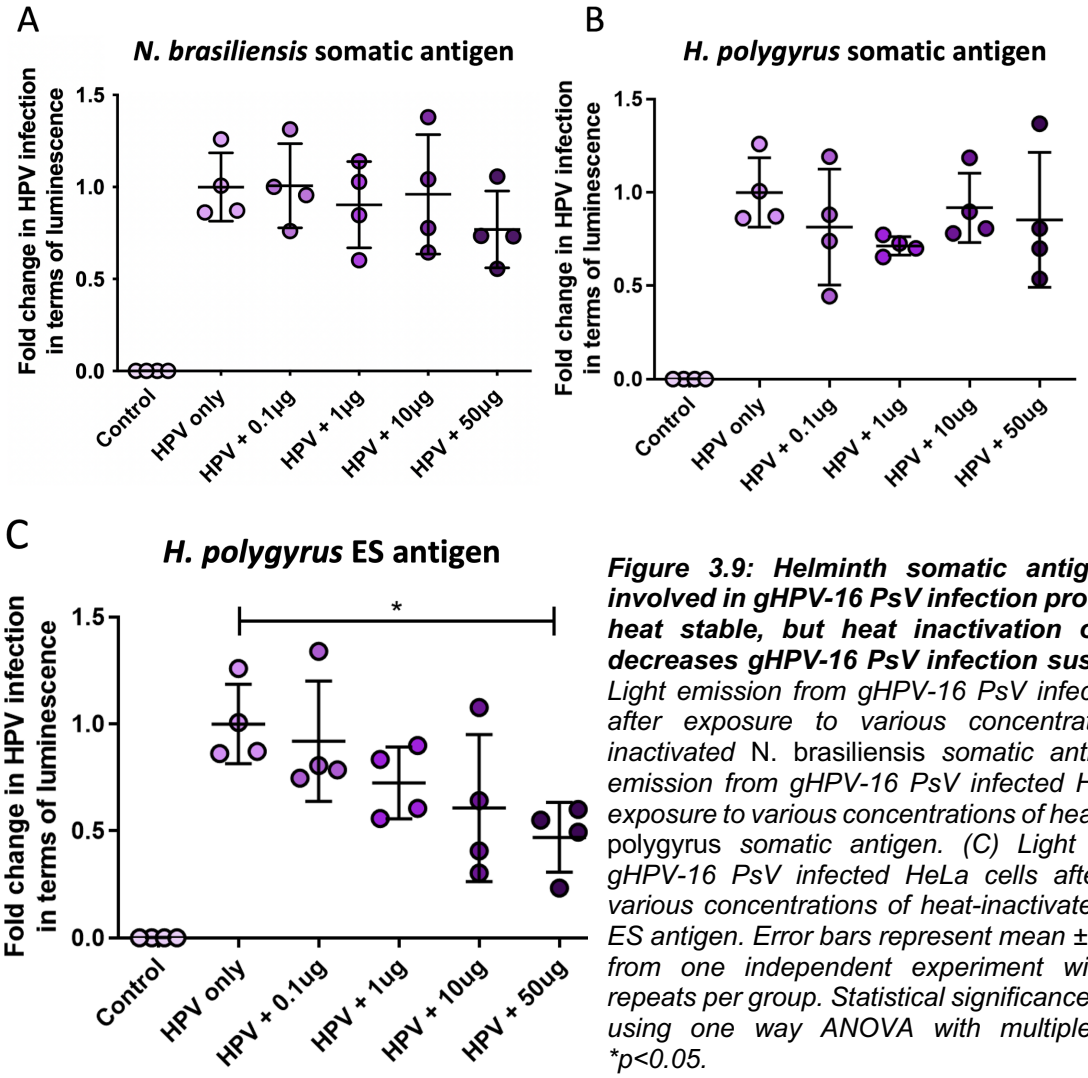

Figure 3.9: Helminth somatic antigen molecules involved in gHPV-16 PsV infection protection are not heat stable, but heat inactivation of ES antigen decreases gHPV-16 PsV infection susceptibility. *(A) Light emission from gHPV-16 PsV infected HeLa cells after exposure to various concentrations of heat-inactivated* N. brasiliensis *somatic antigen. (B) Light emission from gHPV-16 PsV infected HeLa cells after exposure to various concentrations of heat-inactivated* H. polygyrus *somatic antigen. (C) Light emission from gHPV-16 PsV infected HeLa cells after exposure to various concentrations of heat-inactivated* H. polygyrus *ES antigen. Error bars represent mean ± SEM. Data are from one independent experiment with 4 technical repeats per group. Statistical significance was measured using one way ANOVA with multiple comparisons. *p<0.05.*

3.2.10. Helminth exposure increases HPV restriction molecule expression.

To mechanistically determine why there is an observed decrease in HPV infection following exposure to helminth antigens, I investigated how helminth antigen exposure altered the expression of surface molecules potentially involved in HPV infection, choosing a known HPV receptor (namely heparan sulphate proteoglycan (HSPG) and a known HPV restriction factor (namely vimentin). HeLa cells were exposed to various helminth antigens and after 12hrs the cells were lysed and prepared for western blotting.

When imaging the vimentin blot, a band was observed just above the 55 kDa molecular weight marker, confirming that vimentin was being visualized (molecular weight 57 kDa). When HeLa cells were exposed to *N. brasiliensis* somatic antigen, there was a significant increase in the expression of vimentin compared to unexposed cells (p=0.0482; Figure 3.10A).

Unfortunately, it was not possible to obtain a third repeat with exposure to the other antigens due to the third vimentin repeat blot being cut incorrectly (Supplementary Figure 3.1).

When visualizing the HSPG blot, we expected to see bands of various molecular weights after heparinase digestion as HSPGs can have various backbones of differing weights. The two main HSPGs on epithelial cells are syndecan (20-38 kDa) and glypican (±53 kDa). Unfortunately, the western blot for HSPG was largely unsuccessful. However, the two bands for glypican and syndecan could still be seen for the control HeLa cells, HeLa cells exposed to *N. brasiliensis* somatic antigen and AES. While no statistics can be performed, it appears that exposure to *N. brasiliensis* somatic antigen may increase the expression of both HSPGs (Figure 3.10B).

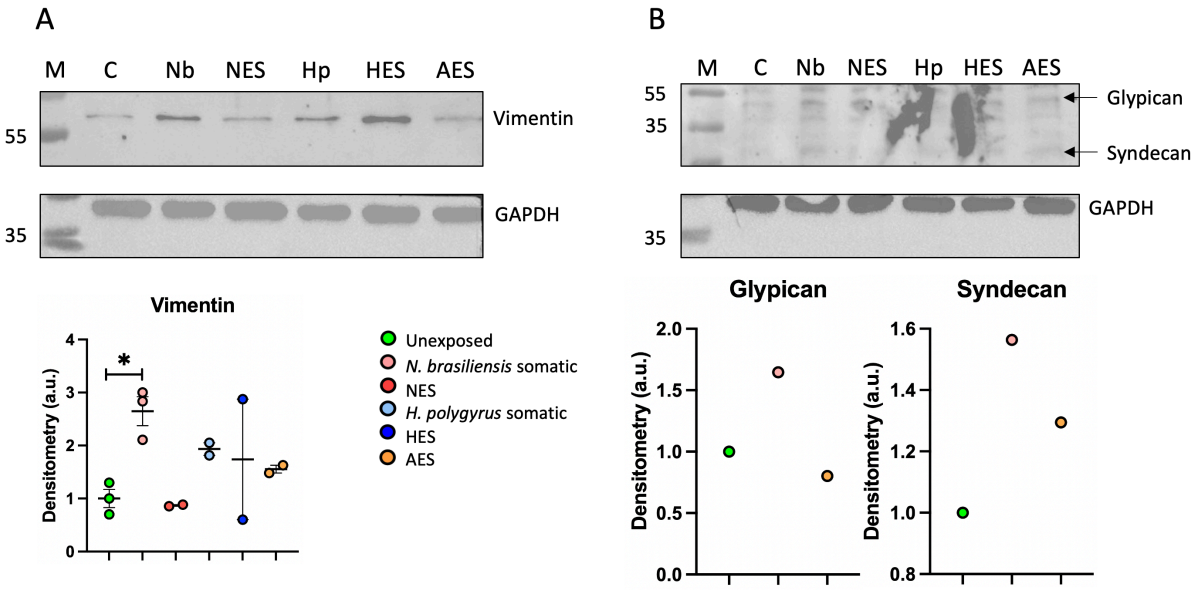

Figure 3.10: Helminth antigen exposure increases the expression of HSPG and vimentin. *(A) Representative western blot of vimentin expression of HeLa cells following 12hrs exposure to no antigen (C),* N. brasiliensis *somatic (Nb) and ES (NES),* H. polygyrus *somatic (Hp) and ES (HES) and AES antigens. First lane (M) contains the molecular weight marker. (B) Western blot of HSPG expression of HeLa cells following 12hrs exposure to no antigen,* N. brasiliensis *somatic and AES antigen. Densitometry is normalised to GAPDH. Error bars represent mean ± SEM. Data are pooled from 2 or 3 (A) or 1 (B) independent experiments. Statistical significance was measured using one-way ANOVA with multiple comparisons. *p<0.05*

3.3 Discussion

Together, these data from an optimised *in vitro* model suggest that exposure to helminth antigens may decrease susceptibility to HPV infection. The molecules of somatic antigens that are responsible for this decrease in HPV infection appear to be a heat labile protein, where heat inactivation of HES reversed the increased susceptibility and rather decreased susceptibility to HPV infection (Figure 3.9).

The first aim of this chapter was to develop an *in vitro* model to assess how helminth exposure may alter HPV infection. Experiments to identify whether prior HPV genome integration and/or transformation altered HPV infection showed that HeLa cells (HPV integrated and transformed) were more readily infected than C-33A (transformed) and NIKS (untransformed) cells. While these are three different cell lines, they all originate from the cervix (HeLa and C-33A) or are the target cells of HPV (NIKS). There is always the possibility that the difference in infectivity observed was not due to HPV integration and/or transformation, but rather due to differences between the cell lines.

A possible explanation for the difference observed when HeLa cells were exposed to HES could be due to the type of antigen. Both antigens appear to contain heat labile molecules; following heat inactivation, these molecules appear to have opposite effects on gHPV-16 PsV infection. If only one molecule from each antigen was involved, we would expect to see the same result in gHPV-16 PsV infection following heat inactivation. This suggests that ES may contain a second molecule whose effects were either inhibited by the heat labile molecule (indicating this second molecule is a heat stable protein, lipid or carbohydrate), or whose effects are only caused following heat inactivation (indicating this second molecule is also heat labile). These molecules from the two different antigens could have differential effects on the cellular processes, which could explain the difference in susceptibility. For example, the molecules from the two antigens may trigger cellular changes that create a more permissive environment for HPV entry and infection, and may induce responses that inhibit or limit viral infection. This could occur through the stimulation of different cellular pathways, the differential interaction with cell receptors or through altering metabolism or cytokine production by the cell.

While there is little *in vitro* work exploring the relationship between helminth and viral infections, there are a number of *in vivo* studies that will be discussed in the next chapter. A recent study found that tegument-enriched antigen from *Fasciola hepatica* significantly reduced SARS-CoV-2 infection of Vero cells[182]. Additionally, previous work by Jacobs et al.[192] discovered that exposure of HeLa cells to *N. brasiliensis* somatic antigen decreased HPV PsV internalisation. This was, unexpectedly, associated with a decrease in cell surface vimentin. A limitation of the vimentin results observed in the current study is that western blots cannot discriminate between cell surface (HPV restriction molecule) and cellular (EMT marker) vimentin. However, the increase in vimentin expression observed in the current study explains the phenotype observed; an increase in the expression of vimentin could inhibit HPV, thereby decreasing HPV infection. While nothing can be concluded from the single blot performed measuring HSPG expression, it does appear that there may be an increase in the expression of HSPG following exposure to STH antigens. Further repeats and replicates of vimentin and HSPG western blots are required before any conclusion can be drawn.

One important factor to consider when interpreting these data, is whether increasing doses of the STH antigens may have a cytotoxic effect on the cells, and therefore give the false illusion that there is reduced infection when there would actually be a reduction in live cells able to express the Gluc reporter. This has been previously explored in HeLa cells and it was shown that STH antigens had no effect on cell viability or growth[192,220].

Although *in vitro* data are useful for elucidating mechanisms, these data cannot be extrapolated to *in vivo* infections, as there are more variables involved, such as the immune system and location of the helminth infection vs the HPV infection. I therefore wished to validate the above findings in an *in vivo* model to more realistically model a human coinfection. These results are outlined in Chapter 4.

3.7 Supplementary material

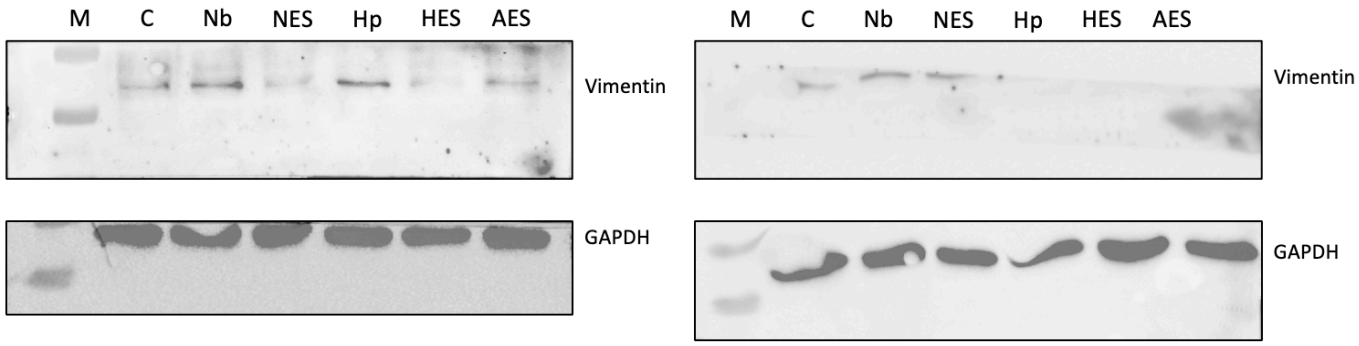

Supplementary Figure 3.1: Repeats of vimentin western blots. *Images of the other two repeats performed measuring vimentin expression of HeLa cells following 12hrs exposure to no antigen (C),* N. brasiliensis *somatic (Nb) and ES (NES),* H. polygyrus *somatic (Hp) and ES (HES) and AES antigens. First lane (M) contains the molecular weight marker.*

Chapter 4: Impact of helminth exposure on HPV infection *in vivo.*

4.1 Introduction

In Chapter 3, I demonstrated that exposure to helminth antigens reduces gHPV-16 PsV infection *in vitro* (except when HeLa cells were exposed to HES), which associated with an increase in vimentin expression. Results from *in vitro* experiments do not always extrapolate to *in vivo* studies. This can be due to a number of factors. For example, in the current project, the somatic antigen is unlikely to come into direct contact with the basal keratinocytes of the FGT (a distal organ). Additionally, *in vitro* experiments are carried out in a highly controlled environment and cells are grown as a monolayer; this does not accurately reflect the complex interactions that occur between epithelial cells and other cells, including those of the immune system in a 3D structure. Therefore, I wished to test my *in vitro* findings in an *in vivo* mouse model.

The systemic effects of helminths in the FGT have not been well explored. However existing studies do imply significant effects. For example, Blackwell et al. determined that helminth infection had varying effects on fecundity of the host, depending on the species of helminth[221], thereby presenting helminth infections at distal sites influencing the female reproductive system. Changes in susceptibility to STVIs is supported by epidemiological data showing *S. haematobium* infection increasing the risk of HIV infection[188]. This is likely to be due to increased density of HIV target cells in the genital mucosa from the lesions caused by helminth egg transit through this tissue[222]. A preclinical study testing the association between another relevant STVI, HSV-2 and a helminth infection in BALB/c mice demonstrated coinfection to result in increased genital pathology. This was due to elevated epithelial necrosis caused by helminth-induced vaginal eosinophilia[191]. While there have been no *in vivo* models exploring relationships between helminth infection and HPV infection, there are epidemiological studies exploring this association. One study reported on the effects of a *S. haematobium* infection on HPV infection and cervical neoplasias. *S. haematobium* causes genital lesions called “sandy patches”, resulting from deposition of helminth ova in the genital

tissue. Despite the increased epithelial damage, there was no association between *S. haematobium* infection and HPV acquisition or persistence[223].

Systemic effects by helminth infections that do not colonise the FGT have also been reported. Gravitt et al. identified that women with an STH infection were 1.6 times more likely to have an HPV infection than STH-uninfected women in Peru and also demonstrated a Th2 cytokine signature in the cervical fluids of STH-infected women[193]. A similar finding was also reported from Togo: here, women with a STH infection were 2.22 times more likely to have an HPV infection[194]. The STH-infected women also had a higher HPV load and a mixed type 1/type 2 immune profile[195]. It is important to note that these epidemiological studies explore an established HPV infection, whereas the *in vitro* data in Chapter 3 models the initial HPV infection.

In this *in vivo* system, a well-established cervicovaginal challenge model using HPV pseudovirions was developed to quantify HPV infection. For *in vitro* analysis, the gHPV-16 PsV is used as it can be quantified in the supernatant of cultured cells[210], whereas for *in vivo* analysis, the Firefly luciferase HPV PsV (fHPV-16 PsV) was used, as the luciferase enzyme is retained in the infected cell[224]. This is more suitable for an *in vivo* model because extracellular luciferase may be washed away naturally by genital mucus, and therefore may not accurately reflect the level of HPV-16 PsV intensity.

Here, I explore the effect that a helminth infection has on fHPV-16 PsV infection and further explore the effect of the coinfection on innate immunity and epithelial phenotypes.

4.2 Results

4.2.1. fHPV-16 PsVs infection requires nonoxynol-9 treatment.

In order for HPV to infect its target cells – the basal keratinocytes of the epithelium – there must be epithelial disruption to allow the virus to infect these cells. The same is true for HPV PsVs. Previous work by Roberts et al. showed that vaginal treatment with N9, a chemical surfactant and spermicide, resulted in higher HPV-16 PsV infection when compared to vaginal cytobrush mediated epithelial disruption, or no disruption[121]. It has also been shown that

following *N. brasiliensis* infection, the resultant vaginal eosinophilia in the FGT of BALB/c mice increased epithelial damage[191]. To determine whether N9 was required for this model or if *N. brasiliensis* infection caused sufficient epithelial damage to promote successful fHPV-16 PsV infection (thus removing the need for N9 and its potential unintended effects), half of the mice were infected with *N. brasiliensis.* After 9 days, when the Th2 response had peaked, half of the *N. brasiliensis*-infected mice and half of the uninfected mice were intravaginally administered N9. All mice were later infected with fHPV-16 PsVs. Two days post PsV infection, mice were imaged using the IVIS.

Mice not pre-treated with N9 displayed no evidence of fHPV-16 PsV infection, represented by minimal detectable light emission in the FGT (Figure 4.1). Mice pre-treated with N9 had a significantly higher fHPV-16 PsV infection compared to mice that were not N9 pre-treated (p=0.0357). There was no significant difference between the light emission, and therefore fHPV-16 PsV infection, between non-pretreated mice that were only infected with fHPV-16 PsV and non-pretreated mice coinfected with *N. brasiliensis* and fHPV-16 PsVs (p=0.30), indicating that the eosinophilia was not sufficient to cause enough (if any) epithelial damage required for the successful infection of fHPV-16 PsVs. We therefore confirmed that N9 is necessary for fHPV-16 PsV infection and would therefore form part of the *in vivo* model.

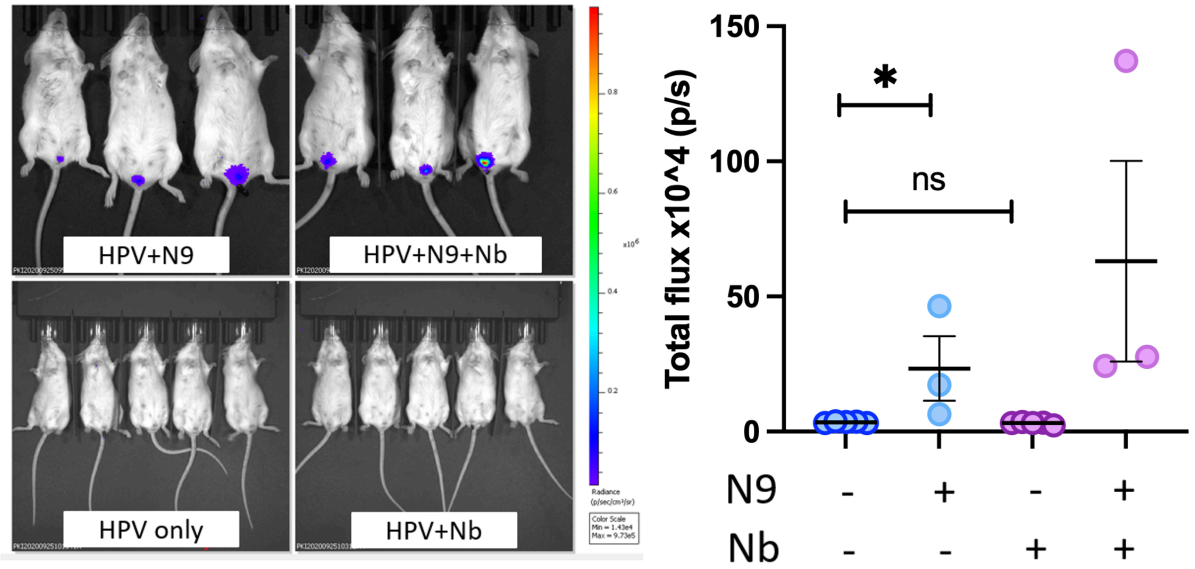

Figure 4.1: N9 is required for detectable fHPV-16 PsV infection*. Images and measurement of light emission from the FGT following intravaginal D-luciferin administration. Data from one experiment where HPV+N9 and*

*HPV+N9+Nb (n=5) and HPV and HPV+Nb (n=3). Error bars represent mean ± SEM. Statistical significance was calculated using a Brown-Forsythe and Welch ANOVA test. *p<0.05*

4.2.2. N9 alters innate immune cell profile in the FGT.

Since N9 causes epithelial disruption, it is likely that treatment with N9 results in some inflammation and possibly an alteration in the innate immune cell profile in the FGT. We therefore excised the FGT and iLN (the draining lymph node of the FGT) to assess this effect (Supplementary Figure 4.1).

It was found that pre-treatment with N9 did not significantly increase the proportion of $CD11b^{+}SSC^{hi}Siglec\text{-}F^{+}$ (eosinophils), $CD11b^{+}Ly6C^{hi}Ly6G^{-}$ (inflammatory monocytes), $CD11b^{+}Ly6C^{+}Ly6G^{+}$ (neutrophils) or $CD11b^{+}F480^{+}$ (macrophages) in the FGT (Figure 4.2A) or iLN (Supplementary Figure 4.2A). However, there was a significant increase in the total number of eosinophils (p=0.0357) and neutrophils in the FGT (p=0.0357; Figure 4.2B), while there was no change in the total number of any of the investigated cell types in the iLN (Supplementary Figure 4.2B). Due to the change in immune cell profiles caused by the use of N9 in the FGT, it was decided to treat all control groups with N9 going forward to control for this.

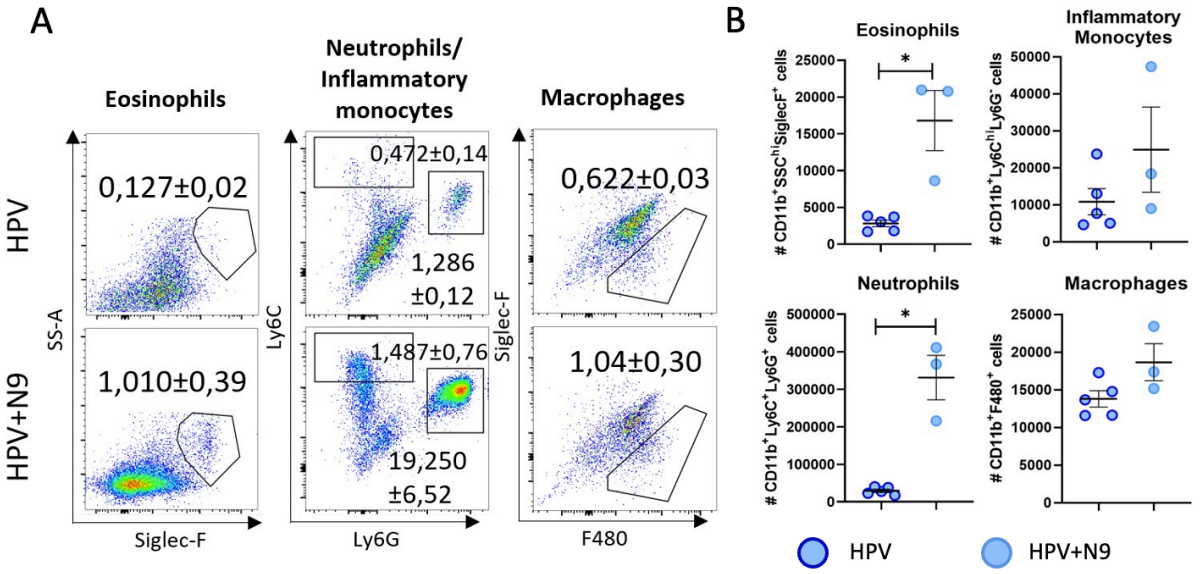

Figure 4.2: N9 alters the innate immune cell profile in the FGT. *(A) Representative FACS plots with mean ± standard error of the mean (SEM) of proportion of $CD11b^{+}SSC^{hi}Siglec\text{-}F^{+}$ eosinophils, $CD11b^{+}Ly6C^{hi}Ly6G^{-}$ inflammatory monocytes, $CD11b^{+}$ $Ly6C^{+}Ly6G^{+}$ neutrophils, and $CD11b^{+}F480^{+}$ macrophages of single cells in the*

*FGT;. (B) Number of cells with mean ± standard error of the mean (SEM) of eosinophils, inflammatory monocytes, neutrophils and macrophages in the iLN. Data from one experiment where HPV only (n=5) and HPV+N9 (n=3). Cell populations gated on CD45+CD11b+ singlets. Error bars represent mean ± SEM. Statistical significance was calculated by Welch's t-test for normally distributed data and Mann-Whitney t-tests when data was not normally distributed. *p<0.05*

4.2.3. Optimisation of fHPV-16 PsV infection time before imaging.

To further develop this model, the length of time between fHPV-16 PsV infection and imaging on the IVIS that yielded a strong enough signal for detection needed to be established[225]. Briefly, female mice were pretreated with N9 and then infected with fHPV-16 PsVs after 6 hours. Roughly every 6 hours for the following two days, mice were imaged on the IVIS.

It was found that there was no detectible light emission until 24hrs post infection, indicating that the fHPV-16 PsV had not yet successfully infected the basal keratinocytes in the FGT. From 24hrs to 40hrs, there was a noticeable increase in detectable light emission. By 41hours, there was a strong signal in the FGT of the mice (Figure 4.3). From these data, imaging 41hrs post fHPV-16 PsV infection was chosen.

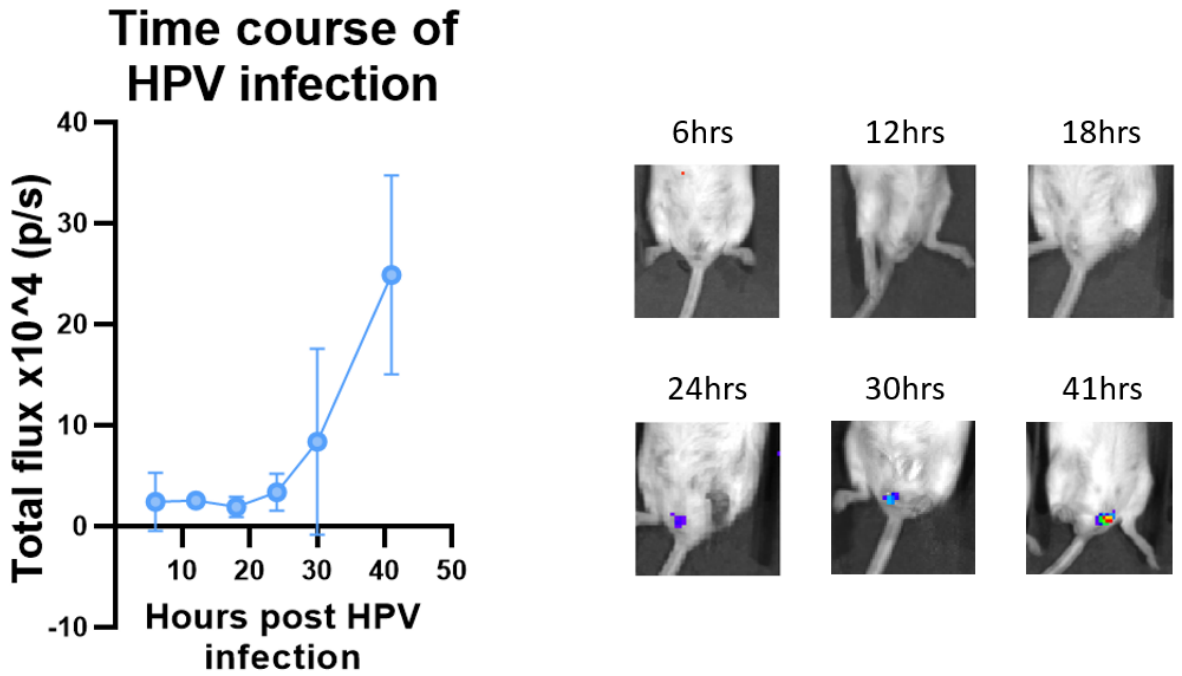

***Figure 4.3: Light emission from fHPV-16 PsV infection increases with time**. Measurement and representative images of* in vivo *light emission from the FGT following intravaginal D-luciferin administration at 6hrs, 12hrs,*

18hrs, 24hrs, 30hrs and 41hrs post fHPV-16 PsV infection. Data represent one experiment where n=5. Error bars represent mean ± SEM.

4.2.4. Exposure to rodent nematode somatic antigen decreases fHPV-16 PsV infection *in vivo.*

To validate the finding that helminth exposure decreased gHPV-16 PsV infection as in the *in vitro* model, half of the female mice were exposed to 10µg/ml *N. brasiliensis* somatic antigen when infected with the fHPV-16 PsVs. There was a significant decrease in fHPV-16 PsV infection in the helminth antigen-exposed mice (p=0.0286; Figure 4.4A). This was associated with a significant decrease in the proportion of eosinophils (p=0.0269), inflammatory monocytes (p=0.0245) and macrophages (p=0.0264) in the FGT (Figure 4.4B).

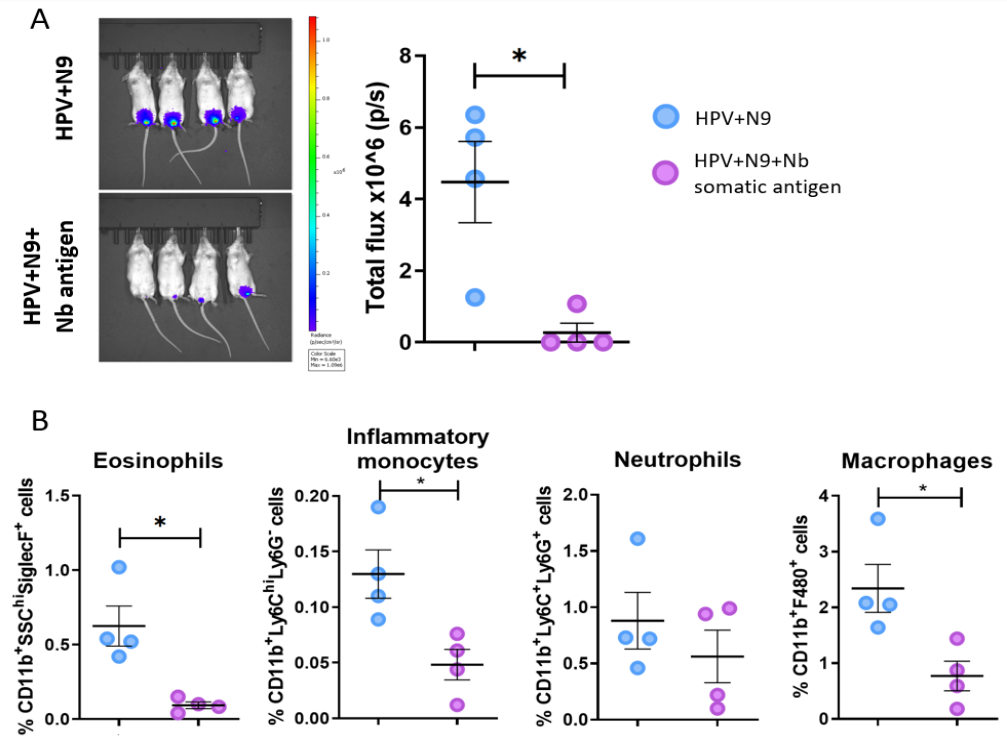

***Figure 4.4: Helminth antigen exposure decreases fHPV-16 PsV infection and alters innate immune cell profiles* in vivo**. *(A) Images and measurement of light emission from the FGT following intravaginal D-luciferin administration. (B) Proportions of CD11b+SSChiSiglec-F+ eosinophils, CD11b+Ly6ChiLy6G- inflammatory monocytes, CD11b+ Ly6C+Ly6G+ neutrophils, and CD11b+F480+ macrophages of single cells in the FGT two days post fHPV-16 PsV infection. Data from one experiment where HPV+N9 (n=4) and HPV+N9+Nb antigen (n=4). Error bars represent mean ± SEM. Statistical significance was calculated by Welch's t tests. *p<0.05.*

4.2.5. Infection with *N. brasiliensis* significantly decreased fHPV-16 PsV infection *in vivo.*

To more realistically model the relationship between a helminth infection and HPV infection, mice were infected with 500 L3 *N. brasiliensis* nine days before fHPV-16 PsVs infection. Two days later, mice were imaged on the IVIS, and the FGT and iLN were excised for analysis. The *N. brasiliensis* infection was considered successful if the mice lost up to 10% body weight.

Mice infected with *N. brasiliensis* had a significantly lower fHPV-16 PsV infection compared to fHPV-16 PsV-only infected mice ($p=0.0068$; Figure 4.5A). In the FGT, there was a significant increase in the number and proportion of eosinophils in the HPV+N9+Nb group compared to the HPV+N9 group ($p=0.0401$ and 0.0054 respectively; Figure 4.5B). In the iLN, there were significantly higher proportions of eosinophils ($p=0.048$) and a trend towards increased proportion of neutrophils ($p=0.0544$) in the iLN of *N. brasiliensis* co-infected mice (Figure 4.5C).

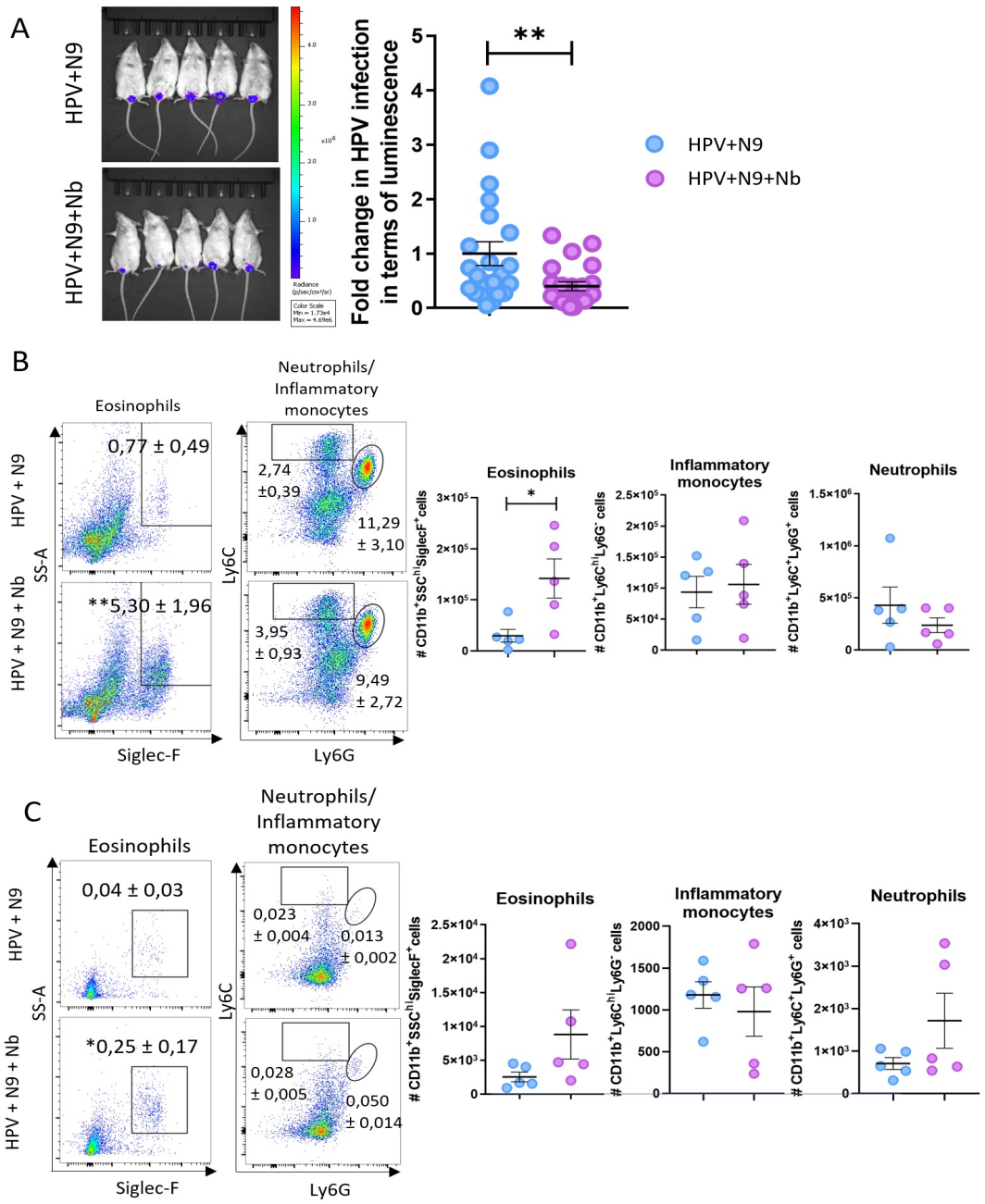

***Figure 4.5: Helminth infection decreases fHPV-16 PsV infection* in vivo**. *(A) Images and measurement of light emission from the FGT following intravaginal D-luciferin administration. (B) Representative flow plots with mean proportion ± SEM of CD11b+SSChiSiglec-F+ eosinophils, CD11b+Ly6ChiLy6G- inflammatory monocytes, CD11b+ Ly6C+Ly6G+ neutrophils, and CD11b+F480+ macrophages of single cells; and number of cells (graphs) in the FGT. (C) Representative flow plots with mean proportion ± SEM of CD11b+SSChiSiglec-F+ eosinophils, CD11b+Ly6ChiLy6G- inflammatory monocytes, CD11b+ Ly6C+Ly6G+ neutrophils, and CD11b+F480+ macrophages of single cells; and total number of each cell type (graphs) in the iLN. Data is representative of three independent experiments. HPV+N9 (n=5) and HPV+N9+Nb (n=5). Error bars represent mean ± SEM. Statistical significance was calculated using a Welch's t-test when data was normally distributed and a Mann-Whitney t-test when data was not normally distributed. *p<0.05, **p<0.01*

4.2.6. Eosinophils from *N. brasiliensis*-infected mice FGTs have altered phenotype.

Given that there was a difference in the number and proportion of eosinophils in the FGT of *N. brasiliensis*-infected mice, the eosinophils identified above were further analysed. Overall, when compared via t-SNE analysis there did not appear to be any difference in the eosinophil population in the FGT of HPV-only infected mice and HPV-*N. brasiliensis*-infected mice (Figure 4.6A). There was also no statistically significant difference in the forward and side scatter of these eosinophils (Figure 4.6B). However, when assessing the geometric mean of Siglec-F, Ly6C, Ly6G and CD11b, it was found that the eosinophils in the FGT of coinfected mice expressed significantly less Ly6C ($p=0.0136$) and significantly more CD11b ($p=0.0319$; Figure 4.6C-F). The same markers were assessed on the eosinophils taken from the FGT of mice who were vaginally exposed to *N. brasiliensis* somatic antigen (section 4.2.4). The same increase in CD11b was observed on eosinophils from *N. brasiliensis* antigen-exposed mice compared to unexposed mice. However, there was no change seen in Ly6C expression (Supplementary Figure 4.3).

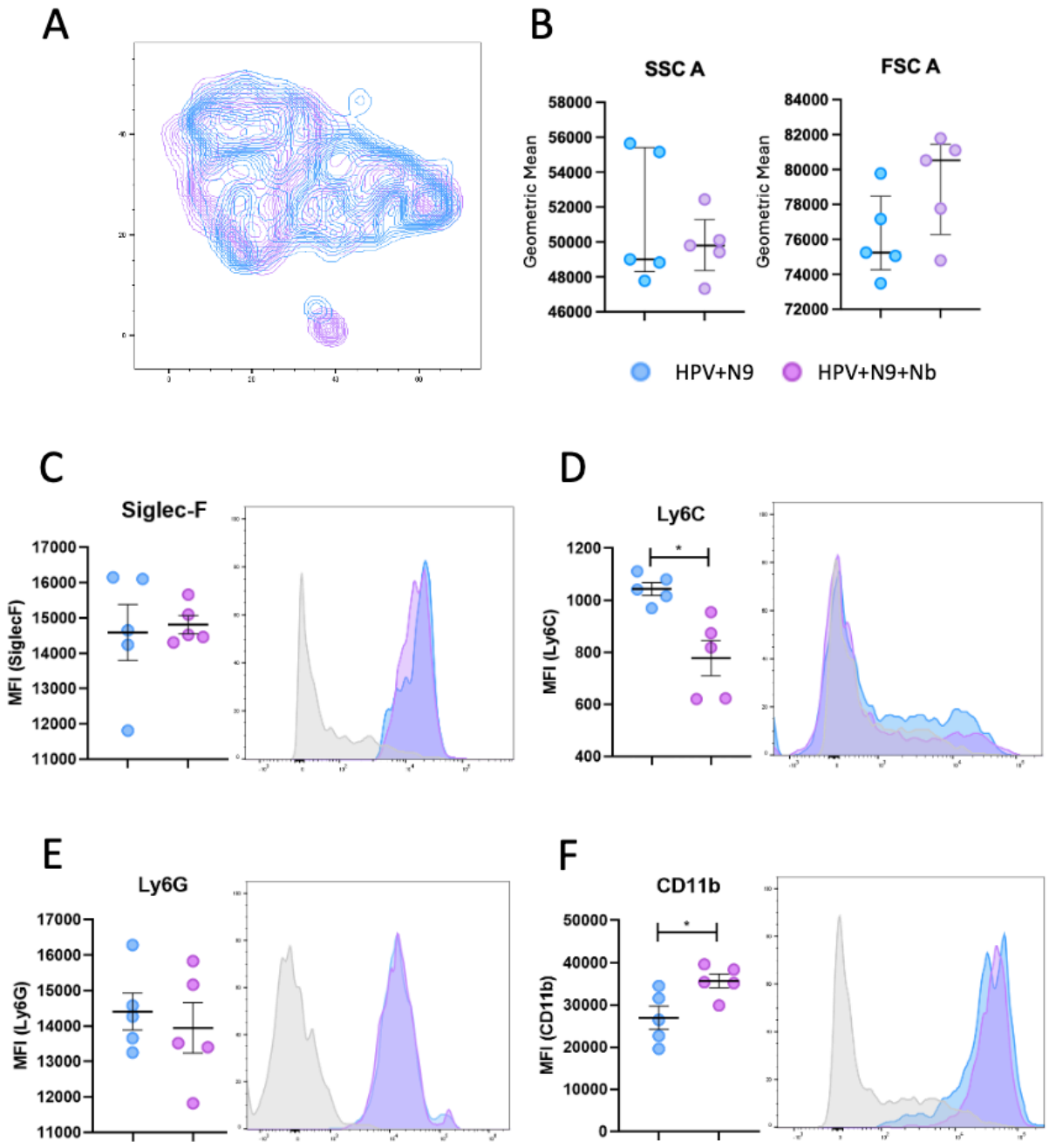

Figure 4.6: **N. brasiliensis** ***infection alters cell surface markers of eosinophils in the FGT****. (A) t-SNE plot of eosinophils from HPV infected mice (blue) and HPV-*N. brasiliensis *coinfected mice (purple), (B) side and forward scatter geometric mean of eosinophils. MFI and histograms of (C) Siglec-F, (D) Ly6C, (E) Ly6G and (F) CD11b. Grey represents unstained control. Error bars represent mean ± SEM. Statistical significance was calculated using a Welch's t-test when data was normally distributed and a Mann-Whitney t-test when data was not normally distributed. *p<0.05*

4.2.7. Protection from fHPV-16 PsV infection is eosinophil dependent.

Since infection with *N. brasiliensis* resulted in significantly higher eosinophils in the FGT (Figure 4.5B), these cells were manipulated to determine whether this immune cell population contributed towards the protection from fHPV-16 PsV infection. This was assessed through the use of an anti-IL-5 antibody, administered on day 5 and day 7 post *N. brasiliensis* infection, to deplete IL-5 and therefore prevent eosinophilia.

It was found that when eosinophilia was prevented, the protection from fHPV-16 PsV infection was lost ($p=0.0317$) and returned to comparable levels of *N. brasiliensis*-uninfected mice (Figure 4.7A). In the iLN of these mice, it was expectedly found that the number of eosinophils was significantly lower in the HPV+N9 mice compared to HPV+N9+Nb+isotype mice ($p=0.01485$) and the proportion of eosinophils between these two groups trended towards a decrease ($p=0.0621$). As expected, the number and proportion of eosinophils in the mice treated with the anti-IL-5 antibody were comparable to the *N. brasiliensis*-uninfected, and neared significance when compared to the isotype control mice ($p=0.0523$ and $p=0.0793$ respectively). Additionally, there was a significant increase in the proportion of neutrophils in HPV+N9+Nb+isotype mice compared to HPV+N9 mice ($p=0.0236$) and a trend towards a decrease in the number of these neutrophils ($p=0.0681$). Similarly, mice that received the anti-IL-5 antibody had significantly reduced number of neutrophils ($p=0.0393$) and trended towards a decrease in the proportion of neutrophils ($p=0.0899$) compared to the *N. brasiliensis* mice that received the isotype control. There was no difference in the number or proportion of inflammatory monocytes or macrophages between the three groups (Figure 4.7B).

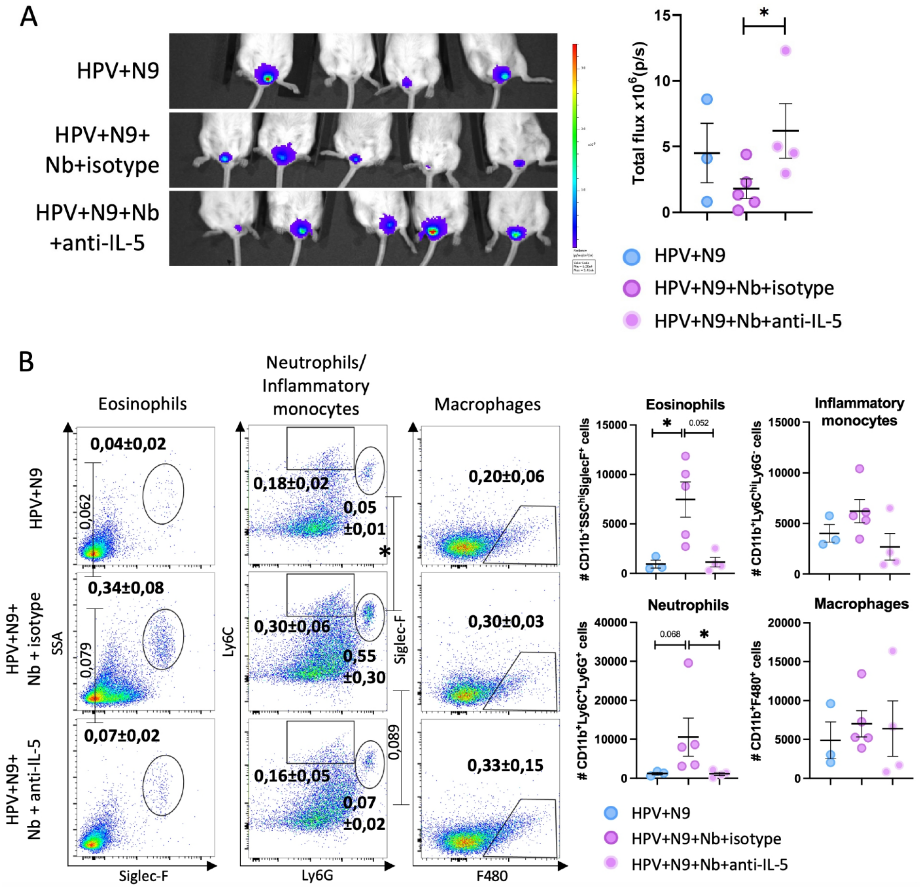

Figure 4.7: Protection from fHPV-16 PsV infection is lost following eosinophilia prevention*. (A) Images and measurement of light emission from the FGT following intravaginal D-luciferin administration. (B) Representative flow plots with mean ± SEM of proportion of CD11b+SSChiSiglec-F+ eosinophils, CD11b+Ly6ChiLy6G- inflammatory monocytes, CD11b+ Ly6C+Ly6G+ neutrophils, and CD11b+F480+ macrophages of single cells; and number of each cell population (graphs) in the iLN. Error bars represent mean ± SEM. Statistical significance was calculated by Brown-Forsythe and Welch ANOVA test for normally distributed data and Kruskal-Wallis ANOVA for data that was not normally distributed. One mouse in the HPV+N9 group and one in the HPV+N9+Nb+anti-IL-5 group were excluded due to failed fHPV-16 PsV infection. *p<0.05*

4.2.8. Helminth infection increases the expression of HSPG in the FGT

As mentioned, HPV infection requires the virus (or pseudovirion) to bind to HSPG on the cell surface. Therefore, I wished to determine whether altered HSPG expression was involved in the inhibition of HPV infection *in vivo*.

As in Chapter 3, I was expecting to find proteins of varying sizes, but specifically a protein that was ±53 kDa (glypican) and 20-38 kDa (syndecan). Proteins at these weights were observed. Surprisingly, it was found that coinfected mice had a non-significant but noticeable increase in expression of glypican, one of the two main core proteins of HSPG (Figure 4.8).

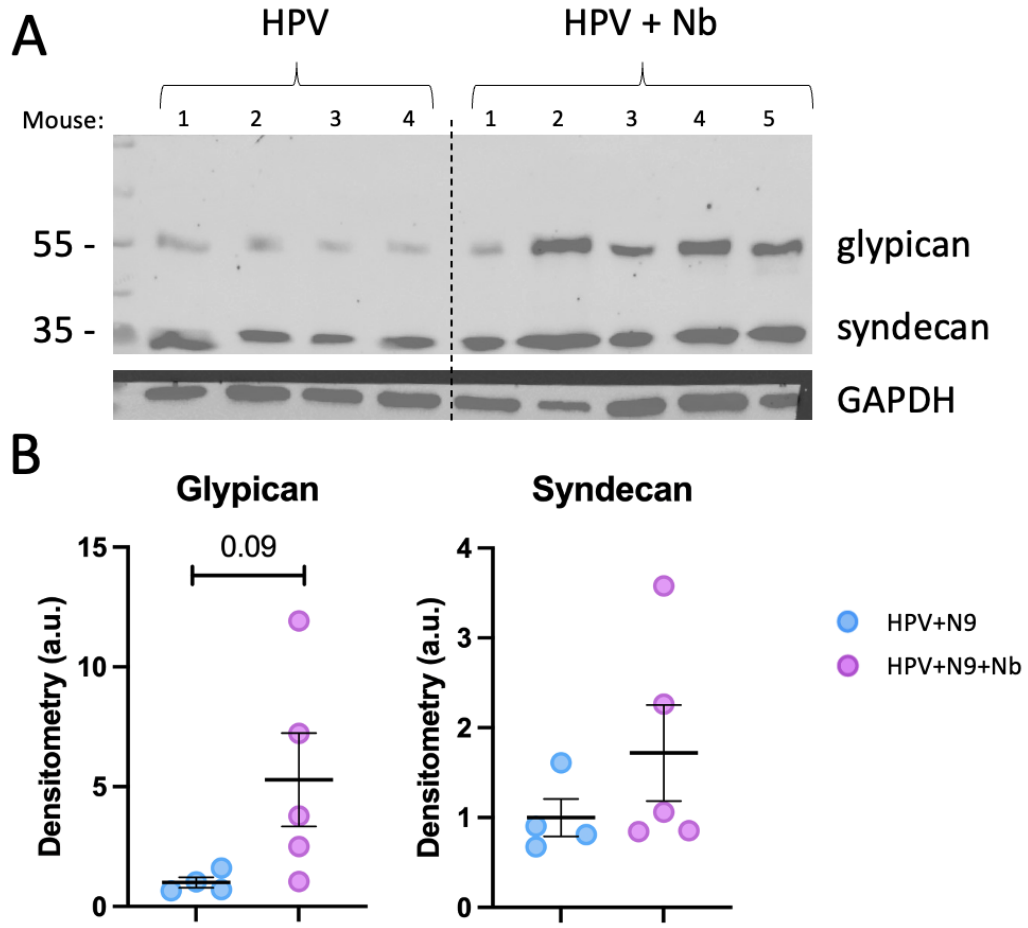

Figure 4.8:* N. brasiliensis *infection increases the expression of glypican. *(A) Western blot of total HSPG (glypican and syndecan) expression, (B) densitometry readings of glypican and syndecan normalised to GAPDH. Each lane is representative of FGT protein lysate from an individual mouse. An unpaired t-test was used to compare expression between the two groups where HPV+N9 n=4 and HPV+N9+Nb n=5.*

4.3 Discussion

Taken together, these data confirm the findings of the previous chapter; they show that exposure to *N. brasiliensis* antigen or a live infection with *N. brasiliensis* inhibits fHPV-16 PsV infection in an *in vivo* cervicovaginal challenge model, with live infection fHPV-16 PsV inhibition being in an eosinophil-dependent manner.

As mentioned, a successful HPV infection requires disruption of the epithelial layer in order for the virus (or pseudovirus) to reach and infect the basal keratinocytes. A lack of disruption would render the virus unable to navigate to the basal layer and therefore would be unable to infect any cells. As mentioned, the virus requires binding to the basement membrane in order to infect the basal keratinocytes; this basement membrane is only present at the basal layer. Here, we confirmed that a lack of disruption of the epithelial layer results in no detectable HPV-16 PsV infection, further adding to the findings of Roberts et al.[121] and solidifying the notion that some form of disruption, such as chemical disruption by N9, is essential for *in vivo* HPV PsV infection.

N9 is known to cause epithelial permeability and sloughing[226]; it is therefore understandable that a local inflammatory response may occur. When the innate immune cell profile was assessed in both the FGT and its draining lymph node (the iLN), it was discovered that N9 pretreatment resulted in an increase in the number of eosinophils and neutrophils in the FGT, but not the iLN. Due to the effect of N9 on the local immune profile, N9 was used in all groups going forward to control for this.

To accurately assess any change in HPV-16 PsV infection, there needed to be a sufficient infection whereby the production of the FLuc would be high enough to observe any differences between the two groups. Should the levels be too low, differences in infection could be missed. Therefore, a time course was performed to assess the increase in Fluc production. There was no noticeable increase in fHPV-16 PsV infection until 24h post infection. This finding is in keeping with the knowledge that the virus had reached the late endosome by 16-24h post infection[227], with half of pseudovirions successfully infecting cells by 12hrs and completing infection by 36h post infection[131]. While the experiment was terminated at 41hrs post fHPV-16 PsV infection, we were confident that this signal was strong enough to compare at this time point and therefore chose 41hrs as the infection time. Handisurya et al. similarly found that the luciferase activity peaked at day 2-3 post PsV infection[228]. This ensures that most, if not all, pseudovirions would have infected the basal cells and had enough time for the production of Fluc reporter.

I then used this optimized time point to assess how exposure to *N. brasiliensis* antigen may alter fHPV-16 PsV infection. When mice were treated intravaginally with *N. brasiliensis* somatic antigen, there was a significant decrease in the infection of fHPV-16 PsVs. The antigen appeared to have an anti-inflammatory effect in the FGT; mice that were intravaginally exposed to the antigen had a marked reduction in eosinophils, inflammatory monocytes and macrophages, with a trend towards a decrease in the proportion of neutrophils. Unfortunately, cell counts had not been recorded, and therefore, cell numbers were not able to be calculated. As discussed above, pretreatment with N9 caused an increase in the number of eosinophils and neutrophils. Pretreatment with *N. brasiliensis* antigen appeared to have abrogated this effect. Helminth antigens are known to have anti-inflammatory properties; these properties have been exploited in the treatment of inflammatory diseases[229]. There is an abundance of literature showing how helminth antigen or infection reduces allergic lung inflammation and/or asthma[230–235]. Infection and/or exposure to helminth antigen appears to reduce allergen-induced Th2 cytokines, eosinophilia, airway inflammation and airway hyperreactivity[231–235]. One of the ways in which this occurs is the upregulation of Tregs and TGF-β production[230]. Helminths and helminth antigens have even been used in human trials; inflammatory bowel disease (IBD) has been successfully treated with *T. suis* eggs or infection with *N. americanus*[236–238]*.* Here we show that exposure to helminth antigen induces an anti-inflammatory response at the site of exposure, which is in keeping with the above results. This suggests that there is a molecule in the *N. brasiliensis* antigen that may have future therapeutic potential, such as the inclusion of this molecule in lubricants and spermicides, which would be used during intercourse when the epithelial disruption occurs.

To more accurately model a live infection, I infected mice with *N. brasiliensis* and challenged with fHPV-16 PsV at 9 days post-infection, a time point coinciding with the peak of type 2 production[239]. Here, a significant decrease in fHPV-16 PsV infection was observed in mice that were infected previously with *N. brasiliensis.* This supports the *in vitro* data as well as the *in vivo* antigen exposure results. Based on the epithelial damage caused by helminth-induced eosinophilia in the FGT shown by Chetty et al., it was hypothesized that the increased tissue damage that occurred due to the helminth-induced eosinophilia in the FGT may lead to further epithelial damage and thus increase the accessibility of the basal keratinocytes. This was not observed in the current study; however, vaginal eosinophilia was observed, both in

number and proportion. This is in direct contradiction to the reduce eosinophils in the FGT following *N. brasiliensis* somatic antigen challenge. A possible explanation could be that there are proteases within this somatic antigen which may act in a similar manner to the ES from *N. americanus*, where it was found that this ES contained a protease that cleaved eotaxin and reduced eosinophil recruitment[65]. Interestingly, Chetty et al. found an increase in neutrophils in the FGT of *N. brasiliensis*-infected mice. The proportion of neutrophils in the FGT of *N. brasiliensis* infected mice in the study by Chetty et al.[191] was comparable to that of the neutrophil proportion of HPV+N9 and HPV+N9+Nb mice (Figure 4.5). Since mice treated with N9 resulted in an increase in neutrophils, the lack of additional increase in neutrophils from *N. brasiliensis* infection may suggest that neutrophilia in the FGT from N9 and from *N. brasiliensis* infection is not additive, but rather that only a certain level of neutrophilia can be induced in the FGT.

The discovery of eosinophilia in the FGT of mice infected with an intestinal worm led us to further explore the involvement of these immune cells. When performing t-SNE analysis on these cells, it did not appear that there were any obvious subpopulations specific to either fHPV-16 PsV-only or coinfected mice. There was also no change in forward or side scatter, indicating no change in the size or granularity of the eosinophils. However, when exploring the expression of various eosinophil markers, it was discovered that there was reduced Ly6C and increased CD11b expression on the eosinophils from the FGT of coinfected mice. Ly6C expression on myeloid cells is an inflammatory marker[240], and CD11b is known to be involved in eosinophil recruitment[241,242]. Therefore, this may show that infection with *N. brasiliensis* may elicit an anti-inflammatory response in the FGT of infected mice. The observation of increased CD11b expression by eosinophils of *N. brasiliensis*-infected mice is understandable, given the marked eosinophilia in the FGT following infection. This also suggests that the increase in eosinophils in the FGT is likely due to increased recruitment as opposed to increase in proliferation of resident eosinophils. Further investigation is needed to assess whether local eosinophil population expansion is involved in FGT eosinophilia. The expression of these markers on eosinophils from the FGT of mice who were vaginally exposed to *N. brasiliensis* somatic antigen was also assessed. The same increase in CD11b expression in antigen-exposed mice suggests that these eosinophils were also likely to be due to recruitment, although it was found that there were fewer eosinophils in the FGT of these mice. There was,

however, no increase in the expression of Ly6C on eosinophils from antigen-exposed mice, suggesting that these eosinophils were not proinflammatory.

Given the differences in eosinophil abundance and cell marker expression, it was hypothesized that these cells may be playing a role in the reduction of fHPV-16 PsV infection *in vivo.* To test this hypothesis, mice were pretreated with an anti-IL-5 antibody, which neutralizes IL-5 and therefore does not allow for eosinophil recruitment or proliferation[243,244]. When the eosinophil population was interrogated, it was confirmed that the antibody treatment had worked, shown by the reduced eosinophil count and proportion in the iLN of *N. brasiliensis* and anti-IL-5 treated mice, which was comparable to *N. brasiliensis*-uninfected mice. Surprisingly, there was also a reduction in neutrophils in the iLN of antibody treated mice compared to infected, isotype control treated mice. While unconventional, it has been shown that tissue infiltrating neutrophils in mice and humans express IL-5Rα, suggesting that IL-5 may be involved in the recruitment of neutrophils[245,246]. Therefore, the neutralization of IL-5 may have had a bystander effect on the neutrophil population in the FGT. As hypothesized, the protection against fHPV-16 PsV infection in mice infected with *N. brasiliensis* was abrogated when these mice were treated with the anti-IL-5 antibody, indicating that the eosinophilia caused by the *N. brasiliensis* infection may have a role in the protection. Eosinophils are known to play a role in tissue repair[247]. Therefore, the eosinophilia elicited in the FGT during a helminth infection may contribute towards repairing the damage to the epithelium induced by N9 treatment, thus reducing the access of the fHPV-16 PsVs to the basal keratinocytes and therefore reducing fHPV-16 PsV infection. Due to the reduction of eosinophils in the FGT of mice who were challenged with *N. brasiliensis* antigen, this could not be the reason for inhibiting fHPV-16 PsV infection. One theory could be that since the antigen used to challenge the mice is produced by homogenising the whole worm, there may be additional factors in this homogenate that could have various effects on fHPV-16 PsV infection; factors in the homogenate could competitively bind HPV receptors or possibly cleave these receptors. These factors are unlikely to reach the FGT during a live infection, hence the probable different mode of inhibition. Further work is needed to explore the potential pathway for inhibition by *N. brasiliensis* antigen.

Lastly, the role of HSPG expression was interrogated. Following western blot analysis of FGT tissue homogenates of fHPV-16-only infected mice and helminth-HPV16-PsV coinfected mice, it was observed that there was an increase in expression of glypican, but not syndecan, in coinfected mice. Syndecan is the primary HSPG expressed on epithelial cells, whereas glypican is not required for HPV cell entry[248]. Therefore, the increase in glypican expression is unlikely to be linked to altered fHPV-16 PsV infection and may instead be due to alteration in expression of other receptors involved in HPV infection, HPV restriction molecules or an unidentified immune process.

Taken together, these data suggest that *N. brasiliensis* infection results in FGT eosinophilia, which may limit the epithelial damage caused by N9 treatment and protect against the initial HPV-16 PsV infection.

4.4 Supplementary material

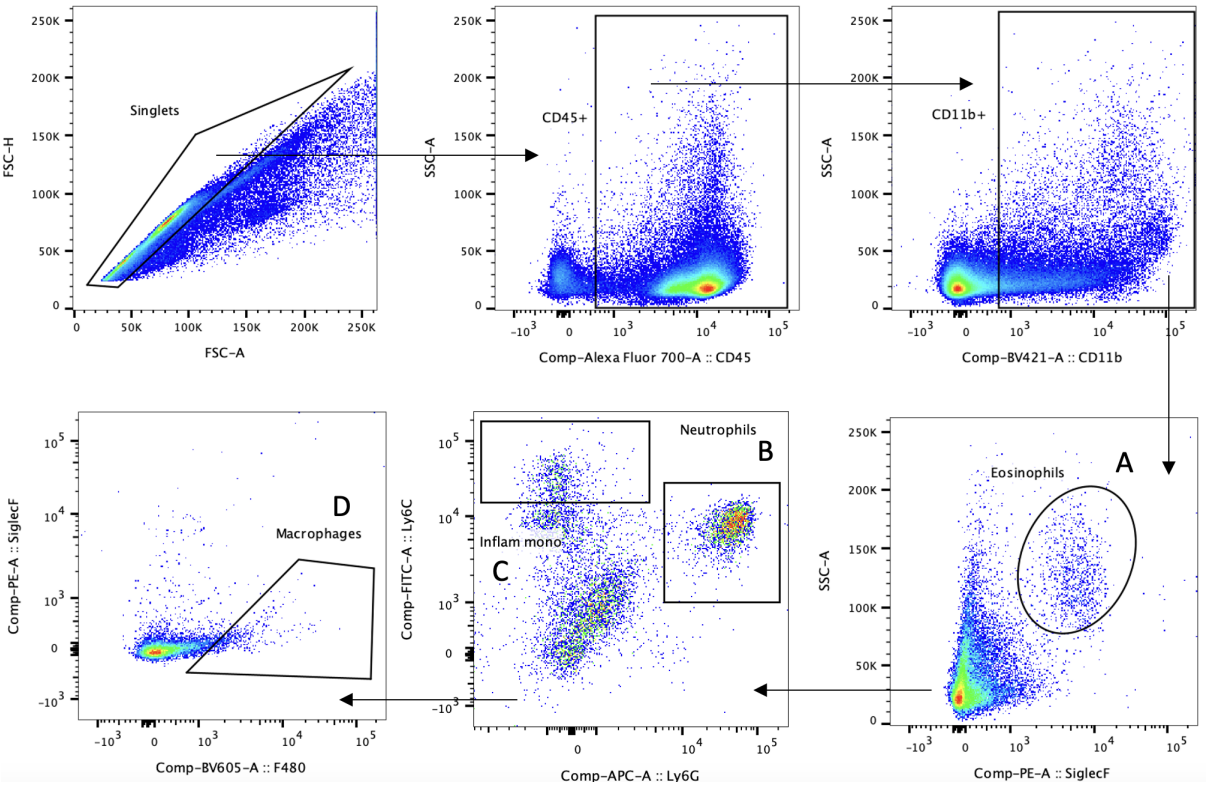

Supplementary Figure 4.1: FGT and iLN myeloid gating strategy. *At 2 days post fHPV-16 PsV infection, the FGT and iLN of each mouse was excised. These organs were prepared into single cell suspensions and stained with fluorochrome-conjugated antibodies. Samples were analysed by flow cytometry and the following populations*

were identified: (A) CD45+CD11b+Siglec-F+ eosinophils, (B) CD45+CD11b+Ly6G+ neutrophils, (C) CD45+CD11b+Lyc6C^{hi} inflammatory monocytes and (D) CD45+CD11b+F4/80+ macrophages.

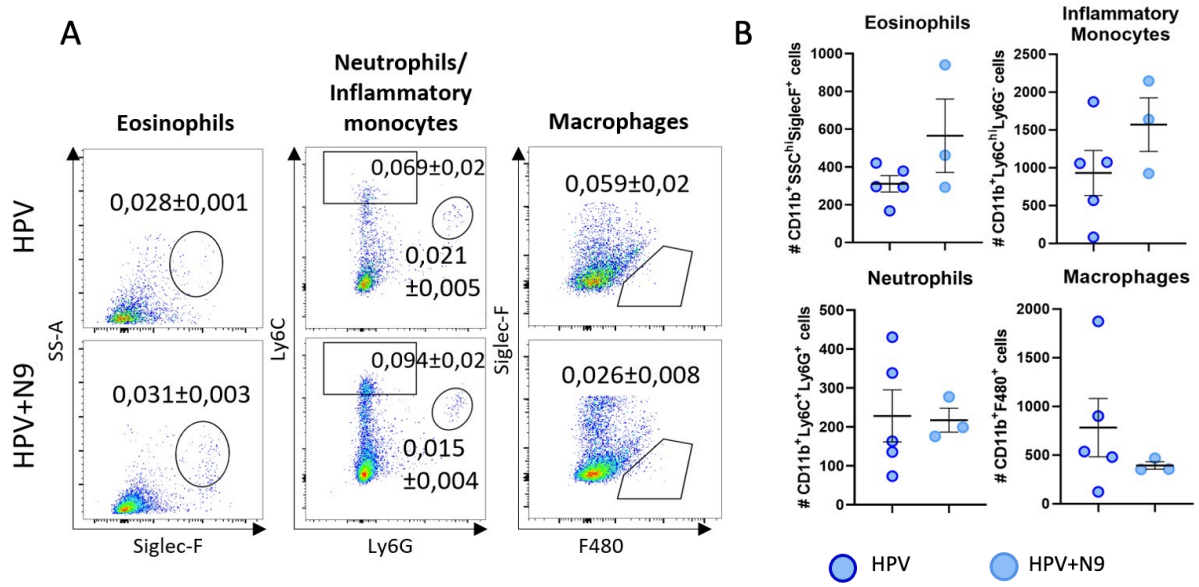

Supplementary Figure 4.2: N9 does not alter the innate immune cell profile in the iLN. *(A) Representative FACS plots with mean ± standard error of the mean (SEM) of proportion of CD11b^{+}SSC^{hi}Siglec-F^{+} eosinophils, CD11b^{+}Ly6C^{hi}Ly6G^{-} inflammatory monocytes, CD11b^{+} Ly6C^{+}Ly6G^{+} neutrophils, and CD11b^{+}F480^{+} macrophages of single cells in the iLN; (B) Cell numbers with mean ± standard error of the mean (SEM) of eosinophils, inflammatory monocytes, neutrophils and macrophages in the iLN. Data from one experiment where HPV only (n=5) and HPV+N9 (n=3). Cell populations gated on CD45+CD11b+ singlets. Error bars represent mean ± SEM. Statistical significance was calculated by Welch's t-test for normally distributed data and Mann-Whitney t-tests when data was not normally distributed.*

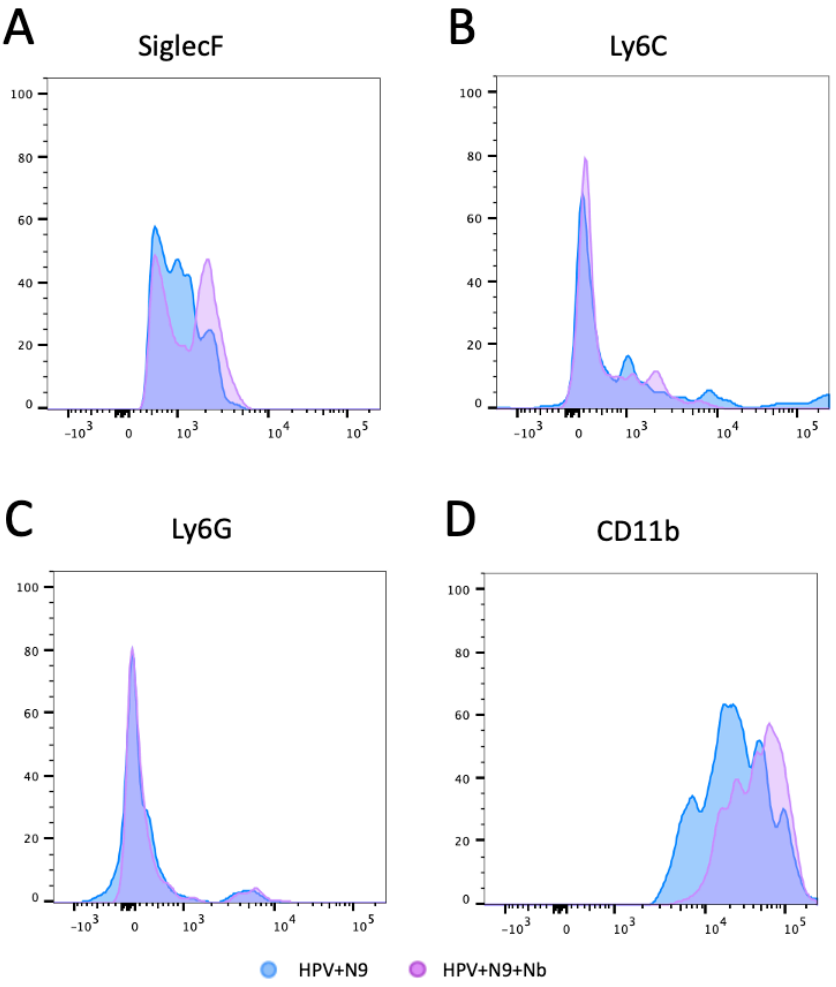

Supplementary Figure 4.3: **N. brasiliensis** ***somatic antigen exposure increases CD11b and Siglec-F expression of eosinophils in the FGT.*** *Histograms of (A) Siglec-F, (B) Ly6C, (C) Ly6G and (D) CD11b.*

Chapter 5: The effect of an STH infection on cervical cancer.

5.1 Introduction

While it has been shown that helminth infection increases host susceptibility to cancer-causing viruses in the FGT[193,249], it is poorly understood how a helminth infection affects cancer growth and behaviour in the FGT directly. As shown by Chetty et al., there is a type 2 immune environment and an induction of eosinophilia in the FGT of *N. brasiliensis*-infected mice[191]. Women with advanced (type III) CINs or cervical carcinomas had increased concentration of TSLP (the Th2-promoting cytokine), IL-10, as well as increased immunosuppressive cells, such as Tregs, at the lesion compared to women with lower (type I and II) CINs[205,206]. Additionally, eosinophils (recruited by TSLP), have been shown to increase proliferation and reduce apoptosis of cervical cancer cell lines *in vitro*[250]; and eosinophilic infiltrates were shown to correlate with reduced survival in human cervical cancer tumours[251].

Investigating the growth and progression of human cancers in murine models was made possible through the generation of immunocompromised mice. Nude mice have a genetic mutation in the *Foxn1* gene, resulting in hair loss and a deteriorated or absent thymus[212] (unable to produce T cells) and therefore unable to mount an immune response against and reject foreign tissue, such as engrafted tissue or tumour cells[213,252]. Similarly, severe combined immunodeficient (SCID) mice lack both B and T cells. Studies have shown that there is no difference in the growth of xenograft tumours between these two strains. However, there appears to be more frequent spontaneous metastasis in SCID mice[253]. Numerous studies have made use of the nude mouse model to assess the effects of various compounds on HeLa cell (experimentally depicting *ex vivo* cervical cancer) growth[254–258]. In these studies, female nude mice were subcutaneously inoculated with $1x10^6$ or more HeLa cells, with most papers choosing the right flank as an inoculation point to avoid inhibiting normal movement of the mouse. Some papers chose to use a BME to assist with tumour formation; one group showed that in the presence of BME, as few as $1x10^2$ HeLa cells could successfully form a tumour[259].

There are a number of methods of assessing the growth of these tumours (named xenografts). The simplest and most commonly used method is to measure the width and length of the tumour and calculate the volume of the tumour (Figure 5.1). More technical methods that are able to give more descriptive data, such as an accurate volume, include the use of luciferase-expressing or fluorescently labelled cells and track growth using the IVIS (Figure 5.2)[260].

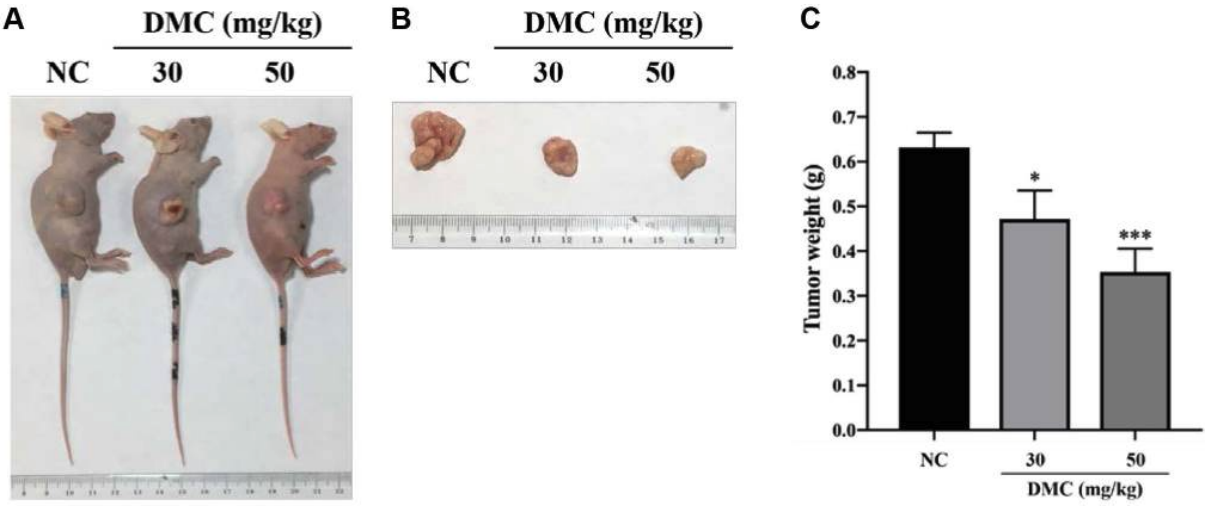

Figure 5.1: Example 1 – Antitumor evaluation of demethoxycurcumin (DMC) in xenografts in HeLa cell-bearing mice. *(A) The tumour growth of each mouse was monitored and representative tumours on control (NC) and DMC-treated (30 mg/kg and 50 mg/kg) mice from the three groups after 22 days of treatment are presented. (B) Representative tumours from three groups are shown. (C) DMC at both doses (30 and 50 mg/kg) significantly suppressed tumour growth when compared to the control group. Significantly different from the control at *p<0.05 and ***p<0.001. Images and data taken from Chueh et al., 2020*[255].

While imaging using the IVIS machine would have been the preferred method generating a generous source of data, in this project it was decided to use the simpler method of calliper measurements. This decision was reached because the fluorescently labelled cell lines were unavailable at the host institution and were expensive to import/produce. Additionally, mice would need to be anaesthetised for every image; repeated isoflurane use is known to cause multiple impairments such as cognitive and motor function, and changes in the cardiovascular system[261–263]. The negative side effects would not be ethical and would be an unnecessary procedure with the availability of an alternative method (callipers). Additionally, tumour

weight and cell counts can also be measured following euthanasia and tumour excision[255] following either method of tumour size monitoring.

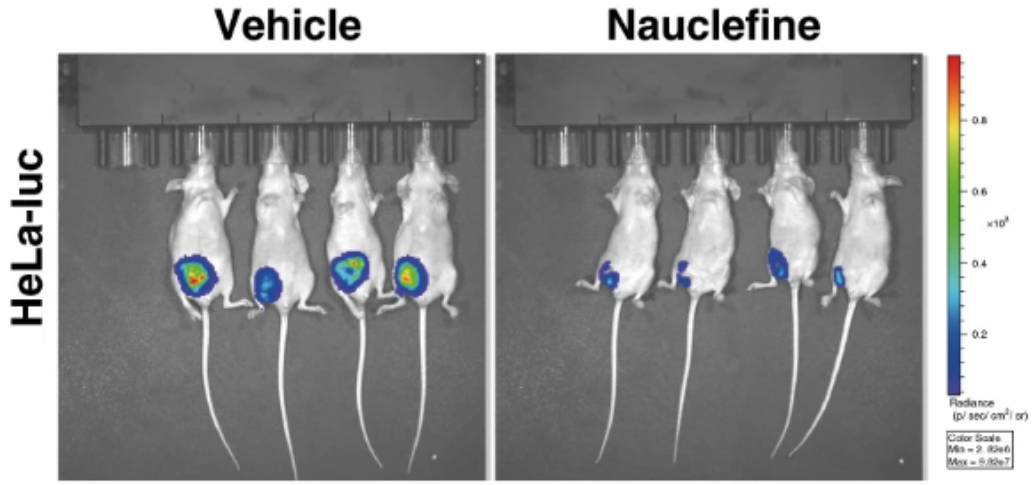

Figure 5.2: Example 2 - Nauclefine inhibits growth of human tumour xenografts in mice. *Mice (n = 4) implanted with WT or mutant HeLa cells were intratumorally injected with vehicle or nauclefine. The luciferase substrate was intraperitoneally injected to visualise tumour size. Adapted from Ai et al. 2020* [260].

A common cause of cancer is the development of a mutation or degradation of a tumour suppressor protein such as p53. Moreover, it is well known that >90% of cervical cancer cases can be attributed to an infection with an oncogenic HPV strain[142]. As mentioned, the proteins E6 and E7 of oncogenic strains of HPV interfere with p53 by promoting its degradation, and therefore allow the cell cycle to continue without assessing DNA damage[264]. P53 has not been shown to be significantly up- or down-regulated in cervical cancer compared to normal tissue[265] or to contain increased rates of mutations[266]. However, the downregulation of p53 has been associated with cervical cancer disease progression[267]. In intestinal helminth infections, p53 has been shown to be essential for type 2 immunity against helminths[268]. While the role of schistosome infection on p53 expression and mutation has been well researched, there is limited data on how soil-transmitted helminths may alter p53 expression.

Once a robust tumour has formed, cancer cells may change their phenotype by undergoing EMT. This renders the cancer cell more motile and increases its ability to invade surrounding tissue and eventually cause metastatic growths of the primary tumour. Distal tumours may invade lymph nodes and/or organs. These metastases are associated with poorer outcomes

and may lead to death if the cancer invades a vital organ. Previous studies have harboured conflicting results when investigating the effect of helminth exposure on markers of EMT. Some markers involved in EMT include β-catenin, E-cadherin and N-cadherin, which are further investigated in this chapter.

Below I investigate how STH infection may alter cervical cancer tumour growth and how p53 may be involved, as well as assess the metastatic potential of tumours in STH-infected mice through the quantification of EMT markers.

5.2. Results

5.2.1. Development of an *in vivo* murine model to assess how an STH exposure or infection alters cervical cancer growth.

The development of an *in vivo* mouse model was needed to explore the association between an STH infection and cervical cancer growth. A variety of papers used nude mice as the experimental animal. Murata et al. used various cell lines with or without the addition of BME. Almost all mice inoculated with HeLa cells with 1:1 BME supplementation grew tumours, with as few as $1x10^1$ HeLa cells, whereas mice inoculated with HeLa cells without BME only grew tumours when inoculated with $1x10^6$ HeLa cells[259]. This demonstrates how supplying a scaffold (BME) assists in the successful development of xenograft tumours. Various other studies have used this approach, with most using a 1:1 HeLa:BME ratio[255,258] and only one group successfully growing tumours without BME[269].

Due to the high cost of BME, I first attempted to develop this model by resuspending HeLa cells in PBS only[269]. Initially, to assess how exposure to STH antigens may alter cervical cancer growth, half of the nude mice received $5x10^5$ C33-A cells resuspended in PBS while the other half were inoculated with $5x10^5$ C-33A cells resuspended in PBS and 10µg *N. brasiliensis* somatic antigen. After 30 days, there was no sign of any tumour formation in any of the mice and the experiment was terminated (data not shown).

In a second attempt at developing the model without BME, half the mice were infected with 500 L3 *N. brasiliensis* nine days before cell inoculation. Due to the success seen in previous

literature using HeLa cells, this cell line was attempted at a higher concentration of $5x10^6$ HeLa cells per mouse, resuspended in PBS. After 28 days, what appeared to be small tumours were excised. Upon flow cytometric analysis, it was discovered that they were not tumours, but rather enlarged inguinal lymph nodes (data not shown).

It was then decided that using BME would be beneficial and more cost effective. Nude mice were infected with *N. brasiliensis* L3 as above. HeLa cells ($5x10^5$ per mouse) were combined with 1:1 BME in a total volume of 100µl per mouse. Initially, the tumours formed and did not disappear, but gradually reduced in size (Figure 5.3A). As expected, mice infected with *N. brasiliensis* lost about 10% body weight in the days following the infection (Figure 5.3B) and reached a maximum clinical score (Appendix 1) of 2. The mice quickly recovered and returned to their original body weight. At 2 weeks post HeLa cell inoculation, one tumour from the *N. brasiliensis*-infected mice completely disappeared. From this time point, the remaining 7 tumours began increasing in size (Figure 5.3A). Naïve mice continued to increase their body weight, whereas *N. brasiliensis* infected mice maintained a very slow weight increase (Figure 5.3B). Mice from both groups did not change from a clinical score of 0. Mice were sacrificed at 36 days post inoculation, as the largest tumour was nearing the humane endpoint of 1.7cm in length.

A second repeat was attempted with the above conditions; however, no tumours formed and any evidence of tumours had completely disappeared by day 9. Mice were monitored for 36 days whereby it was decided to terminate the experiment (data not shown).

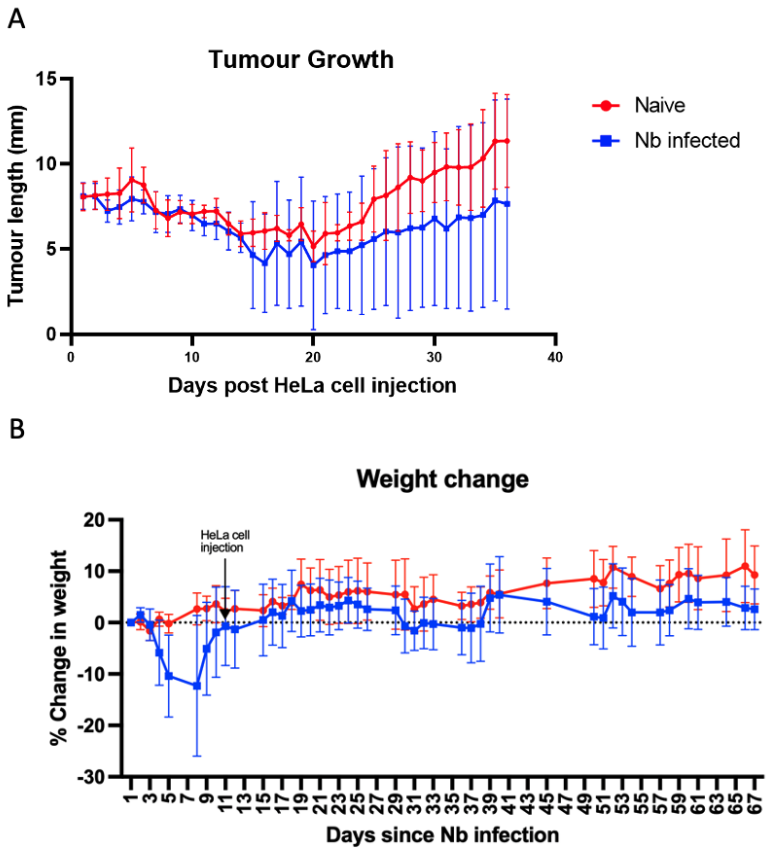

Figure 5.3: Change in tumour size and body weight with time. *(A) Longest length measurement of tumours taken daily with digital callipers. (B) Percent body weight change from baseline weight. Error bars represent mean ± SEM. Data are from one experiment where n=5 for each group.*

5.2.2. STH infection reduces cervical cancer tumour size.

While there was large variation between the two groups, there was a general trend towards reduced tumour size at 36 days post HeLa inoculation in the *N. brasiliensis*-infected mice (Figure 5.4A and B) and a significant reduction in tumour volume in *N. brasiliensis*-infected mice (p=0.048; Figure 5.4C). Interestingly, there appeared to be no difference in the number of live cells per tumour, indicating that the larger tumours from the naïve mice may have had large areas of necrotic tumour (Figure 5.4D). There was also a non-significant trend towards lower tumour weight in the *N. brasiliensis*-infected mice (Figure 5.4E). Please note, images of tumours were taken with the same scalpel blade on the left to ensure that all images of the tumours are within the same scale, and therefore accurately depicting tumour size difference.

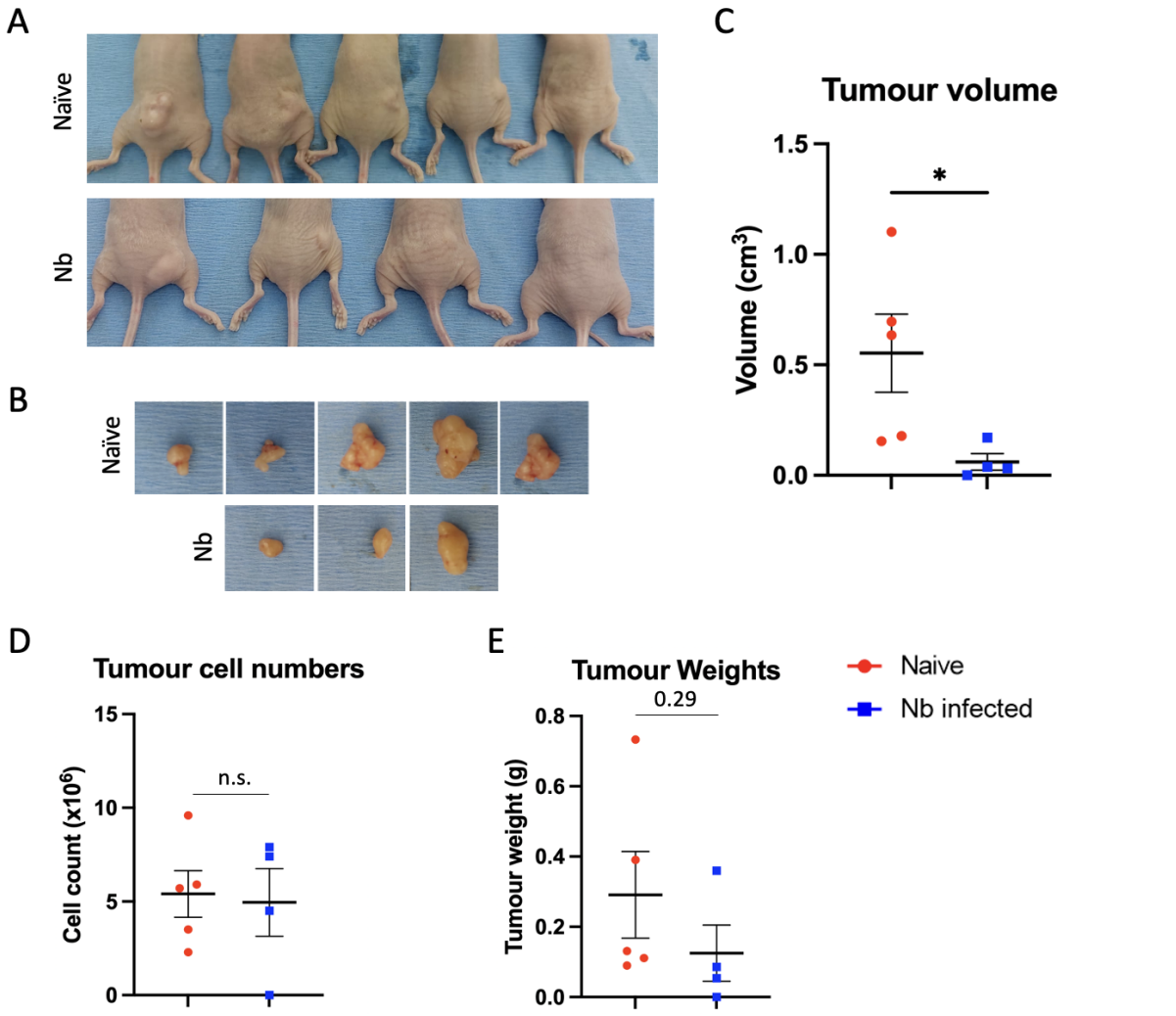

Figure 5.4: STH infection reduces cervical cancer tumour size. *(A) Image of mice with HeLa cell xenograft tumours after 36 days post inoculation. (B) Images of tumours of naïve (top) and* N. brasiliensis*-infected (bottom) mice. (C) Volume of tumours taken from (B). (D) Total live cell counts from tumour single cell suspensions. (E) HeLa xenograft tumour weights on day 36 post inoculation. Data are from one independent experiment where naïve n=5 and* N. brasiliensis*-infected n=4 (one mouse did not grow a tumour). A Welch's t-test was used to compare tumour volumes, cell numbers and weights. Error bars represent the mean ± SEM.*

5.2.3. STH infection does not significantly alter tumour immune cell infiltrates.

When mice were sacrificed on day 36, the tumours were excised and prepared as a single cell suspension for flow cytometric analysis (Supplementary Figure 5.1). When assessing the tumour immune cell infiltrates, it was found that the number of eosinophils, inflammatory monocytes, neutrophils, macrophages and alternatively activated (M2) macrophages infiltrating the tumour was unaffected by *N. brasiliensis* infection (Figure 5.5A-D graphs). There was also no difference in the proportion of eosinophils, inflammatory monocytes,

neutrophils, and macrophages (Figure 5.5A-D flow plots). There was, however, a trend towards an increase in the number and proportion of tumour infiltrating inflammatory monocytes (p=0.11; Figure 5.5B).

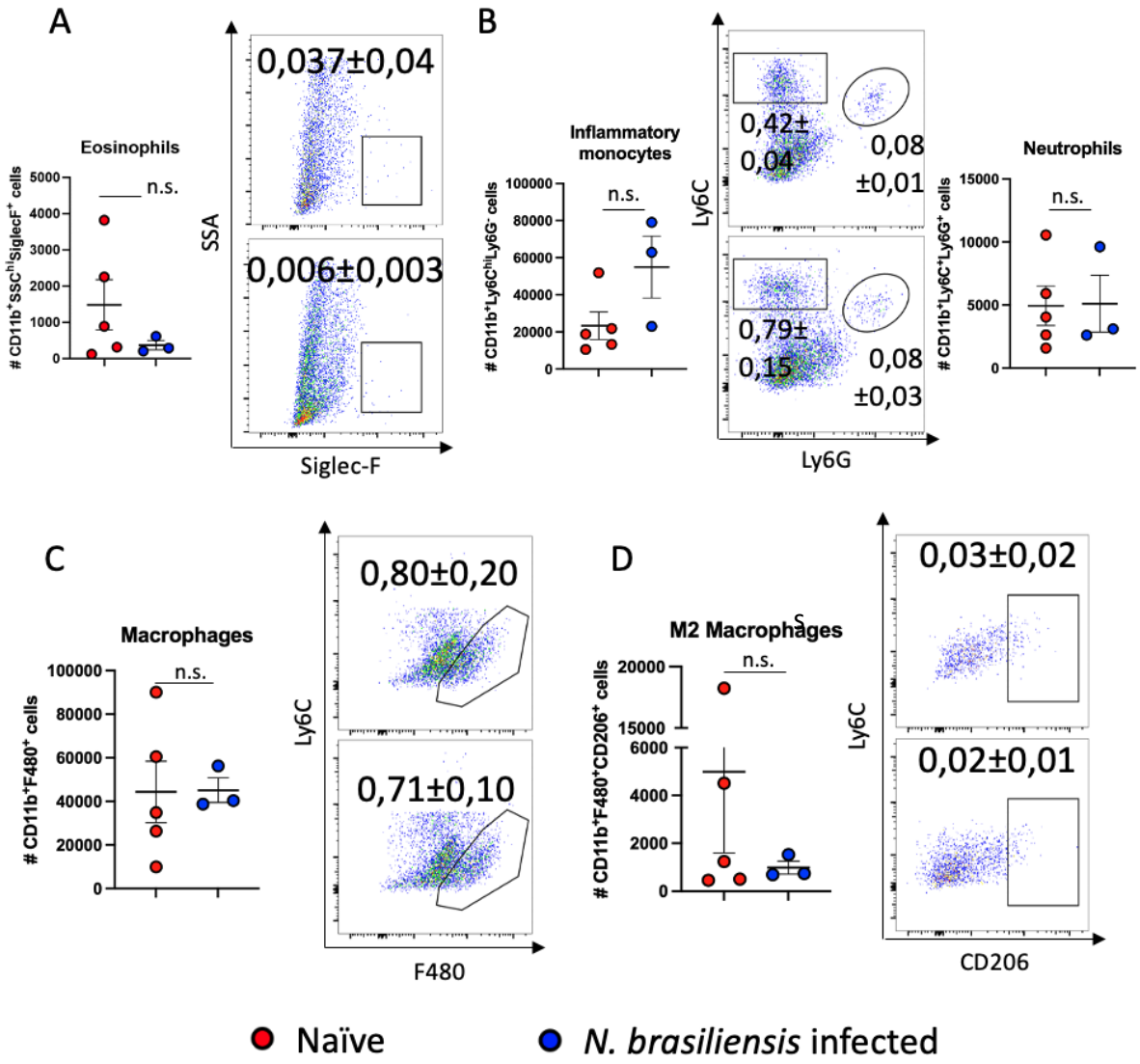

Figure 5.5: STH infection does not significantly alter tumour immune cell infiltrates. *Graphs represent the number of (A) CD11b+ SSC^{hi}Siglec-F+ cells (eosinophils), (B) CD11b+Ly6C^{hi}Ly6G- (inflammatory monocytes) and CD11b+Ly6C+Ly6G+ cells (neutrophils), (C) CD11b+F480+ cells (macrophages) and (D) CD11b+F480+CD206+ cells (M2 macrophages). Numbers on flow plots represent the proportion ± standard deviation of (A) eosinophils, (B) inflammatory monocytes and neutrophils, (C) macrophages and (D) M2 macrophages, of CD45+ single cells, where top flow plots are representative of the tumours from naïve mice and the flow plots below are representative of tumours from* N. brasiliensis*-infected mice. Cells gated on CD45+ single cells. Data are from one experiment, where naïve mice n=5 and* N. brasiliensis*-infected mice n=4 (one mouse did not grow a tumour). A Welch's t-test or Mann-Whitney t-test was used to compare numbers and proportions of immune cells between the two groups depending on the normality of data. Error bars represent mean ± SEM.*

5.2.4. STH infection alters EMT markers of cervical cancer cells.

The tumours excised above were additionally assessed for changes in markers of EMT (Supplementary Figure 5.2). Unsurprisingly, there was no change in the number or proportion of β-catenin, E-cadherin, or N-cadherin-expressing cells; all 3 markers are expressed by HeLa cells (Figure 5.6Ai, Bi, Ci). However, the mean fluorescence intensity (MFI), demonstrated by the geometric mean (GM), between the naïve and *N. brasiliensis*-infected mice was altered, indicating that the tumour cells from the two groups were expressing different amounts of the markers per cell. Mice previously infected with *N. brasiliensis* had a significant reduction in the expression of N-cadherin per cell ($p=0.003$; Figure 5.6Cii), as well as a trend towards reduced E-cadherin expression per cell ($p=0.08$; Figure 5.6Bii). There was a small population (17%) of cells that expressed both E-cadherin and N-cadherin, suggesting that their expression is not mutually exclusive (data not shown).

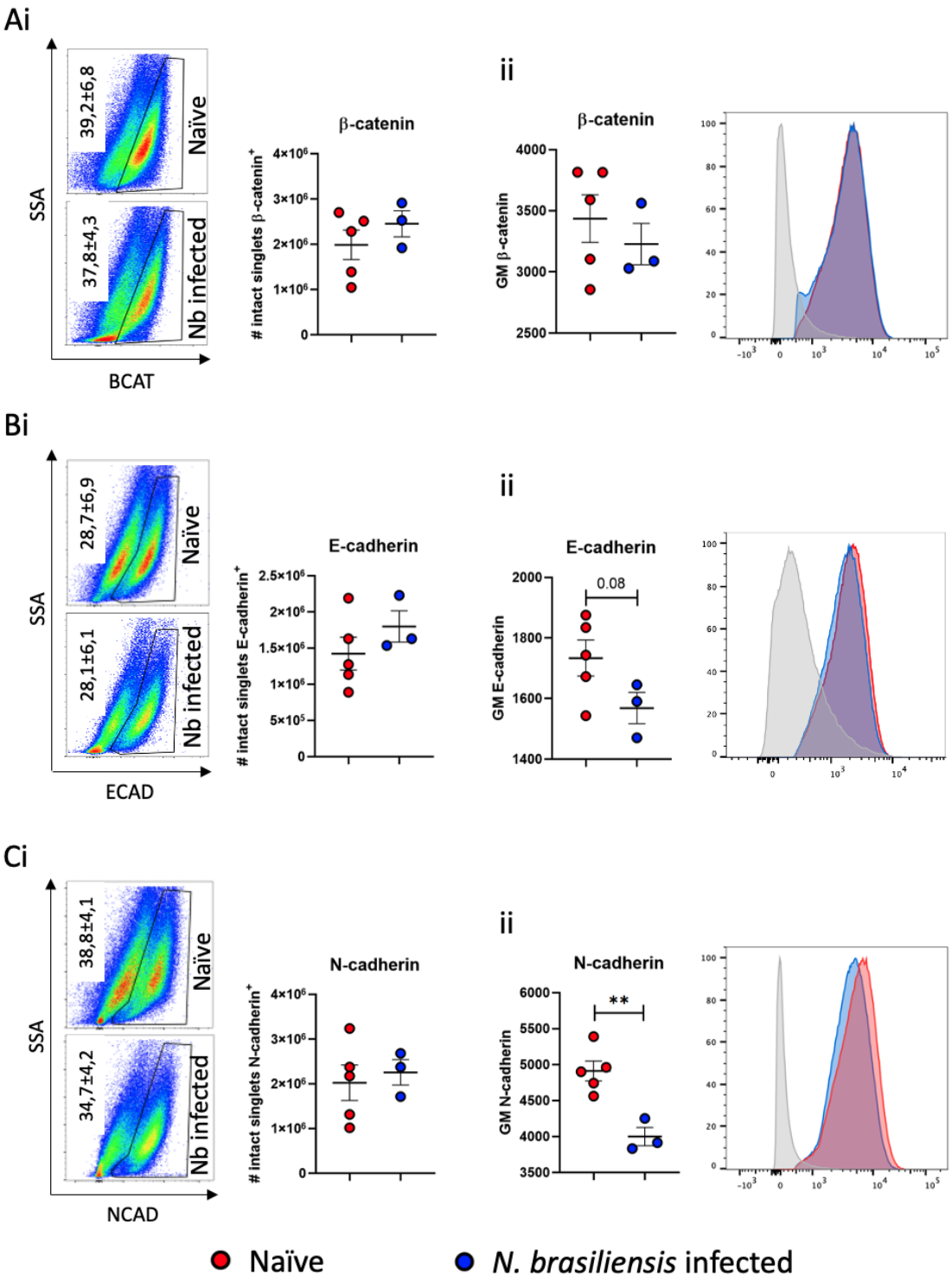

Figure 5.6: STH infection reduces the amount of EMT marker expression in HeLa cell tumours*. (i) Proportion of single intact cells (flow plots) and number of cells (graphs) expressing (A) β-catenin, (B) E-cadherin, and (C) N-cadherin. (ii) Geometric mean (MFI) of (A) β-catenin, (B) E-cadherin, and (C) N-cadherin. Grey peaks represent unstained control. Proportion of cells expressing each marker were calculated as the frequency of intact single cells. Data are from one independent experiment, where naïve n=5 and* N. brasiliensis*-infected n=4 (one mouse did not grow a tumour). A Welch's t-test was used to compare the proportion, number, and MFI between the two groups. Error bars represent mean ± SEM. *p<0.05, **p<0.01.*

5.2.5. Exposure to STH antigen alters p53 expression in a cervical cancer cell line.

The observed reduction in cervical cancer tumour growth prompted us to explore the anti-cancer abilities of various STH antigens. To assess this, I exposed the cervical cancer cell line, HeLa, to 50µg of *N. brasiliensis* somatic, NES, *H. polygyrus* somatic, HES or AES antigens, and assessed the expression of the tumour suppressor protein, p53, via western blot.

Being 53 kDa, I expected to see a protein of this molecular weight, which was seen in all three experiments. There was an observed trend towards an increase in p53 expression following exposure to both *N. brasiliensis* antigens. Contrasting results were obtained between the three experiments when assessing the expression of p53 of HeLa cells following exposure to HES and AES (Figure 5.7A and B).

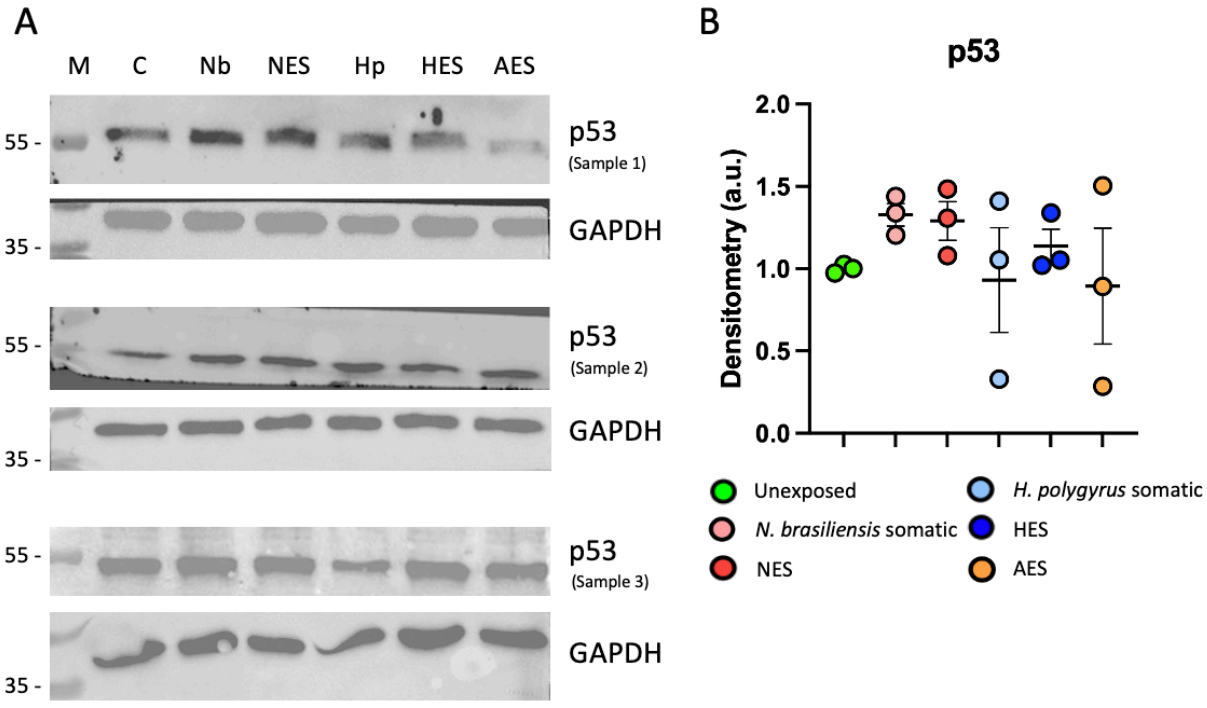

Figure 5.7: **N. brasiliensis *antigen exposure alters p53 expression***. *Images of western blots of p53 expression following HeLa cell exposure of* N. brasiliensis *somatic (N) and ES (NES) antigen,* H. polygyrus *somatic (Hp) and ES (HES) antigen and* A. lumbricoides *ES (AES) antigen for 12h. (B) Densitometry readings of p53 expression. Data from three independent experiments. Statistical significance was calculated using a Brown Forsythe and Welch ANOVA to compare densitometry to unexposed cells. Densitometry readings were normalised to the average of the unexposed cells. Error bars represent mean ± SEM.*

5.2.6. STH antigen exposure alters EMT marker expression of cervical cancer cells.

To further explore how STH exposure alters cervical cancer properties, I assessed the expression of the two EMT markers, namely β-catenin (88 kDa) and N-cadherin (127 kDa), on STH antigen-exposed HeLa cells. These cells were exposed to 50µg of *N. brasiliensis* somatic, NES, *H. polygyrus* somatic, HES or AES antigens, and EMT expression was assessed via western blot.

Proteins were seen at the expected sizes. Similarly, no significant changes could be calculated due to the sample size, but there did not appear to be any alteration in the expression of β-catenin (Figure 5.8A and C). However, there appeared to be an increase in the expression of N-cadherin following exposure to *N. brasiliensis* somatic antigen (Figure 5.8B and C).

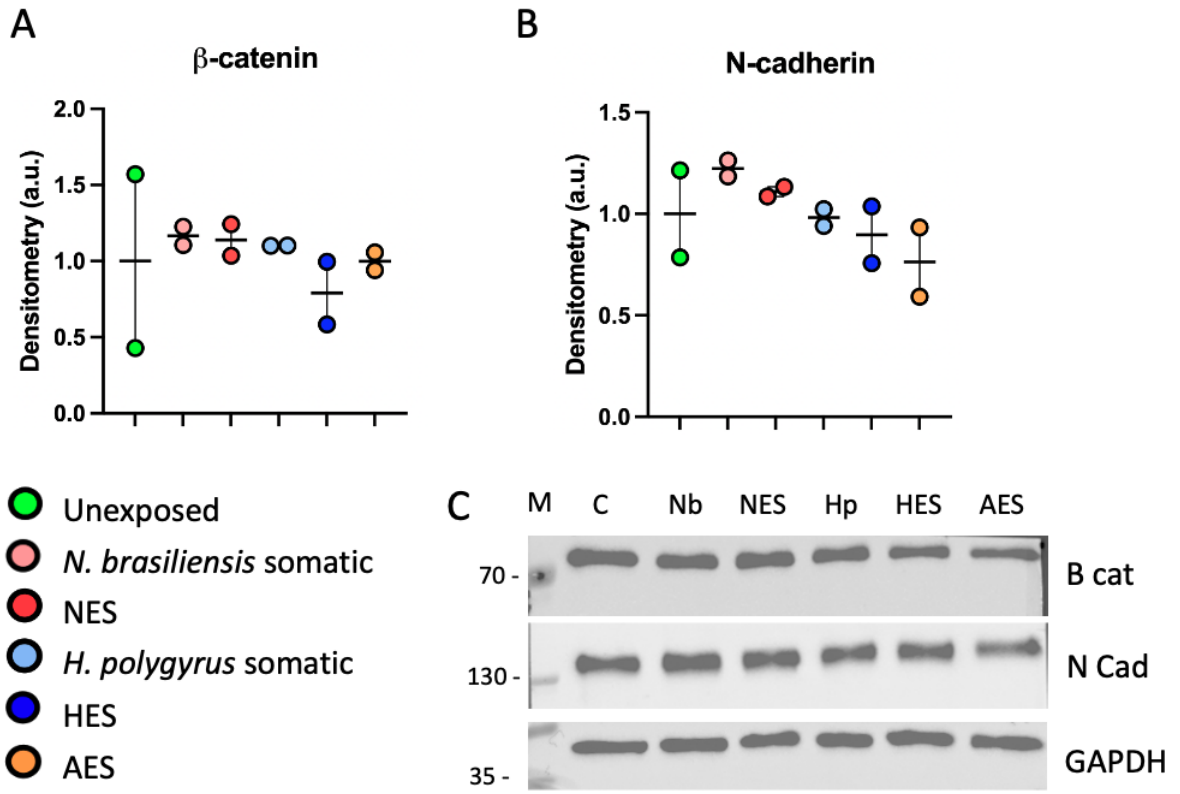

Figure 5.8: N. brasiliensis antigen exposure alters N-cadherin expression*. Densitometry normalised to GAPDH of (A) β-catenin (B cat) and (B) N-cadherin (N cad) expression of HeLa cells following 12hr exposure to* N. brasiliensis *somatic and ES antigen,* H. polygyrus *somatic and ES antigen and* A. lumbricoides *ES antigen. (C) Representative western blot. Data are from two independent experiments. Brown-Forsythe and Welch ANOVA test was used to compare densitometry values to unexposed cells. Densitometry readings were normalised to the average of the unexposed cells. Error bars represent mean ± SEM.*

5.3. Discussion

The data presented in this chapter indicate that an STH infection may reduce cervical cancer growth, possibly due to an increase in p53 expression. However, due to decreased expression E- and N-cadherin on xenograft tumours, the effect of STH infection on these EMT marker expression appears to be conflicting.

Due to the COVID-19 pandemic as well as the difficulty of the model, it was not possible to perform more than one successful repeat of the xenograft experiment, despite many attempts. The COVID-19 pandemic slowed down the animal breeding unit to the point where breeding was only occurring to maintain strains. Once breeding resumed, it was difficult to acquire the number of female mice needed in a narrow age range.

As mentioned, HeLa cells are a human cervical cancer-derived cell line that has a history of HPV-18 infection. Since the rest of this thesis focusses on HPV, this cell line was preferred over the HPV-negative cell line C-33A to assess subsequent cervical cancer progression as the cervical cancer from which the C-33A cells were originated from was not caused by an HPV infection.

While there was large variability in tumour sizes within each group (Figure 5.3A and Figure 5.4A-C; E), there was a trend toward a reduction in tumour growth in *N. brasiliensis*-infected mice as well as significantly smaller tumours (in terms of volume) following 36 days of tumour growth (Figure 5.4B). As mentioned, one mouse did not develop a tumour. It is unknown whether this was due to an unsuccessful inoculation or whether the *N. brasiliensis* infection played a role.

It is well known that one of the early signs of cervical cancer is weight loss[142]. However, the mice in both groups did not appear to lose weight when the tumours were established (Figure 5.3B). This result may highlight the limitations of the *ex vivo* xenograft model, indicating that while it is an appropriate model to assess tumour growth, it does not fully reflect the systemic and location-specific effects that cervical cancer may impose, or include the anti-tumour

effect of T cells. The regression of solid tumours has been shown to be largely due to tumour infiltrating T cells, whereas this infiltration is not observed in non-regressing tumours[270]. These T cells kill cancerous cells in a similar manner to graft rejection; the cells are recognised as foreign, through presentation of mutated gene products[271]. The production of IFN-γ by CD4+ Th1 cells has been shown to be a vital component of anti-tumour immunity[272]; its release leads to the production of various molecules involved in direct (granzymes and perforins[273]) or indirect (anti-angiogenic factors[274]) killing of tumour cells. Given that STH infection results in the polarisation of T cells towards Th2 and favourable prognosis is seen in tumours with Th1 tumour-infiltrating CD4+ T cells[275], it is important to investigate how this STH-induced polarisation may alter the anti-tumour effect of T cells.

It was interesting to note that while the tumours in *N. brasiliensis*-infected mice were smaller than those in naïve mice (Figure 5.4A-C; E), there were comparable numbers of live cells in each tumour (Figure 5.4D). This may indicate that the larger tumours from the naïve mice may have had areas of necrosis. This is a well-known phenomenon in rapidly growing tumours; cells proliferate faster than the blood vessels can grow, resulting in nutrient-deprived areas of the tumour and eventually these cells will die[276].

Flow cytometric analysis of the tumours showed that there was a large number of CD45+CD11b- cells within the tumour. While CD11b is a myeloid marker, certain subtypes of macrophages and dendritic cells do not express CD11b[277,278]. Additionally, these cells could be NK cells or B cells[279,280], which are still produced by nude mice.

Due to the increase in peripheral eosinophils noted in Chapter 4, I was interested in investigating whether *N. brasiliensis* infection would affect eosinophil and other immune cell infiltrates of the tumours. It has been shown that, in cervical cancer, there is increased eosinophil infiltration as the tumour progresses[278], initiated by increased levels of TSLP (which also promotes tumour angiogenesis[281]). However, this increase in eosinophil infiltration could be as a result of the tumour progressing and not the reason that the tumour is progressing. Conversely, IL-33 has been shown to be raised in the FGT of *N. brasiliensis*-infected mice[279]. This alarmin has been shown to be indirectly involved in the recruitment of eosinophils through the upregulation of CCL11 and stimulation of ILC2s (which in turn produce IL-5 to

recruit eosinophils)[282]. Once the eosinophils infiltrate the tumours, they degranulate, through mechanisms such as danger signals from necrotic cells, cytokines such as IL-33, activation by other immune cells and antibody-mediated crosslinking, which leads to tumour cell cytotoxicity and reduced tumour growth[282,283]. This was an attractive theory when I started to notice that the tumours of infected mice began growing at a slower rate than the tumours of naïve mice. However, upon investigation, it was found that there was no difference in the number or proportions of tumour infiltrating eosinophils of *N. brasiliensis*-infected mice (Figure 5.5A). These eosinophils do appear to be lower side scatter (50k-125k) compared to standard Balb/c mice (100k-200k). This has been shown previously to be a feature of eosinophils from nude mice[284].

There was, however, a trend towards an increase in tumour infiltrating inflammatory monocytes in tumours from *N. brasiliensis*-infected mice (Figure 5.5B). The lack of significance may be due to the low sample size of tumours from *N. brasiliensis* infected mice, therefore rendering the experiment underpowered. These monocytes may have differing roles in tumour progression depending on the stage of tumour growth. During primary tumour formation, classical monocytes suppress T cell functions[285,286], promote angiogenesis[287] and extracellular matrix remodelling to favour metastasis[288], through differentiating into tumour-associated macrophages (TAMs). They have also been shown, in *in vitro* studies, to promote tumour cell cytotoxicity[289]. During the later stages of tumour growth, these monocytes continue to be recruited and differentiate into TAMs and encourage tumour progression and metastasis[290,291]. This therefore indicates that inflammatory monocytes may result in increased tumour growth, immune evasion and metastasis. My finding that tumour infiltrating inflammatory monocytes may be increased in STH-infected mice was therefore surprising, as a decrease in growth was observed. However, this finding may also indicate that STH infection may increase infiltrating inflammatory monocytes and increase the tumours metastatic potential.

Increased activation of the canonical (β-catenin dependent) Wnt signalling has been observed in numerous solid cancers[292,293]. During canonical Wnt signalling, β-catenin has been shown to accumulate in the nucleus where it acts as a transcription factor for many cell cycle-promoting genes[294,295]. Activation of this pathway is also linked with EMT induction, as

canonical Wnt signalling inhibition resulted in reduced EMT marker expression (vimentin and Snail) and inhibited cell invasion[296]. Therefore, its overexpression has been linked to increased tumorigenesis. B-catenin also associates with E-cadherin, a well-known cell adhesion molecule[297]. Loss of E-cadherin (discussed below) frees the cytoplasmic β-catenin, allowing it to relocate to the nucleus[298]. One study showed that exposure of a murine colorectal cancer cell line to the intestinal worm *H.* polygyrus resulted in an increased expression of β-catenin, whereas exposure of a human colorectal cancer cell line to the same antigen resulted in a reduced expression of β-catenin[294]. These data suggest that the alteration in the expression of β-catenin following exposure to helminth antigen may be species-specific. In contrast, the current data showed that there was no change in β-catenin expression by HeLa cells *in vitro* (Figure 5.8A and C) or in tumours from *N. brasiliensis*-infected mice (Figure 5.6Ai and ii). The discrepancy between our data and those published by Jacobs et al. may reflect the difference in STH species, cancer type and experimental procedure. The exposure of HeLa cells to helminth somatic antigen may not accurately reflect physiological conditions, as it is highly unlikely that a high enough concentration of somatic antigen will reach systemic sites to influence tumour progression during helminth infection. Together, this suggests that STH exposure/infection may, in this setting, have no effect on canonical Wnt signalling, and the observed reduction in cervical cancer tumour growth is therefore unlikely to be due to an alteration in β-catenin signalling.

As stated above, E-cadherin is an extracellular cell adhesion protein that binds to β-catenin in the cell cytoplasm[298]. A reduction in E-cadherin frees the cytoplasmic β-catenin, allowing the β-catenin to translocate to the nucleus and stimulate the Wnt pathway[294,295]. Therefore, a loss of E-cadherin would result in reduced cell adhesion and potential increased canonical Wnt signalling and is therefore associated with EMT. E-cadherin was found to be reduced in the colonic epithelial cells of *H. polygyrus*-[299] and *N. brasiliensis*-infected mice[300], suggesting that the epithelial barrier may be compromised. In the current study, it was only possible to explore E-cadherin expression in an *in vivo* experiment. While the number of cells that expressed E-cadherin was unchanged, there was a trend towards a decrease in the amount of E-cadherin expressed per cell in the tumours of *N. brasiliensis*-infected mice, indicated by the lower geometric mean of tumour cells from mice infected with *N. brasiliensis* (Figure 5.6Bi and ii). When taken together with the data observed for β-catenin expression, there does not

appear to be a relationship between the two markers in terms of EMT. A reduction in E-cadherin expression would suggest an increase in the amount of free β-catenin to translocate to the nucleus. However, as discussed above, there appears to be no change in the amount of β-catenin on the cell surface or in the cytoplasm (Figure 5.6Ai and ii) or throughout the cell, including the nucleus (Figure 5.8A and C).

N-cadherin is a mesenchymal cell marker and is not expressed by normal epithelial cells. It is involved in the cell adhesion of various cell types, such as neural, muscle and migratory fibroblast (mesenchymal) cells. During EMT, there is a switch from E-cadherin to N-cadherin, which results in the cell losing polarity and becoming spindle shaped and motile[301]. This occurs through the increased expression of the transcription factor Snail; over-expression of Snail was shown to be a potent suppressor of E-cadherin expression[302] and Snail expression positively correlated with N-cadherin expression[303], suggesting that Snail may be the driver of this cadherin switch and ultimately EMT. Jacobs et al. showed that exposure of HeLa cells to *N. brasiliensis* somatic antigen had no effect on N-cadherin expression, as well as no effect on N-cadherin expression in murine genital tracts when mice were infected with *N. brasiliensis*[268]. In the current study, when HeLa cells were exposed to various STH antigens, there did not appear to be a change in N-cadherin expression (Figure 5.8B and C), in agreement with the abovementioned data. There was, however, a minor increase in N-cadherin expression when cells were exposed to *N. brasiliensis* antigen, however no statistical significance can be drawn from this experiment. Similarly, the number of cells expressing N-cadherin remained unchanged in an *in vivo* setting (Figure 5.6Ci). However, when mice were infected with *N. brasiliensis,* there was a clear reduction in the amount of N-cadherin expressed by tumour cells (Figure 5.6Cii). This may suggest that, while the number and proportion of tumour cells that express N-cadherin is comparable, the amount of N-cadherin that each cell expressed was reduced by *N. brasiliensis* infection. This may suggest that these tumour cells are less mesenchymal, which may be indicative of reduced potential invasion and metastasis.

Lastly, p53 is a tumour suppressor protein. As mentioned in Chapter 1, this protein is critical in halting cell division if there is DNA damage or cellular stress in order to prevent uncontrolled cell division and ultimately cancer. This may result from a mutation in or the loss

of expression of p53. A previous study has also revealed that p53 is important in anti-helminth immunity[197]; its expression by tuft cells in the intestine is involved in the release of IL-25 and ultimately triggers the type 2 immune response, while clearance of helminth infection was abrogated with p53 knockout due to the inability to mount an anti-helminth type 2 response. Exposure of human and murine colon cancer cell lines to the antigen of *H. polygyrus* revealed an increase in the expression of p53, as well as another cell cycle arrest protein p21[300]. Although only a trend was observed, HeLa cell exposure to *N. brasiliensis* proteins in the current study appeared to result in a trend toward increased expression of p53, whereas exposure to HES and AES led to a more variable response. Together with published findings, these data suggest that different STH species may alter p53 expression differentially depending on the STH species and site of sampling. This increase in p53 expression may have contributed to the reduced growth of cervical cancer tumours in mice infected with *N. brasiliensis*, by arresting the cell cycle to allow for cellular repair or apoptosis[304]. Given a published role for p53 in anti-helminth immunity, it is understandable that this may be a target for helminths. They could secrete a molecule capable of entering a cell that is able to inhibit the expression of p53 and thus reduce the immune response elicited. This may explain why some helminth infections, such as schistosomiasis, are carcinogenic.

Together, these findings suggest that an STH infection may reduce the rate of cervical cancer growth, whilst potentially promoting DNA repair and encouraging apoptosis through and upregulation of the tumour suppressor protein p53. These helminth antigens could be further studied and assessed for the molecules that may be involved in the observed reduction of tumour growth, reduction of EMT marker expression and increased p53 expression to develop novel anti-cancer therapeutics.

5.4 Supplementary material

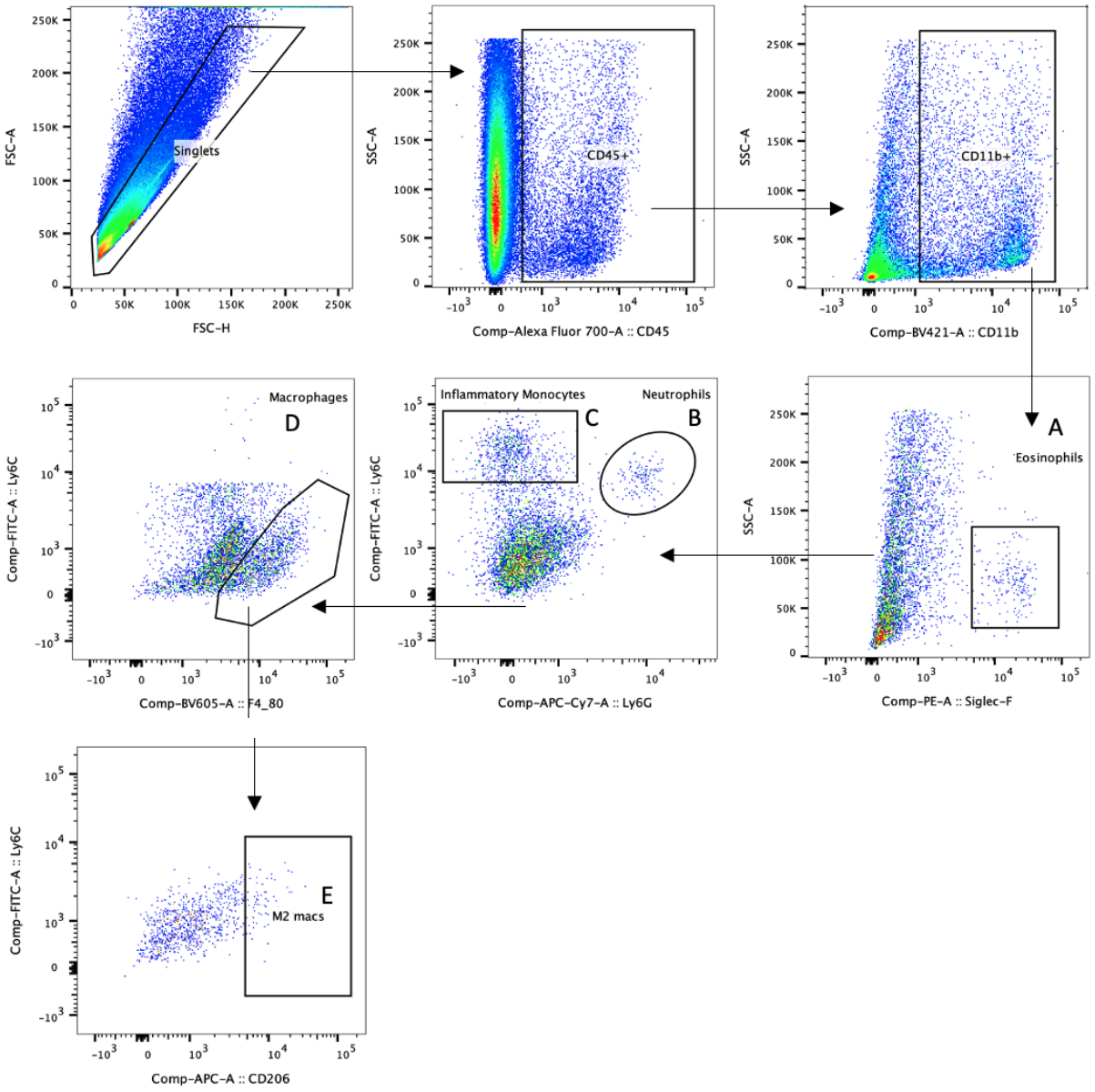

Supplementary Figure 5.1: HeLa cell xenograft myeloid cell infiltrates. *At 36 days post HeLa cell inoculation, the tumour of each mouse was excised. They were prepared into single cell suspensions and stained with fluorochrome-conjugated antibodies. Samples were analysed by flow cytometry and the following populations were identified: (A) CD45+CD11b+Siglec-F+ eosinophils, (B) CD45+CD11b+Ly6G+ neutrophils, (C) CD45+CD11b+Lyc6C^{hi} inflammatory monocytes, (D) CD45+CD11b+F4/80+ macrophages and (E) CD45+CD11b+CD206+ M2 macrophages.*

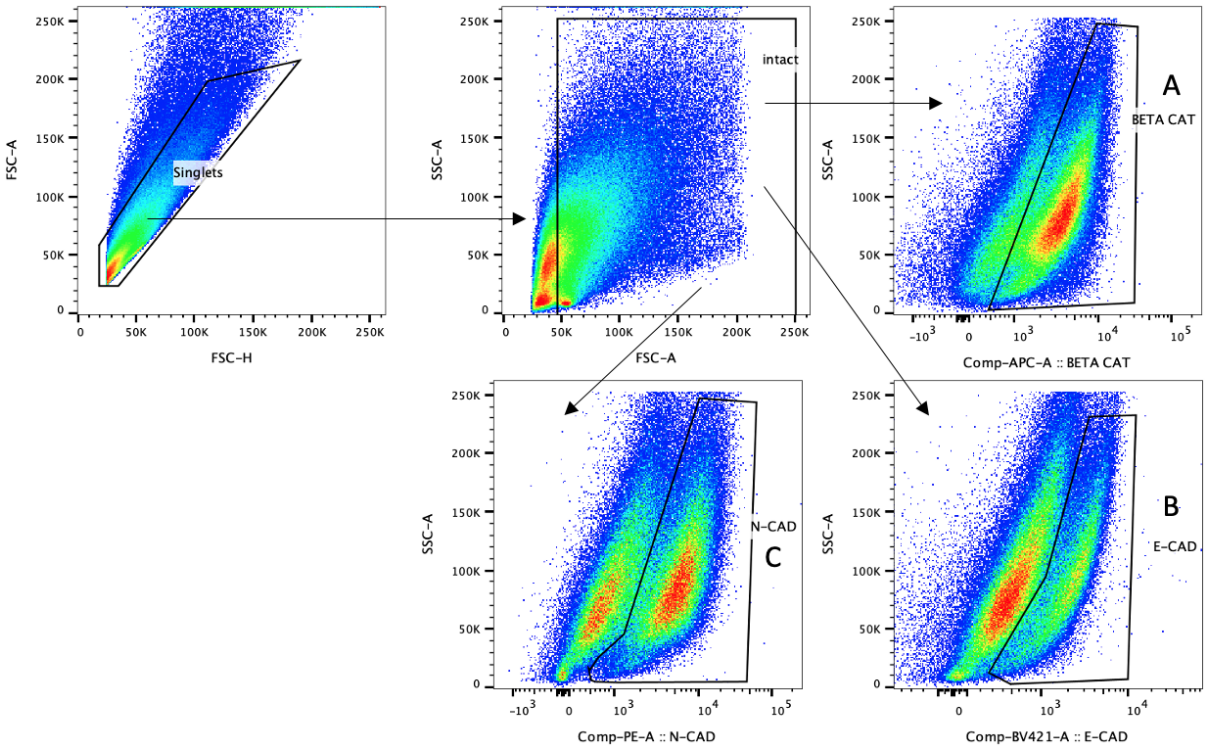

Supplementary Figure 5.2: HeLa cell xenograft EMT marker gating strategy. *At 36 days post HeLa cell inoculation, the tumour of each mouse was excised. They were prepared into single cell suspensions and stained with fluorochrome-conjugated antibodies. Samples were analysed by flow cytometry and the following populations and MFIs were identified: (A) β-catenin+ cells, (B) E-cadherin+ cells and, (C) N-cadherin+ cells.*

Chapter 6: Concluding remarks.

6.1 Summary of results

Through work performed in this thesis, I have demonstrated, both *in vitro* and *in vivo*, that a gastrointestinal helminth reduces HPV-16 PsV infection. *In vitro*, decreased HPV infection was associated with a trend toward increased vimentin (HPV restriction molecule) expression. *In vivo*, decreased HPV-16 PsV infection was dependent on helminth-induced IL-5-dependent immune cell populations, including eosinophils, and independent of HPV-receptor and restriction factor expression. Preliminary experiments utilising a pre-clinical model of cervical cancer cell growth showed that helminth infection reduced tumour volume, E-cadherin and N-cadherin expression, and increased p53 expression.

Initial exploration of the relationship between STH exposure and HPV-16 PsV infection required the development and optimisation of an *in vitro* assay. Exposure of cell lines to various STH antigens resulted in dose-dependent decreased in gHPV-16 PsV infection. The decrease in gHPV-16 PsV infection could be due to an increase in the expression of vimentin, a molecule known to inhibit HPV infection[192]. This supports the published work of Jacobs et al. who showed that cell exposure to *N. brasiliensis* somatic antigen resulted in a decreased uptake of fluorescently labelled HPV-16 PsVs[193,194]. This is, however, in contrast to epidemiological studies that found that an STH infection was associated with increased odds of having an HPV infection[191]. It is important to note that the model developed in Chapter 3 explored the initial infection of the virus, and not a sustained, long-term infection. From these data, we can conclude that STH antigens contain a molecule that is able to inhibit HPV PsV infection, however the exact mechanism remains unknown.

Further investigation into this relationship led to the development of an *in vivo* assay. This assay allowed me to validate the findings from my *in vitro* studies: both vaginal exposure and live infection with the STH *N. brasiliensis* resulted in protection against fHPV-16 PsV infection. Live infection of mice resulted in eosinophilia in both the FGT and iLN, which is in keeping with published literature[191]. These eosinophils were recruited to the FGT and displayed a more anti-inflammatory phenotype. Through antibody depletion experiments, it was shown

that an IL-5 dependent immune cell population, including eosinophils, was strongly involved in the protection against fHPV-16 PsV infection. Chetty et al. determined that the STH-induced eosinophilia in the FGT resulted in increased epithelial damage, which resulted in worsened HSV-2 pathology in mice[193]. It is unclear why the eosinophilia in the FGT in the current study did not cause increased epithelial damage. Or, if there was increased epithelial damage, why this did not cause an increase in fHPV-16 PsV infection through increased access to the basal keratinocytes. While human studies by Gravitt et al.[195] and Omondi et al.[142] showed a positive correlation with increased IL-5 in the FGT of STH-infected women, no data has been published showing FGT eosinophilia in STH-infected women. Further investigation is required to determine how eosinophils protect the FGT epithelium from fHPV-16 PsV infection, however a potential explanation may be that it is as a result of eosinophils also being involved in tissue repair; these eosinophils may have repaired or limited the epithelial damage caused by pre-treatment with N9.

As around 99% of cervical cancer cases can be attributed to a persistent HPV infection[192], investigating the relationship between a STH infection and its effect on cervical cancer growth and behaviour was a logical next step. While the hypothesis was, due to the eosinophilia and type 2 immune environment induced by an STH infection, that an STH infection may increase the growth of cervical cancer cells, it was found that an STH infection actually reduced cervical cancer growth, as shown in a novel *in vivo* xenograft model. No alteration in immune cell infiltrates were observed, however this decrease in tumour volume may be attributed to an increase in p53 expression (and therefore increased cell cycle arrest and apoptosis). These data should be interpreted with caution as it was not possible to assess the p53 expression of the xenografts, but rather only to STH antigen-exposed cells. A mixed EMT marker expression profile was observed in the tumours of *N. brasiliensis*-infected mice when assessing the expression of E-cadherin and N-cadherin. This is supported by a study published by Jacobs et al. who found that HeLa cell exposure to *N. brasiliensis* somatic antigen resulted in decreased N-cadherin expression[192]. In this study, it was also found that this was associated with an increase in cell migration[195], suggesting that STH exposure/infection may increase EMT potential of cervical cancer tumours. However, these data are from *in vitro* data, which may not accurately reflect *in vivo* environments.

6.2 Limitations

While the data in this thesis provide robust preliminary data exploring the relationship between STH infection and HPV infection and cervical cancer growth, there are a few limitations to this study. As discussed, there are a number of differences in the immune systems of mice and humans. Therefore, anti-viral immunity in the FGT of a human may not respond the same as in that of a mouse, and protection may not be equal. This *in vivo* model, developed to assess the relationship between STH infection and HPV-16 PsV infection, required the use of N9, which causes epithelial disruption. While one can argue that this should not be too different in the case of human HPV infection (N9 is used in the lubricant of condoms and in the case of intercourse without a condom, there would also be epithelial damage that occurs), this chemical may have unknown effects which were not explored in this thesis on the immune environment of the FGT and therefore on the anti-viral response.

Additionally, the xenograft model assessing the effect of STH infection on cervical cancer development comes with two main limitations. Firstly, the cervical cancer tumour is grown *ex situ;* i.e. the tumour is grown in the flank as opposed to the FGT. Omondi et al. showed that the peripheral plasma cytokine expression did not mirror that of the cytokine expression in the vaginal washes of STH-infected women[270]. This may suggest that the cervical cancer tumour in the flank may not have been exposed to a similar immune environment and therefore may not respond as it would if grown *in situ*. Lastly, the control of tumours is largely reliant on the cytotoxic effect of T cells[191]. Given that this model used nude mice, which are athymic, we are not able to assess the effect of T cells on cervical cancer growth. This may be significant as Chetty et al. has demonstrated a Th2 immune profile in the FGT of STH-infected mice[205,206]; a Th2 immune profile has additionally been associated with higher grade CIN[301].

6.3 Future work

These preliminary data demonstrating the effects of STH infection in the FGT of female mice leaves much to be explored.

The experiment assessing whether the molecule in the helminth antigens responsible for the reduction in gHPV-16 PsV infection was heat liable did not contain a non-heat-treated control.

Repeating this experiment with the non-heat-treated control would make for stronger results.

While this work specifically explored the effect of STH infection on the *initial* stages of HPV infection, the effect of STH infection on an established HPV infection would provide more representative insights into human scenarios. This could only be achieved through the use of murine papillomavirus (MmuPV), as HPV cannot replicate in murine keratinocytes and form an established infection[305]. These results may provide further insight into why the data in this thesis contradicts those of epidemiological studies[195].

Since the *in vivo* model used assesses the initial infection of the virus/PsV, it is not possible to explore the effect of the adaptive immune system on viral control. Again, this would need to be performed using MmuPV for a longer-term infection model as this papillomavirus is able to replicate in murine cells.

As demonstrated, an STH infection is able to alter the immune profile of the FGT, a completely uncolonized site by the helminth. According to Omondi et al., this immunomodulation may not be completely systemic, as shown by the lack of cytokine expression change in the plasma of STH-infected women[191]. It is therefore intriguing why this immunomodulation would occur in the FGT, but not systemically. Further work is required to determine how the immune profile is altered in the FGT – whether it be from circulating antigens through APCs travelling to lymph nodes or some other mechanism. The results from helminth antigen exposure in the FGT suggest that this may be a possible mechanism, as both a live infection (in the GIT) and FGT exposure to antigen resulted in decreased fHPV-16 PsV infection. However, the immune cell profiles between these two models were not comparable and therefore may point to another mechanism.

The result that STH-induced eosinophilia in the FGT is protective against fHPV-16 PsV infection was surprising given that it has been shown that this eosinophilia leads to increased epithelial damage (this was, however, shown in the absence of N9). Therefore, one would hypothesise that this increased damage would lead to increased access to the basal keratinocytes and therefore increase fHPV-16 infection. Further work, such as histology or cytokine analysis, is

required to determine whether the STH-induced eosinophilia is causing epithelial damage in this model or if this is specific to the HSV-2 model used by Chetty et al.[302].

In order to create a more realistic model of cervical cancer in mice and using this to explore the effect of STH infection on cervical cancer growth, I would like to use a novel preclinical model produced by Henkle et al.[306] Here, they developed a murine model of spontaneous HPV-16-expressing carcinomas in the FGT of mice. The tumours formed from this model grow in immunocompetent mice and expressed HPV-16 E6 and E7 proteins. The ability of these tumours to grow in immunocompetent mice allows us to explore the effect of T cells on anti-cancer immunity as well as how the Th1/Th2 polarisation may affect tumour control. These tumours also progress from intraepithelial lesions through to carcinoma, which would allow us to assess the effect of STH infection on tumour progression. Another model that could be used to more realistically investigate the effect of STH infection on cervical cancer growth would be to use humanised mice. These mice have engrafted human immune cells, allowing researchers to investigate the effect of T cells in short-term oncology studies. This would allow us to use HeLa cells and investigate the effect of the Th2 environment created by STH infection on cervical cancer growth and phenotype. These mice, however, would also require xenografts *ex situ*, and be grown on the flank of the mouse. Another caveat would be that these mice may develop graft vs host disease 3-4 weeks post immune cell engraftment[307], which may affect the results of the study towards the end of the experiment.

Lastly, the findings that STH exposure/infection altered the expression of β-catenin, N-cadherin and p53 left me with further questions. While I can speculate what the results may entail, I would like to further investigate the involvement of the canonical Wnt signalling pathway that may be affected by STH infection. Similarly, the observed trend towards increased p53 expression following STH antigen exposure could point to a number of altered processes that may have an effect on cervical cancer growth. To explore this, I would like to assess apoptosis and cell cycle arrest in HeLa cells following exposure to STH antigens, as well as validate these findings *in vivo* by assessing p53 expression in the xenografts grown in nude mice. This could further explain how STH exposure/infection reduces cervical cancer growth.

Appendix

Appendix 1 – Mice monitoring sheet

UNIVERSITY OF CAPE TOWN
IYUNIVESITHI YASEKAPA • UNIVERSITEIT VAN KAAPSTAD

FHS003: AEC Application Form

FHS AEC number	**019/032**	**Short title**	Helminth regulation of HPV-related cervical cancer
Name of monitor(s)	**Claire Butters, Katherine Smith, Rodney Lucas**	**Monitoring frequency**	Daily after treatment (or as defined in the protocol)

Details of any Procedures [A]:																															
Cage Number:		**Date:**	/ /		/ /		/ /		/ /		/ /		/ /		/ /		/ /		/ /		/ /		/ /		/ /		/ /		/ /		/ /	
Mark:	**Baseline Weight:**	**15% Weight loss:**	**Weight**		**Weight**		**Weight**		**Weight**		**Weight**		**Weight**		**Weight**		**Weight**		**Weight**		**Weight**		**Weight**		**Weight**		**Weight**		**Weight**		**Weight**	
Mouse 1	g	g																													
Mouse 2	g	g																													
Mouse 3	g	g																													
Mouse 4	g	g																													
Mouse 5	g	g																													
			am	pm	am	pm	am	pm	am	pm	am	pm	am	pm	am	pm	am	pm	am	pm	am	pm	am	pm	am	pm	am	pm	am	pm	am	pm
Clinical illness severity [B] Score 0-3																															
Tumour Size & Appearance[C]																															
Distress (D) Euthanize (EE or HE) [D] Found Dead (FD)																															
Monitor																															

[A] **Procedure:** OG = oral gavage, IP = intraperitoneal injection, IA = isofluorane anaesthesia, SC = subcutaneous administration, IV = intravenous administration, IVAG = intravaginal inoculation

[B] **Clinical illness score**: **Score 0 = No discomfort or stress:** Active, inquisitive; hair-coat clean; normal posture, ears upright, extremities normal colour. **Score 1 = mild discomfort or stress:** General lack of grooming, aggression, guarding behaviour, less mobile, altered respiration rate and pattern, 10% weight loss, minor depression or exaggerated responses. **Score 2 = moderate discomfort or stress:** Coat staring, ocular and nasal discharges, very still and alert (reduced ability to feed), isolated, dehydration by lifting the skin (reduced ability to drink), reduced response to provocation. Body condition score 2. **Score 3 = severe discomfort or stress:** Pilo-erection, hunched up, vocalisation, restlessness, inert, 15% weight loss immobility (cannot feed or drink), tremors, convulsions, reacts violently or very weak and unresponsive, primary tumour volume is more that 1.7cm in any direction, primary tumour exhibits 1. discharge, 2. redness of surrounding skin or 3. The development of a crater-like appearance at the site of the lesion. Respiratory distress. Body condition score 1.
If the animal shows signs of moderate discomfort or stress (scoring 2), monitor twice daily. If the animal is not likely to recover and no action can be taken to alleviate its distress, the animal must immediately be euthanized.

[C] **Tumour Appearance**: Normal **(N)**, Large (~700-1200mm^3) **(L)**, Discharge **(D)**, Redness of surrounding skin **(R),** Crater-like appearance **(C)**.

[D] **EE** = experimental endpoint: **HE** = humane endpoint

Body Condition Score 1-5: 1 = Mouse is emaciated (skeletal structure extremely prominent; little or no flesh cover. Vertebrae distinctly segmented), **2** = Mouse is under-conditioned (segmentation of vertebral column evident. Dorsal pelvic bones are readily palpable), **3** = Mouse is well-conditioned (vertebra and dorsal pelvis not prominent; palpable with slight pressure**)**, **4** = Mouse is over-conditioned (spine is a continuous column. Vertebrae palpable only with firm pressure), **5** = Mouse is obese (mouse is smooth and bulky, Bone structure disappears under flesh and subcutaneous fat). A body condition score 1 justifies a humane endpoint.

Humane endpoint: The animal scores a 3 (severe discomfort or stress, including a body condition score of 1) or the animal has shown no improvement and has deteriorated since a score of 2 (moderate discomfort or stress) is recorded, the humane endpoint has been reached and the animal must be euthanised immediately. If animals display **(D)**, **(R)** or **(C) Tumour appearance**, the human endpoint has been reached. **Action:** Immediate euthanasia. **If an animal is kept alive while it is in a state of distress, this will constitute a violation of the principles of the humane care of animals.**

Appendix 2 – Cell culture

Complete DMEM

- Dulbecco's Modified Eagle Medium (DMEM; Sigma Aldrich)
- 10% fetal bovine serum (FBS, Gibco™)
- 1% penicillin/streptomycin (P/S; Thermo Fisher)

F media

- 1 part DMEM
- 3 parts Ham's F-12 media (Sigma Aldrich)
- 5% FBS
- 5% P/S
- 0.4µg/ml hydrocortisone (Calbiochem)
- 5µg/ml insulin (NovoRapid)
- 8.4ng/ml cholera toxin (Sigma Aldrich)
- 10ng/ml epidermal growth factor (Life Technologies)
- 24µg/ml adenine (Sigma Aldrich)

Appendix 3 – helminth antigen reagents

NES culturing solution

- RPMI 1640 medium (Sigma Aldrich)
- 1% gentamycin (Thermo Fisher Scientific)
- 1% P/S
- 1% L-glutamine (Merck)
- 1% glucose

Filter-sterilised and stored at 4°C.

HES culturing media

- RPMI
- 2.22% 25% glucose
- 1% P/S
- 1% L-glutamine
- 1% gentamycin

Appendix 4 – HPV pseudovirion production

5x HSB

- 125mM HEPES (BioWhittaker™)
- 2.5M NaCl
- 0.1% Brij58
- 5mM $MgCl_2$
- 500µM EDTA
- 2.5% ethanol

Filter sterilised

Cell lysis buffer (in PBS)

- 9.5mM $MgCl_2$
- 10% Brij
- 2µl Benzonase
- 2µl Exonuclease V (New England Biolabs)

CsCl solution

- 54g light CsCl or 77.6g heavy CsCl
- Topped up to 200ml with HSB

Filter sterilised

Appendix 5 – flow cytometry

MACs buffer

- 0.5% BSA (Carl Roth)
- 2mM EDTA
- PBS

Appendix 6 – Western Blots

Laemmli sample buffer

- 0.25 M Tris (pH 6.8)
- 4% SDS
- 20% glycerol
- 10% β-mercaptoethanol
- 0.002% bromophenol blue

Tissue lysis buffer

- H_2O
- 1:10 RIPA buffer (Merck)
- 1:100 protease inhibitor (Sigma Aldrich)

8% Resolving gel (10ml)

- 5.3ml H_2O
- 2ml 40% acrylamide
- 2.5ml 1.5M Tris (pH 8.8)
- 100µl 10% SDS
- 100µl 10% AMPS (Promega)
- 10µl TEMED

10% Resolving gel

- 4.8ml H_2O
- 2.5ml 40% acrylamide
- 2.5ml 1.5M Tris (pH 8.8)
- 100µl 10% SDS
- 100µl 10% AMPS
- 10µl TEMED

5% Stacking gel (8ml)

- 5.8ml H_2O
- 1ml 40% acrylamide
- 1ml 1.5M Tris (pH 6.8)
- 80µl 10% SDS
- 80µl 10% AMPS
- 8µl TEMED

Running buffer

- 25 mM Tris
- 190 mM glycine
- 0.1% SDS
- Made up to 1L with ddH_2O

Transfer buffer

- 25 mM Tris
- 190 mM glycine
- 20% methanol
- Made up to 1L with ddH_2O

Ponceau stain (10x)

- 0.25g Ponceau S (Sigma Aldrich)
- 12.5ml acetic acid
- Make up to 250ml with H_2O

TBST

- 100ml 10x TBS
- 1ml Tween
- Filled up to 1l with H_2O

Blocking buffer (20ml)

- 1g milk
- Filled up to 20ml with TBST

References

1. Wakelin, D. Helminths: Pathogenesis and Defenses. in *Medical Microbiology* (ed. Baron, S.) (University of Texas Medical Branch at Galveston, Galveston (TX)).
2. Soil-transmitted helminth infections. https://www.who.int/news-room/fact-sheets/detail/soil-transmitted-helminth-infections.
3. Soil Transmitted Helminth Infections. *Centers for Disease Control and Prevention* https://www.cdc.gov/parasites/sth/index.html#:~:text=Soil%2Dtransmitted%20helminths%20refer%20to,Ancylostoma%20duodenale%20and%20Necator%20americanus). (2022).
4. Pullan, R. L., Smith, J. L., Jasrasaria, R. & Brooker, S. J. Global numbers of infection and disease burden of soil transmitted helminth infections in 2010. *Parasit. Vectors* **7**, 37 (2014).
5. Montresor, A., Mwinzi, P., Mupfasoni, D. & Garba, A. Reduction in DALYs lost due to soil-transmitted helminthiases and schistosomiasis from 2000 to 2019 is parallel to the increase in coverage of the global control programmes. *PLoS Negl. Trop. Dis.* **16**, e0010575 (2022).
6. Create a map. *Global Atlas of Helminth Infections* https://www.thiswormyworld.org/maps/create-a-map.
7. Colombo, S. A. P. & Grencis, R. K. Immunity to Soil-Transmitted Helminths: Evidence From the Field and Laboratory Models. *Front. Immunol.* **11**, 1286 (2020).
8. Despommier, D. D., Gwadz, R. W. & Hotez, P. J. *Parasitic Diseases*. (Springer Science & Business Media, 2012).

9. Phillips, N. L. H. & Roth, T. L. Animal Models and Their Contribution to Our Understanding of the Relationship Between Environments, Epigenetic Modifications, and Behavior. *Genes* **10**, (2019).

10. Masopust, D., Sivula, C. P. & Jameson, S. C. Of Mice, Dirty Mice, and Men: Using Mice To Understand Human Immunology. *J. Immunol.* **199**, 383–388 (2017).

11. Morse, H. C. Chapter 1 - Building a Better Mouse: One Hundred Years of Genetics and Biology. in *The Mouse in Biomedical Research (Second Edition)* (eds. Fox, J. G. et al.) 1–11 (Academic Press, Burlington, 2007).

12. Mouse Genome Sequencing Consortium *et al.* Initial sequencing and comparative analysis of the mouse genome. *Nature* **420**, 520–562 (2002).

13. Moore, K. J. Utilization of mouse models in the discovery of human disease genes. *Drug Discov. Today* **4**, 123–128 (1999).

14. Shay, T. *et al.* Conservation and divergence in the transcriptional programs of the human and mouse immune systems. *Proc. Natl. Acad. Sci. U. S. A.* **110**, 2946–2951 (2013).

15. Fukushima, A. *et al.* Genetic background determines susceptibility to experimental immune-mediated blepharoconjunctivitis: comparison of Balb/c and C57BL/6 mice. *Exp. Eye Res.* **82**, 210–218 (2006).

16. Camberis, M., Le Gros, G. & Urban, J., Jr. Animal model of Nippostrongylus brasiliensis and Heligmosomoides polygyrus. *Curr. Protoc. Immunol.* **Chapter 19**, Unit 19.12 (2003).

17. Johnston, C. J. C. *et al.* Cultivation of Heligmosomoides polygyrus: an immunomodulatory nematode parasite and its secreted products. *J. Vis. Exp.* e52412 (2015).

18. Montaño, K. J., Cuéllar, C. & Sotillo, J. Rodent Models for the Study of Soil-Transmitted Helminths: A Proteomics Approach. *Front. Cell. Infect. Microbiol.* **11**, 639573 (2021).

19. Pionnier, N. *et al.* Neutropenic Mice Provide Insight into the Role of Skin-Infiltrating Neutrophils in the Host Protective Immunity against Filarial Infective Larvae. *PLoS Negl. Trop. Dis.* **10**, e0004605 (2016).

20. Giacomin, P. R. *et al.* The role of complement in innate, adaptive and eosinophil-dependent immunity to the nematode Nippostrongylus brasiliensis. *Mol. Immunol.* **45**, 446–455 (2008).

21. Knott, M. L., Matthaei, K. I., Foster, P. S. & Dent, L. A. The roles of eotaxin and the STAT6 signalling pathway in eosinophil recruitment and host resistance to the nematodes Nippostrongylus brasiliensis and Heligmosomoides bakeri. *Mol. Immunol.* **46**, 2714–2722 (2009).

22. Mochizuki, M., Bartels, J., Mallet, A. I., Christophers, E. & Schröder, J. M. IL-4 induces eotaxin: a possible mechanism of selective eosinophil recruitment in helminth infection and atopy. *J. Immunol.* **160**, 60–68 (1998).

23. Gazzinelli-Guimarães, P. H. *et al.* Parasitological and immunological aspects of early Ascaris spp. infection in mice. *Int. J. Parasitol.* **43**, 697–706 (2013).

24. Sutherland, T. E. *et al.* Chitinase-like proteins promote IL-17-mediated neutrophilia in a tradeoff between nematode killing and host damage. *Nat. Immunol.* **15**, 1116–1125 (2014).

25. Witko-Sarsat, V., Rieu, P., Descamps-Latscha, B., Lesavre, P. & Halbwachs-Mecarelli, L. Neutrophils: Molecules, Functions and Pathophysiological Aspects. *Lab. Invest.* **80**, 617–653 (2000).

26. Chen, F. *et al.* Neutrophils prime a long-lived effector macrophage phenotype that mediates accelerated helminth expulsion. *Nat. Immunol.* **15**, 938–946 (2014).

27. Coffman, R. L., Seymour, B. W., Hudak, S., Jackson, J. & Rennick, D. Antibody to interleukin-5 inhibits helminth-induced eosinophilia in mice. *Science* **245**, 308–310 (1989).

28. Levi-Schaffer, F. *et al.* Human eosinophils regulate human lung- and skin-derived fibroblast properties *in vitro*: A role for transforming growth factor β (TGF-β). *Proceedings of the National Academy of Sciences* **96**, 9660–9665 (1999).

29. Angkasekwinai, P. *et al.* Interleukin 25 promotes the initiation of proallergic type 2 responses. *J. Exp. Med.* **204**, 1509–1517 (2007).

30. Gerbe, F. *et al.* Intestinal epithelial tuft cells initiate type 2 mucosal immunity to helminth parasites. *Nature* **529**, 226–230 (2016).

31. Humphreys, N. E., Xu, D., Hepworth, M. R., Liew, F. Y. & Grencis, R. K. IL-33, a potent inducer of adaptive immunity to intestinal nematodes. *J. Immunol.* **180**, 2443–2449 (2008).

32. Haber, A. L. *et al.* A single-cell survey of the small intestinal epithelium. *Nature* **551**, 333–339 (2017).

33. Liu, S.-K., Cypess, R. H. & Van Zandt, P. Gastritis Caused by Multiple Nematospiroides dubius Infections. *J. Parasitol.* **60**, 790–793 (1974).

34. Owhashi, M., Kirai, N. & Horii, Y. Eosinophil chemotactic factor release from neutrophils induced by stimulation with Schistosoma japonicum eggs. *Parasitol. Res.* **83**, 42–46 (1997).

35. Neill, D. R. *et al.* Nuocytes represent a new innate effector leukocyte that mediates type-2 immunity. *Nature* **464**, 1367–1370 (2010).

36. Molofsky, A. B. *et al.* Innate lymphoid type 2 cells sustain visceral adipose tissue eosinophils and alternatively activated macrophages. *J. Exp. Med.* **210**, 535–549 (2013).

37. Cui, W. *et al.* Diet-mediated constitutive induction of novel IL-4+ ILC2 cells maintains intestinal homeostasis in mice. *J. Exp. Med.* **220**, (2023).

38. Impellizzieri, D. *et al.* IL-4 receptor engagement in human neutrophils impairs their migration and extracellular trap formation. *J. Allergy Clin. Immunol.* **144**, 267-279.e4 (2019).

39. Seki, T. *et al.* Interleukin-4 (IL-4) and IL-13 suppress excessive neutrophil infiltration and hepatocyte damage during acute murine schistosomiasis japonica. *Infect. Immun.* **80**, 159–168 (2012).

40. Zhu, Z. *et al.* Pulmonary expression of interleukin-13 causes inflammation, mucus hypersecretion, subepithelial fibrosis, physiologic abnormalities, and eotaxin production. *J. Clin. Invest.* **103**, 779–788 (1999).

41. Halim, T. Y. F. *et al.* Group 2 innate lymphoid cells are critical for the initiation of adaptive T helper 2 cell-mediated allergic lung inflammation. *Immunity* **40**, 425–435 (2014).

42. Soumelis, V. *et al.* Human epithelial cells trigger dendritic cell mediated allergic inflammation by producing TSLP. *Nat. Immunol.* **3**, 673–680 (2002).

43. Ito, T. *et al.* TSLP-activated dendritic cells induce an inflammatory T helper type 2 cell response through OX40 ligand. *J. Exp. Med.* **202**, 1213–1223 (2005).

44. Agrawal, S. *et al.* Cutting edge: different Toll-like receptor agonists instruct dendritic cells to induce distinct Th responses via differential modulation of extracellular

signal-regulated kinase-mitogen-activated protein kinase and c-Fos. *J. Immunol.* **171**, 4984–4989 (2003).

45. Halim, T. Y. F. *et al.* Group 2 innate lymphoid cells license dendritic cells to potentiate memory TH2 cell responses. *Nat. Immunol.* **17**, 57–64 (2016).

46. Noh, J. Y. *et al.* Thymic stromal lymphopoietin regulates eosinophil migration via phosphorylation of l-plastin in atopic dermatitis. *Exp. Dermatol.* **25**, 880–886 (2016).

47. Korenaga, M. *et al.* The role of interleukin-5 in protective immunity to Strongyloides venezuelensis infection in mice. *Immunology* **72**, 502–507 (1991).

48. Rotman, H. L. *et al.* Strongyloides stercoralis: eosinophil-dependent immune-mediated killing of third stage larvae in BALB/cByJ mice. *Exp. Parasitol.* **82**, 267–278 (1996).

49. Urban, J. F., Jr, Katona, I. M., Paul, W. E. & Finkelman, F. D. Interleukin 4 is important in protective immunity to a gastrointestinal nematode infection in mice. *Proc. Natl. Acad. Sci. U. S. A.* **88**, 5513–5517 (1991).

50. Betts, C. J. & Else, K. J. Mast cells, eosinophils and antibody-mediated cellular cytotoxicity are not critical in resistance to Trichuris muris. *Parasite Immunol.* **21**, 45–52 (1999).

51. Patnode, M. L., Bando, J. K., Krummel, M. F., Locksley, R. M. & Rosen, S. D. Leukotriene B4 amplifies eosinophil accumulation in response to nematodes. *J. Exp. Med.* **211**, 1281–1288 (2014).

52. Klion, A. D. & Nutman, T. B. The role of eosinophils in host defense against helminth parasites. *J. Allergy Clin. Immunol.* **113**, 30–37 (2004).

53. Cook, E. B., Stahl, J. L., Schwantes, E. A., Fox, K. E. & Mathur, S. K. IL-3 and TNFα increase Thymic Stromal Lymphopoietin Receptor (TSLPR) expression on eosinophils and enhance TSLP-stimulated degranulation. *Clin. Mol. Allergy* **10**, 8 (2012).

54. Makepeace, B. L., Martin, C., Turner, J. D. & Specht, S. Granulocytes in helminth infection -- who is calling the shots? *Curr. Med. Chem.* **19**, 1567–1586 (2012).

55. Hogan, S. P. *et al.* Eosinophils: biological properties and role in health and disease. *Clin. Exp. Allergy* **38**, 709–750 (2008).

56. Ackerman, S. J., Gleich, G. J., Loegering, D. A., Richardson, B. A. & Butterworth, A. E. Comparative toxicity of purified human eosinophil granule cationic proteins for schistosomula of Schistosoma mansoni. *Am. J. Trop. Med. Hyg.* **34**, 735–745 (1985).

57. Hamann, K. J., Barker, R. L., Loegering, D. A. & Gleich, G. J. Comparative Toxicity of Purified Human Eosinophil Granule Proteins for Newborn Larvae of Trichinella spiralis. *J. Parasitol.* **73**, 523–529 (1987).

58. Abu-Ghazaleh, R. I., Fujisawa, T., Mestecky, J., Kyle, R. A. & Gleich, G. J. IgA-induced eosinophil degranulation. *J. Immunol.* **142**, 2393–2400 (1989).

59. Soussi Gounni, A. *et al.* High-affinity IgE receptor on eosinophils is involved in defence against parasites. *Nature* **367**, 183–186 (1994).

60. Lacy, P. *et al.* Rapid mobilization of intracellularly stored RANTES in response to interferon-gamma in human eosinophils. *Blood* **94**, 23–32 (1999).

61. Horie, S., Gleich, G. J. & Kita, H. Cytokines directly induce degranulation and superoxide production from human eosinophils. *J. Allergy Clin. Immunol.* **98**, 371–381 (1996).

62. Pecaric-Petkovic, T., Didichenko, S. A., Kaempfer, S., Spiegl, N. & Dahinden, C. A. Human basophils and eosinophils are the direct target leukocytes of the novel IL-1 family member IL-33. *Blood* **113**, 1526–1534 (2009).

63. Padigel, U. M., Lee, J. J., Nolan, T. J., Schad, G. A. & Abraham, D. Eosinophils can function as antigen-presenting cells to induce primary and secondary immune responses to Strongyloides stercoralis. *Infect. Immun.* **74**, 3232–3238 (2006).

64. MacKenzie, J. R., Mattes, J., Dent, L. A. & Foster, P. S. Eosinophils promote allergic disease of the lung by regulating CD4(+) Th2 lymphocyte function. *J. Immunol.* **167**, 3146–3155 (2001).

65. Culley, F. J. *et al.* Eotaxin is specifically cleaved by hookworm metalloproteases preventing its action in vitro and in vivo. *J. Immunol.* **165**, 6447–6453 (2000).

66. Reece, J. J., Siracusa, M. C. & Scott, A. L. Innate immune responses to lung-stage helminth infection induce alternatively activated alveolar macrophages. *Infect. Immun.* **74**, 4970–4981 (2006).

67. Herbert, D. R. *et al.* Alternative macrophage activation is essential for survival during schistosomiasis and downmodulates T helper 1 responses and immunopathology. *Immunity* **20**, 623–635 (2004).

68. Zhao, A. *et al.* Th2 cytokine-induced alterations in intestinal smooth muscle function depend on alternatively activated macrophages. *Gastroenterology* **135**, 217-225.e1 (2008).

69. Hayashi, N. *et al.* Kupffer cells from Schistosoma mansoni-infected mice participate in the prompt type 2 differentiation of hepatic T cells in response to worm antigens. *J. Immunol.* **163**, 6702–6711 (1999).

70. Welch, J. S. *et al.* TH2 cytokines and allergic challenge induce Ym1 expression in macrophages by a STAT6-dependent mechanism. *J. Biol. Chem.* **277**, 42821–42829 (2002).

71. Raes, G. *et al.* Differential expression of FIZZ1 and Ym1 in alternatively versus classically activated macrophages. *J. Leukoc. Biol.* **71**, 597–602 (2002).

72. Webb, D. C., McKenzie, A. N. & Foster, P. S. Expression of the Ym2 lectin-binding protein is dependent on interleukin (IL)-4 and IL-13 signal transduction: identification of a novel allergy-associated protein. *J. Biol. Chem.* **276**, 41969–41976 (2001).

73. Linehan, E. *et al.* Aging impairs peritoneal but not bone marrow-derived macrophage phagocytosis. *Aging Cell* **13**, 699–708 (2014).

74. Kawai, Y. *et al.* T cell-dependent and -independent expression of intestinal epithelial cell-related molecules in rats infected with the nematode Nippostrongylus brasiliensis. *APMIS* **115**, 210–217 (2007).

75. Hashimoto, K. *et al.* Depleted intestinal goblet cells and severe pathological changes in SCID mice infected with Heligmosomoides polygyrus. *Parasite Immunol.* **31**, 457–465 (2009).

76. Mitchell, G. F., Hogarth-Scott, R. S., Edwards, R. D. & Moore, T. Studies on immune responses to parasite antigens in mice. III. Nippostrongylus brasiliensis infections in hypothymic nu/nu mice. *Int. Arch. Allergy Appl. Immunol.* **52**, 95–104 (1976).

77. Metenou, S. *et al.* Highly heterogeneous, activated, and short-lived regulatory T cells during chronic filarial infection. *Eur. J. Immunol.* **44**, 2036–2047 (2014).

78. Taylor, M. D., van der Werf, N. & Maizels, R. M. T cells in helminth infection: the regulators and the regulated. *Trends Immunol.* **33**, 181–189 (2012).

79. Chen, W. *et al.* Conversion of Peripheral CD4+CD25− Naive T Cells to CD4+CD25+ Regulatory T Cells by TGF-β Induction of Transcription Factor Foxp3. *J. Exp. Med.* **198**, 1875–1886 (2003).

80. Douglas, B. *et al.* Transgenic expression of a T cell epitope in Strongyloides ratti reveals that helminth-specific CD4+ T cells constitute both Th2 and Treg populations. *PLoS Pathog.* **17**, e1009709 (2021).

81. Smith, K. A. *et al.* Chronic helminth infection promotes immune regulation in vivo through dominance of CD11cloCD103- dendritic cells. *J. Immunol.* **186**, 7098–7109 (2011).

82. Taylor, M. D., Harris, A., Nair, M. G., Maizels, R. M. & Allen, J. E. F4/80+ alternatively activated macrophages control CD4+ T cell hyporesponsiveness at sites peripheral to filarial infection. *J. Immunol.* **176**, 6918–6927 (2006).

83. van der Kleij, D. *et al.* A novel host-parasite lipid cross-talk. Schistosomal lyso-phosphatidylserine activates toll-like receptor 2 and affects immune polarization. *J. Biol. Chem.* **277**, 48122–48129 (2002).

84. Grainger, J. R. *et al.* Helminth secretions induce de novo T cell Foxp3 expression and regulatory function through the TGF-β pathway. *J. Exp. Med.* **207**, 2331–2341 (2010).

85. Johnston, C. J. C. *et al.* A structurally distinct TGF-β mimic from an intestinal helminth parasite potently induces regulatory T cells. *Nat. Commun.* **8**, 1–13 (2017).

86. Groux, H. *et al.* A CD4+ T-cell subset inhibits antigen-specific T-cell responses and prevents colitis. *Nature* **389**, 737–742 (1997).

87. Satoguina, J. S. *et al.* Tr1 and naturally occurring regulatory T cells induce IgG4 in B cells through GITR/GITR-L interaction, IL-10 and TGF-beta. *Eur. J. Immunol.* **38**, 3101–3113 (2008).

88. Layland, L. E., Rad, R., Wagner, H. & da Costa, C. U. P. Immunopathology in schistosomiasis is controlled by antigen-specific regulatory T cells primed in the presence of TLR2. *Eur. J. Immunol.* **37**, 2174–2184 (2007).

89. Sawant, D. V. *et al.* Regulatory T cells limit induction of protective immunity and promote immune pathology following intestinal helminth infection. *J. Immunol.* **192**, 2904–2912 (2014).

90. Smith, K. A. *et al.* Low-level regulatory T-cell activity is essential for functional type-2 effector immunity to expel gastrointestinal helminths. *Mucosal Immunol.* **9**, 428–443 (2015).

91. Harnett, W. Secretory products of helminth parasites as immunomodulators. *Mol. Biochem. Parasitol.* **195**, 130–136 (2014).

92. Dainichi, T. *et al.* Nippocystatin, a cysteine protease inhibitor from Nippostrongylus brasiliensis, inhibits antigen processing and modulates antigen-specific immune response. *Infect. Immun.* **69**, 7380–7386 (2001).

93. Ziegler, T. *et al.* A novel regulatory macrophage induced by a helminth molecule instructs IL-10 in CD4+ T cells and protects against mucosal inflammation. *J. Immunol.* **194**, 1555–1564 (2015).

94. Manoury, B., Gregory, W. F., Maizels, R. M. & Watts, C. Bm-CPI-2, a cystatin homolog secreted by the filarial parasite Brugia malayi, inhibits class II MHC-restricted antigen processing. *Curr. Biol.* **11**, 447–451 (2001).

95. Schnoeller, C. *et al.* A helminth immunomodulator reduces allergic and inflammatory responses by induction of IL-10-producing macrophages. *J. Immunol.* **180**, 4265–4272 (2008).

96. McSorley, H. J., Blair, N. F., Smith, K. A., McKenzie, A. N. J. & Maizels, R. M. Blockade of IL-33 release and suppression of type 2 innate lymphoid cell responses by helminth secreted products in airway allergy. *Mucosal Immunol.* **7**, 1068–1078 (2014).

97. Vacca, F. *et al.* A helminth-derived suppressor of ST2 blocks allergic responses. *Elife* **9**, (2020).

98. Drurey, C. & Maizels, R. M. Helminth extracellular vesicles: Interactions with the host immune system. *Mol. Immunol.* **137**, 124–133 (2021).

99. Buck, A. H. *et al.* Exosomes secreted by nematode parasites transfer small RNAs to mammalian cells and modulate innate immunity. *Nat. Commun.* **5**, 5488 (2014).

100. Eichenberger, R. M. *et al.* Hookworm Secreted Extracellular Vesicles Interact With Host Cells and Prevent Inducible Colitis in Mice. *Front. Immunol.* **9**, 850 (2018).

101. Coakley, G. *et al.* Extracellular Vesicles from a Helminth Parasite Suppress Macrophage Activation and Constitute an Effective Vaccine for Protective Immunity. *Cell Rep.* **19**, 1545–1557 (2017).

102. Hansen, E. P. *et al.* Exploration of extracellular vesicles from Ascaris suum provides evidence of parasite-host cross talk. *J Extracell Vesicles* **8**, 1578116 (2019).

103. Zhu, L. *et al.* Molecular characterization of S. japonicum exosome-like vesicles reveals their regulatory roles in parasite-host interactions. *Sci. Rep.* **6**, 25885 (2016).

104. Tritten, L., Clarke, D., Timmins, S., McTier, T. & Geary, T. G. Dirofilaria immitis exhibits sex- and stage-specific differences in excretory/secretory miRNA and protein profiles. *Vet. Parasitol.* **232**, 1–7 (2016).

105. Walk, S. T., Blum, A. M., Ewing, S. A.-S., Weinstock, J. V. & Young, V. B. Alteration of the murine gut microbiota during infection with the parasitic helminth Heligmosomoides polygyrus. *Inflamm. Bowel Dis.* **16**, 1841–1849 (2010).

106. Reynolds, L. A. *et al.* Commensal-pathogen interactions in the intestinal tract: lactobacilli promote infection with, and are promoted by, helminth parasites. *Gut Microbes* **5**, 522–532 (2014).

107. Zaiss, M. M. *et al.* The Intestinal Microbiota Contributes to the Ability of Helminths to Modulate Allergic Inflammation. *Immunity* **43**, 998–1010 (2015).

108. Su, C. W. *et al.* Helminth-Induced and Th2-Dependent Alterations of the Gut Microbiota Attenuate Obesity Caused by High-Fat Diet. *Cell Mol Gastroenterol Hepatol* **10**, 763–778 (2020).

109. Kennedy, M. H. E. *et al.* Small Intestinal Levels of the Branched Short-Chain Fatty Acid Isovalerate Are Elevated during Infection with Heligmosomoides polygyrus and Can Promote Helminth Fecundity. *Infect. Immun.* **89**, e0022521 (2021).

110. Su, Z., Segura, M. & Stevenson, M. M. Reduced protective efficacy of a blood-stage malaria vaccine by concurrent nematode infection. *Infect. Immun.* **74**, 2138–2144 (2006).

111. Elias, D., Britton, S., Aseffa, A., Engers, H. & Akuffo, H. Poor immunogenicity of BCG in helminth infected population is associated with increased in vitro TGF-beta production. *Vaccine* **26**, 3897–3902 (2008).

112. Hartmann, W., Brunn, M.-L., Stetter, N., Gabriel, G. & Breloer, M. Pre-existing helminth infection impairs the efficacy of adjuvanted influenza vaccination in mice. *PLoS One* **17**, e0266456 (2022).

113. Brown, J. *et al.* Impact of malaria and helminth infections on immunogenicity of the human papillomavirus-16/18 AS04-adjuvanted vaccine in Tanzania. *Vaccine* **32**, 611–617 (2014).

114. Marchant, A. *et al.* Newborns develop a Th1-type immune response to Mycobacterium bovis bacillus Calmette-Guérin vaccination. *J. Immunol.* **163**, 2249–2255 (1999).

115. Emeny, R. T. *et al.* Priming of human papillomavirus type 11-specific humoral and cellular immune responses in college-aged women with a virus-like particle vaccine. *J. Virol.* **76**, 7832–7842 (2002).

116. Pinto, L. A. *et al.* Cellular immune responses to human papillomavirus (HPV)-16 L1 in healthy volunteers immunized with recombinant HPV-16 L1 virus-like particles. *J. Infect. Dis.* **188**, 327–338 (2003).

117. CDC. About HPV. https://www.cdc.gov/hpv/parents/about-hpv.html (2021).

118. Human Papillomavirus (HPV) Vaccine. *Pan American Health Organisation* https://www.paho.org/en/human-papillomavirus-hpv-vaccine.

119. Crow, J. M. HPV: The global burden. *Nature* **488**, S2-3 (2012).

120. Xu, Y.-F., Zhang, Y.-Q., Xu, X.-M. & Song, G.-X. Papillomavirus virus-like particles as vehicles for the delivery of epitopes or genes. *Arch. Virol.* **151**, 2133–2148 (2006).

121. Roberts, J. N. *et al.* Genital transmission of HPV in a mouse model is potentiated by nonoxynol-9 and inhibited by carrageenan. *Nat. Med.* **13**, 857–861 (2007).

122. Horvath, C. A. J., Boulet, G. A. V., Renoux, V. M., Delvenne, P. O. & Bogers, J.-P. J. Mechanisms of cell entry by human papillomaviruses: an overview. *Virol. J.* **7**, 11 (2010).

123. Roden, R. B., Kirnbauer, R., Jenson, A. B., Lowy, D. R. & Schiller, J. T. Interaction of papillomaviruses with the cell surface. *J. Virol.* **68**, 7260–7266 (1994).

124. Day, P. M., Gambhira, R., Roden, R. B. S., Lowy, D. R. & Schiller, J. T. Mechanisms of human papillomavirus type 16 neutralization by l2 cross-neutralizing and l1 type-specific antibodies. *J. Virol.* **82**, 4638–4646 (2008).

125. Evander, M. *et al.* Identification of the alpha6 integrin as a candidate receptor for papillomaviruses. *J. Virol.* **71**, 2449–2456 (1997).

126. Huang, H.-S. & Lambert, P. F. Use of an in vivo animal model for assessing the role of integrin α(6)β(4) and syndecan-1 in early steps in papillomavirus infection. *Virology* **433**, 395–400 (2012).

127. Dziduszko, A. & Ozbun, M. A. Annexin A2 and S100A10 regulate human papillomavirus type 16 entry and intracellular trafficking in human keratinocytes. *J. Virol.* **87**, 7502–7515 (2013).

128. Woodham, A. W. *et al.* Small molecule inhibitors of the annexin A2 heterotetramer prevent human papillomavirus type 16 infection. *J. Antimicrob. Chemother.* **70**, 1686–1690 (2015).

129. Laniosz, V., Dabydeen, S. A., Havens, M. A. & Meneses, P. I. Human papillomavirus type 16 infection of human keratinocytes requires clathrin and caveolin-1 and is brefeldin a sensitive. *J. Virol.* **83**, 8221–8232 (2009).

130. Day, P. M., Lowy, D. R. & Schiller, J. T. Papillomaviruses infect cells via a clathrin-dependent pathway. *Virology* **307**, 1–11 (2003).

131. Schelhaas, M. *et al.* Entry of human papillomavirus type 16 by actin-dependent, clathrin- and lipid raft-independent endocytosis. *PLoS Pathog.* **8**, e1002657 (2012).

132. Florin, L. *et al.* Identification of a dynein interacting domain in the papillomavirus minor capsid protein l2. *J. Virol.* **80**, 6691–6696 (2006).

133. Aydin, I. *et al.* Large scale RNAi reveals the requirement of nuclear envelope breakdown for nuclear import of human papillomaviruses. *PLoS Pathog.* **10**, e1004162 (2014).

134. Pyeon, D., Pearce, S. M., Lank, S. M., Ahlquist, P. & Lambert, P. F. Establishment of human papillomavirus infection requires cell cycle progression. *PLoS Pathog.* **5**, e1000318 (2009).

135. Jeon, S. & Lambert, P. F. Integration of human papillomavirus type 16 DNA into the human genome leads to increased stability of E6 and E7 mRNAs: implications for cervical carcinogenesis. *Proc. Natl. Acad. Sci. U. S. A.* **92**, 1654–1658 (1995).

136. Stanley, M. Immune responses to human papillomavirus. *Vaccine* **24 Suppl 1**, S16-22 (2006).

137. Scheffner, M., Werness, B. A., Huibregtse, J. M., Levine, A. J. & Howley, P. M. The E6 oncoprotein encoded by human papillomavirus types 16 and 18 promotes the degradation of p53. *Cell* **63**, 1129–1136 (1990).

138. Dyson, N., Howley, P. M., Münger, K. & Harlow, E. The human papilloma virus-16 E7 oncoprotein is able to bind to the retinoblastoma gene product. *Science* **243**, 934–937 (1989).

139. Myers, J. E. *et al.* Detecting episomal or integrated human papillomavirus 16 DNA using an exonuclease V-qPCR-based assay. *Virology* **537**, 149–156 (2019).

140. McBride, A. A. & Warburton, A. The role of integration in oncogenic progression of HPV-associated cancers. *PLoS Pathog.* **13**, e1006211 (2017).

141. Williams, V. M., Filippova, M., Soto, U. & Duerksen-Hughes, P. J. HPV-DNA integration and carcinogenesis: putative roles for inflammation and oxidative stress. *Future Virol.* **6**, 45–57 (2011).

142. Cervical Cancer. *World Health Organisation* https://www.who.int/news-room/fact-sheets/detail/human-papillomavirus-(hpv)-and-cervical-cancer (2022).

143. Katerji, M. & Duerksen-Hughes, P. J. DNA damage in cancer development: special implications in viral oncogenesis. *Am. J. Cancer Res.* **11**, 3956–3979 (2021).

144. Mello, V. & Sundstrom, R. K. *Cervical Intraepithelial Neoplasia*. (StatPearls Publishing, 2023).

145. Ribatti, D., Tamma, R. & Annese, T. Epithelial-Mesenchymal Transition in Cancer: A Historical Overview. *Transl. Oncol.* **13**, 100773 (2020).

146. Greenburg, G. & Hay, E. D. Epithelia suspended in collagen gels can lose polarity and express characteristics of migrating mesenchymal cells. *J. Cell Biol.* **95**, 333–339 (1982).

147. Pirinen, R. T., Hirvikoski, P., Johansson, R. T., Hollmén, S. & Kosma, V. M. Reduced expression of alpha-catenin, beta-catenin, and gamma-catenin is associated with high cell proliferative activity and poor differentiation in non-small cell lung cancer. *J. Clin. Pathol.* **54**, 391–395 (2001).

148. Kase, S. *et al.* Expression of E-cadherin and beta-catenin in human non-small cell lung cancer and the clinical significance. *Clin. Cancer Res.* **6**, 4789–4796 (2000).

149. Liu, C.-Y., Lin, H.-H., Tang, M.-J. & Wang, Y.-K. Vimentin contributes to epithelial-mesenchymal transition cancer cell mechanics by mediating cytoskeletal organization and focal adhesion maturation. *Oncotarget* **6**, 15966–15983 (2015).

150. Tsai, J. H., Donaher, J. L., Murphy, D. A., Chau, S. & Yang, J. Spatiotemporal regulation of epithelial-mesenchymal transition is essential for squamous cell carcinoma metastasis. *Cancer Cell* **22**, 725–736 (2012).

151. Cervical Cancer. *Western Cape Government* https://www.westerncape.gov.za/general-publication/cervical-cancer (2021).

152. South Africa: Human Papillomavirus and Related Cancers, Fact Sheet 2023. *HPV Information Centre* chrome-extension://efaidnbmnnnibpcajpcglclefindmkaj/https://hpvcentre.net/statistics/reports/ZAF_FS.pdf (2023).

153. Protection from cervical cancer. *UNICEF* https://www.unicef.org/southafrica/parents-frequently-asked-questions-hpv-cervical-cancer (2022).

154. Ebrahimi, N. *et al.* Human papillomavirus vaccination in low- and middle-income countries: progression, barriers, and future prospective. *Front. Immunol.* **14**, 1150238 (2023).

155. U.S. Cancer Statistics Working Group. United States Cancer Statistics: Data Visualizations. *Centers for Disease Control and Prevention* https://gis.cdc.gov/Cancer/USCS/#/Trends/ (2023).

156. Sung, H. *et al.* Global Cancer Statistics 2020: GLOBOCAN Estimates of Incidence and Mortality Worldwide for 36 Cancers in 185 Countries. *CA Cancer J. Clin.* **71**, 209–249 (2021).

157. Globocan. Cancer Today - Population Fact Sheets. *International Agency for Research on Cancer (IARC)* (2020).

158. Scherer, W. F., Syverton, J. T. & Gey, G. O. Studies on the propagation in vitro of poliomyelitis viruses. IV. Viral multiplication in a stable strain of human malignant epithelial cells (strain HeLa) derived from an epidermoid carcinoma of the cervix. *J. Exp. Med.* **97**, 695–710 (1953).

159. Eagle, H. Propagation in a fluid medium of a human epidermoid carcinoma, strain KB. *Proc. Soc. Exp. Biol. Med.* **89**, 362–364 (1955).

160. Strauss, N. & Hendee, E. D. The effect of diphtheria toxin on the metabolism of HeLa cells. *J. Exp. Med.* **109**, 145–163 (1959).

161. Henrietta Lacks: science must right a historical wrong. *Nature* **585**, 7 (2020).

162. Hasan, U. A. *et al.* TLR9 expression and function is abolished by the cervical cancer-associated human papillomavirus type 16. *J. Immunol.* **178**, 3186–3197 (2007).

163. Karim, R. *et al.* Human papillomavirus (HPV) upregulates the cellular deubiquitinase UCHL1 to suppress the keratinocyte's innate immune response. *PLoS Pathog.* **9**, e1003384 (2013).

164. Nees, M. *et al.* Papillomavirus type 16 oncogenes downregulate expression of interferon-responsive genes and upregulate proliferation-associated and NF-kappaB-responsive genes in cervical keratinocytes. *J. Virol.* **75**, 4283–4296 (2001).

165. Tummers, B. *et al.* The interferon-related developmental regulator 1 is used by human papillomavirus to suppress NFκB activation. *Nat. Commun.* **6**, 6537 (2015).

166. Sasagawa, T., Takagi, H. & Makinoda, S. Immune responses against human papillomavirus (HPV) infection and evasion of host defense in cervical cancer. *J. Infect. Chemother.* **18**, 807–815 (2012).

167. Hacke, K. *et al.* Regulation of MCP-1 chemokine transcription by p53. *Mol. Cancer* **9**, 82 (2010).

168. Coleman, N. *et al.* Immunological events in regressing genital warts. *Am. J. Clin. Pathol.* **102**, 768–774 (1994).

169. Ghim, S. *et al.* Spontaneously regressing oral papillomas induce systemic antibodies that neutralize canine oral papillomavirus. *Exp. Mol. Pathol.* **68**, 147–151 (2000).

170. Franco, E. L. *et al.* Epidemiology of acquisition and clearance of cervical human papillomavirus infection in women from a high-risk area for cervical cancer. *J. Infect. Dis.* **180**, 1415–1423 (1999).

171. Brown, D. R. *et al.* A longitudinal study of genital human papillomavirus infection in a cohort of closely followed adolescent women. *J. Infect. Dis.* **191**, 182–192 (2005).

172. Spellberg, B. & Edwards, J. E. Type 1/Type 2 Immunity in Infectious Diseases. *Clin. Infect. Dis.* **32**, 76–102 (2001).

173. Osborne, L. C. *et al.* Coinfection. Virus-helminth coinfection reveals a microbiota-independent mechanism of immunomodulation. *Science* **345**, 578–582 (2014).

174. Wilen, C. B. *et al.* Tropism for tuft cells determines immune promotion of norovirus pathogenesis. *Science* **360**, 204–208 (2018).

175. Wescott, R. B. & Todd, A. C. Interaction of Nippostrongylus brasiliensis and Influenza Virus in Mice. I. Influence of the Nematode on the Virus. *J. Parasitol.* **52**, 242–247 (1966).

176. Nayak, D. P. & Kelley, G. W. SYNERGISTIC EFFECT OF ASCARIS MIGRATION AND INFLUENZA INFECTION IN MICE. *J. Parasitol.* **51**, 297–298 (1965).

177. Rouse, B. T. & Sehrawat, S. Immunity and immunopathology to viruses: what decides the outcome? *Nat. Rev. Immunol.* **10**, 514–526 (2010).

178. Gopallawa, I., Dehinwal, R., Bhatia, V., Gujar, V. & Chirmule, N. A four-part guide to lung immunology: Invasion, inflammation, immunity, and intervention. *Front. Immunol.* **14**, 1119564 (2023).

179. Oyesola, O. O. *et al.* Exposure to lung-migrating helminth protects against murine SARS-CoV-2 infection through macrophage-dependent T cell activation. *Science Immunology* **8**, eadf8161 (2023).

180. King, I. L. *et al.* Intestinal helminth infection impacts the systemic distribution and function of the naive lymphocyte pool. *Mucosal Immunol.* **10**, 1160–1168 (2017).

181. McFarlane, A. J. *et al.* Enteric helminth-induced type I interferon signaling protects against pulmonary virus infection through interaction with the microbiota. *J. Allergy Clin. Immunol.* **140**, 1068-1078.e6 (2017).

182. Serrat, J. *et al.* Antigens from the Helminth Fasciola hepatica Exert Antiviral Effects against SARS-CoV-2 In Vitro. *Int. J. Mol. Sci.* **24**, (2023).

183. Rolot, M. *et al.* Helminth-induced IL-4 expands bystander memory CD8+ T cells for early control of viral infection. *Nat. Commun.* **9**, 4516 (2018).

184. Scheer, S. *et al.* S. mansoni bolsters anti-viral immunity in the murine respiratory tract. *PLoS One* **9**, e112469 (2014).

185. Furze, R. C., Hussell, T. & Selkirk, M. E. Amelioration of influenza-induced pathology in mice by coinfection with Trichinella spiralis. *Infect. Immun.* **74**, 1924–1932 (2006).

186. Dietze, K. K. *et al.* Filariae-Retrovirus Co-infection in Mice is Associated with Suppressed Virus-Specific IgG Immune Response and Higher Viral Loads. *PLoS Negl. Trop. Dis.* **10**, e0005170 (2016).

187. Downs, J. A. *et al.* Urogenital schistosomiasis in women of reproductive age in Tanzania's Lake Victoria region. *Am. J. Trop. Med. Hyg.* **84**, 364–369 (2011).

188. Kjetland, E. F. *et al.* Association between genital schistosomiasis and HIV in rural Zimbabwean women. *AIDS* **20**, 593–600 (2006).

189. Morawski, B. M. *et al.* Hookworm infection is associated with decreased CD4+ T cell counts in HIV-infected adult Ugandans. *PLoS Negl. Trop. Dis.* **11**, e0005634 (2017).

190. Yegorov, S. *et al.* Schistosoma mansoni treatment reduces HIV entry into cervical CD4+ T cells and induces IFN-I pathways. *Nat. Commun.* **10**, 1–12 (2019).

191. Chetty, A. *et al.* Il4ra-independent vaginal eosinophil accumulation following helminth infection exacerbates epithelial ulcerative pathology of HSV-2 infection. *Cell Host Microbe* **29**, 579-593.e5 (2021).

192. Jacobs, B.-A. *et al.* Hookworm exposure decreases human papillomavirus uptake and cervical cancer cell migration through systemic regulation of epithelial-mesenchymal transition marker expression. *Sci. Rep.* **8**, 11547 (2018).

193. Gravitt, P. E. *et al.* Soil-Transmitted Helminth Infections Are Associated With an Increase in Human Papillomavirus Prevalence and a T-Helper Type 2 Cytokine Signature in Cervical Fluids. *J. Infect. Dis.* **213**, 723–730 (2016).

194. Holali Ameyapoh, A. *et al.* Hookworm Infections and Sociodemographic Factors Associated With Female Reproductive Tract Infections in Rural Areas of the Central Region of Togo. *Front. Microbiol.* **12**, 738894 (2021).

195. Omondi, M. A. *et al.* Hookworm infection associates with a vaginal Type 1/Type 2 immune signature and increased HPV load. *Front. Immunol.* **13**, 1009968 (2022).

196. Pastille, E. *et al.* Intestinal helminth infection drives carcinogenesis in colitis-associated colon cancer. *PLoS Pathog.* **13**, e1006649 (2017).

197. Jacobs, B.-A., Prince, S. & Smith, K. A. Gastrointestinal Nematode-Derived Antigens Alter Colorectal Cancer Cell Proliferation and Migration through Regulation of Cell Cycle and Epithelial-Mesenchymal Transition Proteins. *Int. J. Mol. Sci.* **21**, (2020).

198. Hayes, K. S. *et al.* Chronic Trichuris muris infection causes neoplastic change in the intestine and exacerbates tumour formation in APC min/+ mice. *PLoS Negl. Trop. Dis.* **11**, e0005708 (2017).

199. Chala, B. *et al.* Development of Urinary Bladder Pre-Neoplasia by Schistosoma haematobium Eggs and Chemical Carcinogen in Mice. *Korean J. Parasitol.* **55**, 21–29 (2017).

200. Tuffour, I. *et al.* Schistosoma Egg Antigen Induces Oncogenic Alterations in Human Prostate Cells. *Anal. Cell. Pathol.* **2018**, 4675380 (2018).

201. Wu, C. *et al.* Schistosoma japonicum SjE16.7 Protein Promotes Tumor Development via the Receptor for Advanced Glycation End Products (RAGE). *Front. Immunol.* **11**, 1767 (2020).

202. Habib, S. L., Said, B., Awad, A. T., Mostafa, M. H. & Shank, R. C. Novel adenine adducts, N7-guanine-AFB1 adducts, and p53 mutations in patients with schistosomiasis and aflatoxin exposure. *Cancer Detect. Prev.* **30**, 491–498 (2006).

203. Callejas, B. E. *et al.* Helminth-derived molecules inhibit colitis-associated colon cancer development through NF-κB and STAT3 regulation. *Int. J. Cancer* **145**, 3126–3139 (2019).

204. León-Cabrera, S. *et al.* Extraintestinal helminth infection reduces the development of colitis-associated tumorigenesis. *Int. J. Biol. Sci.* **10**, 948–956 (2014).

205. Feng, Q. *et al.* Th2 type inflammation promotes the gradual progression of HPV-infected cervical cells to cervical carcinoma. *Gynecol. Oncol.* **127**, 412–419 (2012).

206. Bais, A. G. *et al.* A shift to a peripheral Th2-type cytokine pattern during the carcinogenesis of cervical cancer becomes manifest in CIN III lesions. *J. Clin. Pathol.* **58**, 1096–1100 (2005).

207. Buck, C. B., Pastrana, D. V., Lowy, D. R. & Schiller, J. T. Generation of HPV Pseudovirions Using Transfection and Their Use in Neutralization Assays. in *Human Papillomaviruses: Methods and Protocols* (eds. Davy, C. & Doorbar, J.) 445–462 (Humana Press, Totowa, NJ, 2006).

208. Buck, C. B., Pastrana, D. V., Lowy, D. R. & Schiller, J. T. Efficient intracellular assembly of papillomaviral vectors. *J. Virol.* **78**, 751–757 (2004).

209. BioRender.com. Genetic viral life cycle. (2023).

210. Tannous, B. A. Gaussia luciferase reporter assay for monitoring biological processes in culture and in vivo. *Nat. Protoc.* **4**, 582–591 (2009).

211. Carse, S., Lang, D., Katz, A. A. & Schäfer, G. Exogenous Vimentin Supplementation Transiently Affects Early Steps during HPV16 Pseudovirus Infection. *Viruses* **13**, (2021).

212. Flanagan, S. P. “Nude”, a new hairless gene with pleiotropic effects in the mouse. *Genet. Res.* **8**, 295–309 (1966).

213. Pantelouris, E. M. Athymic development in the mouse. *Differentiation* **1**, 437–450 (1973).

214. Montoliu-Gaya, L. *et al.* CA10 regulates neurexin heparan sulfate addition via a direct binding in the secretory pathway. *EMBO Rep.* **22**, e51349 (2021).

215. Schäfer, G. *et al.* Vimentin Modulates Infectious Internalization of Human Papillomavirus 16 Pseudovirions. *J. Virol.* **91**, (2017).

216. Thierry, F. Transcriptional regulation of the papillomavirus oncogenes by cellular and viral transcription factors in cervical carcinoma. *Virology* **384**, 375–379 (2009).

217. Ranjeva, S. L. *et al.* Recurring infection with ecologically distinct HPV types can explain high prevalence and diversity. *Proc. Natl. Acad. Sci. U. S. A.* **114**, 13573–13578 (2017).

218. Ujma, S. *et al.* Surfactant Protein A Impairs Genital HPV16 Pseudovirus Infection by Innate Immune Cell Activation in A Murine Model. *Pathogens* **8**, (2019).

219. Segura, M., Su, Z., Piccirillo, C. & Stevenson, M. M. Impairment of dendritic cell function by excretory-secretory products: a potential mechanism for nematode-induced immunosuppression. *Eur. J. Immunol.* **37**, 1887–1904 (2007).

220. Jacobs, B.-A. Cancer cell behaviour following parasite exposure. (University of Cape Town, 2018).

221. Blackwell, A. D. *et al.* Helminth infection, fecundity, and age of first pregnancy in women. *Science* **350**, 970–972 (2015).

222. Jourdan, P. M., Holmen, S. D., Gundersen, S. G., Roald, B. & Kjetland, E. F. HIV target cells in Schistosoma haematobium-infected female genital mucosa. *Am. J. Trop. Med. Hyg.* **85**, 1060–1064 (2011).

223. Kjetland, E. F. *et al.* The effects of genital schistosoma haematobium on human papillomavirus and the development of cervical neoplasia after five years in a Zimbabwean population. *Eur. J. Gynaecol. Oncol.* **31**, 169–173 (2010).

224. Hu, J. *et al.* Development of cell-based pseudovirus entry assay to identify potential viral entry inhibitors and neutralizing antibodies against SARS-CoV-2. *Genes & Diseases* **7**, 551–557 (2020).

225. Longet, S., Schiller, J. T., Bobst, M., Jichlinski, P. & Nardelli-Haefliger, D. A murine genital-challenge model is a sensitive measure of protective antibodies against human papillomavirus infection. *J. Virol.* **85**, 13253–13259 (2011).

226. Hillier, S. L. *et al.* In vitro and in vivo: the story of nonoxynol 9. *J. Acquir. Immune Defic. Syndr.* **39**, 1–8 (2005).

227. Aksoy, P., Gottschalk, E. Y. & Meneses, P. I. HPV entry into cells. *Mutat. Res. - Rev. Mut. Res.* **772**, 13–22 (2017).

228. Handisurya, A. *et al.* Murine skin and vaginal mucosa are similarly susceptible to infection by pseudovirions of different papillomavirus classifications and species. *Virology* **433**, 385–394 (2012).

229. Finlay, C. M., Walsh, K. P. & Mills, K. H. G. Induction of regulatory cells by helminth parasites: exploitation for the treatment of inflammatory diseases. *Immunol. Rev.* **259**, 206–230 (2014).

230. Dittrich, A. M. *et al.* Helminth infection with Litomosoides sigmodontis induces regulatory T cells and inhibits allergic sensitization, airway inflammation, and hyperreactivity in a murine asthma model. *J. Immunol.* **180**, 1792–1799 (2008).

231. Mo, H.-M. *et al.* Schistosoma japonicum infection modulates the development of allergen-induced airway inflammation in mice. *Parasitol. Res.* **103**, 1183–1189 (2008).

232. Wilson, M. S. *et al.* Suppression of allergic airway inflammation by helminth-induced regulatory T cells. *J. Exp. Med.* **202**, 1199–1212 (2005).

233. Wohlleben, G. *et al.* Helminth infection modulates the development of allergen-induced airway inflammation. *Int. Immunol.* **16**, 585–596 (2004).

234. Trujillo-Vargas, C. M. *et al.* Helminth-derived products inhibit the development of allergic responses in mice. *Am. J. Respir. Crit. Care Med.* **175**, 336–344 (2007).

235. McSorley, H. J. *et al.* Suppression of type 2 immunity and allergic airway inflammation by secreted products of the helminth Heligmosomoides polygyrus. *Eur. J. Immunol.* **42**, 2667–2682 (2012).

236. Broadhurst, M. J. *et al.* IL-22+ CD4+ T cells are associated with therapeutic trichuris trichiura infection in an ulcerative colitis patient. *Sci. Transl. Med.* **2**, 60ra88 (2010).

237. Croese, J. *et al.* A proof of concept study establishing Necator americanus in Crohn's patients and reservoir donors. *Gut* **55**, 136–137 (2006).

238. Summers, R. W., Elliott, D. E., Urban, J. F., Jr, Thompson, R. A. & Weinstock, J. V. Trichuris suis therapy for active ulcerative colitis: A randomized controlled trial. *Gastroenterology* **128**, 825–832 (2005).

239. Voehringer, D., Shinkai, K. & Locksley, R. M. Type 2 Immunity Reflects Orchestrated Recruitment of Cells Committed to IL-4 Production. *Immunity* **20**, 267–277 (2004).

240. Höchst, B. *et al.* Differential induction of Ly6G and Ly6C positive myeloid derived suppressor cells in chronic kidney and liver inflammation and fibrosis. *PLoS One* **10**, e0119662 (2015).

241. Berends, C. *et al.* Expression of CD35 (CR1) and CD11b (CR3) on circulating neutrophils and eosinophils from allergic asthmatic children. *Clin. Exp. Allergy* **23**, 926–933 (1993).

242. in 't Veen, J. C. *et al.* CD11b and L-selectin expression on eosinophils and neutrophils in blood and induced sputum of patients with asthma compared with normal subjects. *Clin. Exp. Allergy* **28**, 606–615 (1998).

243. Stirling, R. G., van Rensen, E. L., Barnes, P. J. & Chung, K. F. Interleukin-5 induces CD34(+) eosinophil progenitor mobilization and eosinophil CCR3 expression in asthma. *Am. J. Respir. Crit. Care Med.* **164**, 1403–1409 (2001).

244. Pelaia, C. *et al.* Interleukin-5 in the Pathophysiology of Severe Asthma. *Front. Physiol.* **10**, 1514 (2019).

245. Lawrence, M. G. *et al.* Interleukin-5 receptor alpha (CD125) expression on human blood and lung neutrophils. *Ann. Allergy Asthma Immunol.* **128**, 53-60.e3 (2022).

246. Gorski, S. A. *et al.* Expression of IL-5 receptor alpha by murine and human lung neutrophils. *PLoS One* **14**, e0221113 (2019).

247. Coden, M. E. & Berdnikovs, S. Eosinophils in wound healing and epithelial remodeling: Is coagulation a missing link? *J. Leukoc. Biol.* **108**, 93–103 (2020).

248. Selinka, H.-C., Giroglou, T. & Sapp, M. Analysis of the Infectious Entry Pathway of Human Papillomavirus Type 33 Pseudovirions. *Virology* **299**, 279–287 (2002).

249. Reese, T. A. *et al.* Helminth infection reactivates latent γ-herpesvirus via cytokine competition at a viral promoter. *Science* **345**, 573–577 (2014).

250. Xie, F. *et al.* The infiltration and functional regulation of eosinophils induced by TSLP promote the proliferation of cervical cancer cell. *Cancer Lett.* **364**, 106–117 (2015).

251. van Driel, W. J. *et al.* Tumor-associated eosinophilic infiltrate of cervical cancer is indicative for a less effective immune response. *Hum. Pathol.* **27**, 904–911 (1996).

252. Pelleitier, M. & Montplaisir, S. The nude mouse: a model of deficient T-cell function. *Methods Achiev. Exp. Pathol.* **7**, 149–166 (1975).

253. Xie, X. *et al.* Comparative studies between nude and scid mice on the growth and metastatic behavior of xenografted human tumors. *Clin. Exp. Metastasis* **10**, 201–210 (1992).

254. Liu, A. *et al.* Effects of curcumin on growth of human cervical cancer xenograft in nude mice and underlying mechanism. *Food Sci. Technol.* **38**, 106–111 (2017).

255. Chueh, F.-S. *et al.* Demethoxycurcumin Inhibits In Vivo Growth of Xenograft Tumors of Human Cervical Cancer Cells. *In Vivo* **34**, 2469–2474 (2020).

256. Cilwyn-Shalitha, B. & Sasidharan, S. Mechanisms of the In Vivo Antitumor Activity of Polyalthia longifolia Leaf Extract Against HeLa Cell Xenograft Tumor: A Microscopic-Based Histological and Immunohistochemical Microanalyses. *Microanal* **29**, 1153–1167 (2023).

257. Li, W. *et al.* SBF-1 exerts strong anticervical cancer effect through inducing endoplasmic reticulum stress-associated cell death via targeting sarco/endoplasmic reticulum Ca2+-ATPase 2. *Cell Death Dis.* **5**, e1581–e1581 (2014).

258. Liu, H. *et al.* Berberine nanoparticles for promising sonodynamic therapy of a HeLa xenograft tumour. *RSC Adv.* **9**, 10528–10535 (2019).

259. Murata, H. *et al.* Responsiveness to basement membrane extract as a possible trait for tumorigenicity characterization. *Vaccine X* **1**, 100004 (2019).

260. Ai, Y. *et al.* An alkaloid initiates phosphodiesterase 3A–schlafen 12 dependent apoptosis without affecting the phosphodiesterase activity. *Nat. Commun.* **11**, 1–10 (2020).

261. Hohlbaum, K. *et al.* Severity classification of repeated isoflurane anesthesia in C57BL/6JRj mice-Assessing the degree of distress. *PLoS One* **12**, e0179588 (2017).

262. Constantinides, C., Mean, R. & Janssen, B. J. Effects of isoflurane anesthesia on the cardiovascular function of the C57BL/6 mouse. *ILAR J.* **52**, e21-31 (2011).

263. Bajwa, N. M., Lee, J. B., Halavi, S., Hartman, R. E. & Obenaus, A. Repeated isoflurane in adult male mice leads to acute and persistent motor decrements with long-term

modifications in corpus callosum microstructural integrity. *J. Neurosci. Res.* **97**, 332–345 (2019).

264. Hietanen, S., Lain, S., Krausz, E., Blattner, C. & Lane, D. P. Activation of p53 in cervical carcinoma cells by small molecules. *Proceedings of the National Academy of Sciences* **97**, 8501–8506 (2000).

265. Garima, Pandey, S., Pandey, L. K., Saxena, A. K. & Patel, N. The Role of p53 Gene in Cervical Carcinogenesis. *J. Obstet. Gynaecol. India* **66**, 383–388 (2016).

266. Cheah, P.-L. & Looi, L.-M. p53 immunohistochemical expression: messages in cervical carcinogenesis. *Pathology* **34**, 326–331 (2002).

267. Khan, M. A. *et al.* Exploring the p53 connection of cervical cancer pathogenesis involving north-east Indian patients. *PLoS One* **15**, e0238500 (2020).

268. Chang, C.-Y. *et al.* Tumor suppressor p53 regulates intestinal type 2 immunity. *Nat. Commun.* **12**, 3371 (2021).

269. Liu, P. *et al.* Cell-cycle-regulated activation of Akt kinase by phosphorylation at its carboxyl terminus. *Nature* **508**, 541–545 (2014).

270. Halliday, G. M., Patel, A., Hunt, M. J., Tefany, F. J. & Barnetson, R. S. Spontaneous regression of human melanoma/nonmelanoma skin cancer: association with infiltrating CD4+ T cells. *World J. Surg.* **19**, 352–358 (1995).

271. Stoler, D. L. *et al.* The onset and extent of genomic instability in sporadic colorectal tumor progression. *Proc. Natl. Acad. Sci. U. S. A.* **96**, 15121–15126 (1999).

272. Prat, M., Bretti, S., Amedeo, M., Landolfo, S. & Comoglio, P. M. Monoclonal antibodies against murine IFN-gamma abrogate in vivo tumor immunity against RSV-induced murine sarcomas. *J. Immunol.* **138**, 4530–4533 (1987).

273. Smyth, M. J. *et al.* Perforin-mediated cytotoxicity is critical for surveillance of spontaneous lymphoma. *J. Exp. Med.* **192**, 755–760 (2000).

274. Angiolillo, A. L. *et al.* Human interferon-inducible protein 10 is a potent inhibitor of angiogenesis in vivo. *J. Exp. Med.* **182**, 155–162 (1995).

275. Tosolini, M. *et al.* Clinical impact of different classes of infiltrating T cytotoxic and helper cells (Th1, th2, treg, th17) in patients with colorectal cancer. *Cancer Res.* **71**, 1263–1271 (2011).

276. Bland, A. R. & Ashton, J. C. Considerations for Whole-Slide Analysis of Murine Xenografts Experiments. *J. Histochem. Cytochem.* **69**, 627–631 (2021).

277. Merad, M., Sathe, P., Helft, J., Miller, J. & Mortha, A. The dendritic cell lineage: ontogeny and function of dendritic cells and their subsets in the steady state and the inflamed setting. *Annu. Rev. Immunol.* **31**, 563–604 (2013).

278. Duan, M. *et al.* CD11b immunophenotyping identifies inflammatory profiles in the mouse and human lungs. *Mucosal Immunol.* **9**, 550–563 (2016).

279. Ghosn, E. E. B., Yang, Y., Tung, J., Herzenberg, L. A. & Herzenberg, L. A. CD11b expression distinguishes sequential stages of peritoneal B-1 development. *Proc. Natl. Acad. Sci. U. S. A.* **105**, 5195–5200 (2008).

280. Chiossone, L. *et al.* Maturation of mouse NK cells is a 4-stage developmental program. *Blood* **113**, 5488–5496 (2009).

281. Xie, F. *et al.* Cervical carcinoma cells stimulate the angiogenesis through TSLP promoting growth and activation of vascular endothelial cells. *Am. J. Reprod. Immunol.* **70**, 69–79 (2013).

282. Hollande, C. *et al.* Inhibition of the dipeptidyl peptidase DPP4 (CD26) reveals IL-33-dependent eosinophil-mediated control of tumor growth. *Nat. Immunol.* **20**, 257–264 (2019).

283. Varricchi, G. *et al.* Eosinophils: The unsung heroes in cancer? *Oncoimmunology* **7**, e1393134 (2018).

284. Chetty, A. *et al.* Induction of Siglec-FhiCD101hi eosinophils in the lungs following murine hookworm Nippostrongylus brasiliensis infection. *Front. Immunol.* **14**, 1170807 (2023).

285. Li, X. *et al.* Targeting of tumour-infiltrating macrophages via CCL2/CCR2 signalling as a therapeutic strategy against hepatocellular carcinoma. *Gut* **66**, 157–167 (2017).

286. Movahedi, K. *et al.* Different tumor microenvironments contain functionally distinct subsets of macrophages derived from Ly6C(high) monocytes. *Cancer Res.* **70**, 5728–5739 (2010).

287. Bonapace, L. *et al.* Cessation of CCL2 inhibition accelerates breast cancer metastasis by promoting angiogenesis. *Nature* **515**, 130–133 (2014).

288. Porrello, A. *et al.* Factor XIIIA-expressing inflammatory monocytes promote lung squamous cancer through fibrin cross-linking. *Nat. Commun.* **9**, 1988 (2018).

289. Olingy, C. E., Dinh, H. Q. & Hedrick, C. C. Monocyte heterogeneity and functions in cancer. *J. Leukoc. Biol.* **106**, 309–322 (2019).

290. Robinson, A., Han, C. Z., Glass, C. K. & Pollard, J. W. Monocyte Regulation in Homeostasis and Malignancy. *Trends Immunol.* **42**, 104–119 (2021).

291. Qian, B.-Z. *et al.* CCL2 recruits inflammatory monocytes to facilitate breast-tumour metastasis. *Nature* **475**, 222–225 (2011).

292. Zhang, M. *et al.* The lncRNA NEAT1 activates Wnt/β-catenin signaling and promotes colorectal cancer progression via interacting with DDX5. *J. Hematol. Oncol.* **11**, 113 (2018).

293. Tsukamoto, A. S., Grosschedl, R., Guzman, R. C., Parslow, T. & Varmus, H. E. Expression of the int-1 gene in transgenic mice is associated with mammary gland hyperplasia and adenocarcinomas in male and female mice. *Cell* **55**, 619–625 (1988).

294. Cao, M.-Q. *et al.* miR-182-5p promotes hepatocellular carcinoma progression by repressing FOXO3a. *J. Hematol. Oncol.* **11**, 12 (2018).

295. Leung, W. K. C., He, M., Chan, A. W. H., Law, P. T. Y. & Wong, N. Wnt/β-Catenin activates MiR-183/96/182 expression in hepatocellular carcinoma that promotes cell invasion. *Cancer Lett.* **362**, 97–105 (2015).

296. Wei, C.-Y. *et al.* Downregulation of RNF128 activates Wnt/β-catenin signaling to induce cellular EMT and stemness via CD44 and CTTN ubiquitination in melanoma. *J. Hematol. Oncol.* **12**, 21 (2019).

297. Ozawa, M., Baribault, H. & Kemler, R. The cytoplasmic domain of the cell adhesion molecule uvomorulin associates with three independent proteins structurally related in different species. *EMBO J.* **8**, 1711–1717 (1989).

298. Tian, X. *et al.* E-cadherin/β-catenin complex and the epithelial barrier. *J. Biomed. Biotechnol.* **2011**, 567305 (2011).

299. Su, C.-W. *et al.* Duodenal helminth infection alters barrier function of the colonic epithelium via adaptive immune activation. *Infect. Immun.* **79**, 2285–2294 (2011).

300. Hyoh, Y. *et al.* Enhancement of apoptosis with loss of cellular adherence in the villus epithelium of the small intestine after infection with the nematode Nippostrongylus brasiliensis in rats. *Parasitology* **119 (Pt 2)**, 199–207 (1999).

301. Radice, G. L. N-cadherin-mediated adhesion and signaling from development to disease: lessons from mice. *Prog. Mol. Biol. Transl. Sci.* **116**, 263–289 (2013).

302. Cano, A. *et al.* The transcription factor snail controls epithelial-mesenchymal transitions by repressing E-cadherin expression. *Nat. Cell Biol.* **2**, 76–83 (2000).

303. Wang, Y.-L. *et al.* Snail promotes epithelial-mesenchymal transition and invasiveness in human ovarian cancer cells. *Int. J. Clin. Exp. Med.* **8**, 7388–7393 (2015).

304. Ozaki, T. & Nakagawara, A. Role of p53 in Cell Death and Human Cancers. *Cancers* **3**, 994–1013 (2011).

305. IARC Working Group on the Evaluation of Carcinogenic Risks to Humans. *Studies of Animal Papillomaviruses*. (International Agency for Research on Cancer, 2007).

306. Henkle, T. R. *et al.* Development of a Novel Mouse Model of Spontaneous High-Risk HPVE6/E7-Expressing Carcinoma in the Cervicovaginal Tract. *Cancer Res.* **81**, 4560–4569 (2021).

307. Walsh, N. C. *et al.* Humanized Mouse Models of Clinical Disease. *Annu. Rev. Pathol.* **12**, 187–215 (2017).